OCS Study
MMS 86-0027

GULF OF MEXICO CIRCULATION MODELING STUDY

ANNUAL PROGRESS REPORT: YEAR 2

1986

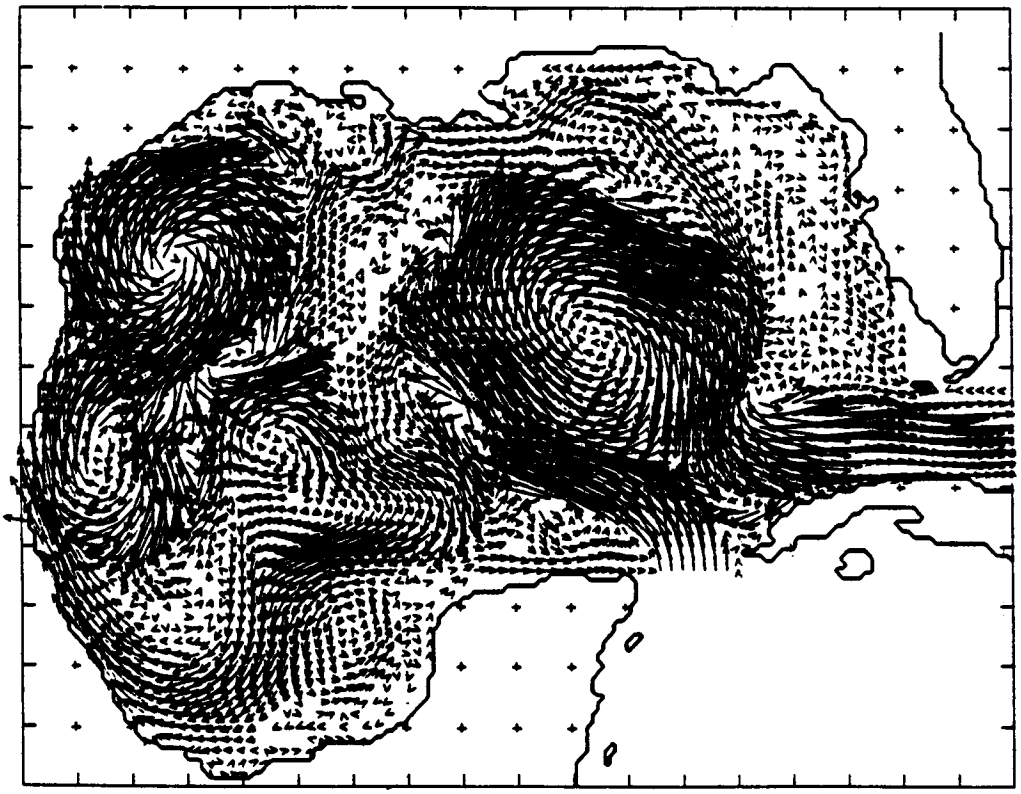

U.S. DEPARTMENT OF THE INTERIOR/MINERALS MANAGEMENT SERVICE

OCS STUDY
MMS 86-0027

GULF OF MEXICO
CIRCULATION MODELING STUDY

ANNUAL PROGRESS REPORT: YEAR 2

1986

by:

Alan J. Wallcraft, Ph.D.

JAYCOR
1608 Spring Hill Road
Vienna, Virginia 22180-2270

Prepared under Contract 14-12-0001-30073

for:

Minerals Management Service
Gulf of Mexico OCS Regional Office
Metairie, Louisiana 70010

Project Officer: Murray L. Brown, Ph.D.

April 1986

REPORT AVAILABILITY

Preparation of this report was conducted under Contract between the Minerals Management Service and JAYCOR. Extra copies of the report may be obtained from the Public Information Section (Mail Stop OPS-3-4) at the following address:

Minerals Management Service
Gulf of Mexico OCS Regional Office
U.S. Department of the Interior
P.O. Box 7944
Metairie, Louisiana 70010
Attn: Public Information Section
Phone: (504) 838-0519

DISCLAIMER

This report has been reviewed by the Minerals Management Service and approved for publication. Approval does not signify that the contents necessarily reflect the views and policies of the Service, nor does mention of the trade names or commercial products constitute endorsement or recommendation for use.

This volume should be cited as:

Wallcraft, A. 1986. Gulf of Mexico Circulation Modeling Study. (Progress Report by JAYCOR submitted to Minerals Management Service, Metairie, LA. Contract No. 14-12-0001-30073.)

TABLE OF CONTENTS

I. INTRODUCTION

This final report gives details of the second year of a four year numerical ocean circulation modeling program for the Gulf of Mexico. The aim of the program is to progressively upgrade in modest increments an existing numerical ocean circulation model of the Gulf so that the final model has a horizontal resolution of about 10 km and vertical resolution approaching 1 to 10 m in the mixed layer, 10 m at the thermocline and 100 m in the deep water. Throughout the four year period, the validity of the upgraded model will be continuously tested, and velocity field time series delivered periodically based on the most realistic simulation of Gulf circulation available.

Experiments in the first year were with the existing NORDA/JAYCOR two layer hydrodynamic primitive equation ocean circulation model of the Gulf on a 0.2 degree grid. They concentrated on correctly specifying the coastline and bottom topography for maximum realism in circulation simulation, and on how best to include wind forcing.

Experiments in the second year were also with the existing NORDA/JAYCOR hydrodynamic model, but most were on a 0.1 degree, rather than 0.2 degree, grid. Wind-forced only, port-forced only, and wind- plus port-forced simulations were generated. Details of selected experiments are presented in this report.

Simulated surface currents sampled every three days for more than 10 years were delivered to MMS from Experiment 201/16.0, which is driven by both wind and port forcing, as representing the best simulation available from the second year effort. Simulated surface currents sampled every three days for two eddy cycles were also delivered to MMS from Experiment 201/17.0, as representing the best simulation available with port forcing only.

Model parameters for all referenced experiments are included in Appendix A.

II. SUMMARY OF YEAR 1

The ocean model contains many innovative features, and the reader is referred to its detailed discussion in Hurlburt and Thompson (1980). In particular, Section 2 (pp. 1613-1614) gives the model equations and Appendix B (pp. 1647-1650) describes the numerical design of the model. Since that time, the capability to handle general basin geometry has been added but this does not affect the description in any major way. Wind forcing is treated identically to interfacial and bottom stress terms, i.e., wind stress appears directly as an additive term in the momentum equation (see p. 1614 of Hurlburt and Thompson (1980)).

In terms of 'realism' Experiment 9 was the most successful Gulf of Mexico numerical simulation prior to the start of this project. The model was driven from rest to statistical equilibrium solely by a steady inflow through the Yucatan Straits which was compensated by outflow through the Florida Straits. Figure 1 compares 'instantaneous' upper ocean flow patterns just before an eddy is shed by the Loop current (a) from the numerical model and (b) from observations by Leipper (1970). The ability of the model to simulate observed features is clearly demonstrated by this comparison, which is remarkable given the simplicity of the model forcing; however, some discrepancies remain. For example, the eddy has not penetrated as far into the Gulf and is more intense than that shown in the observations. Waves can be seen moving around the wall of the Loop Current in both the model and the observations, but in the model they are at the limit of resolution and therefore unrealistically large. Moreover, in the Gulf the waves are more pronounced on the eastern wall of the Loop and can form strong cold intrusions that may contribute to the eddy shedding process (Vukovitch and Maul, 1984). As shed eddies propagate westward (Figure 2a) the model spontaneously develops a counter-rotating vortex pair (Figure 2b), a structure repeatedly observed in the Western Gulf (Figure 3). The roles of the wind and the Loop Current eddies in the formation of this structure have been a matter of some controversy (Merrell and Morrison, 1981). Although wind forcing was not present in this simulation, a major role for winds has not been ruled out. After spin-up the experiment sheds an eddy once every 390 days and the observed eddy shedding cycles are very similar.

There is good observational evidence that the total transport through the Yucatan Straits is about 30 Sverdrups (Sv) (10^6 m^3 sec^{-1}), but there are very little data available on the vertical distribution of the flow. Experiment 9 allocated 26 Sv to the upper layer and 4 Sv to the lower. Allocating less transport to the upper layer would give rise to smaller Loop Current eddies, but exactly what range of eddy sizes is realistic is hard to quantify. However, there is one source of Gulf-wide data that can be used as a guide: maps of sea surface variability for the Gulf have been produced from all hydrographic, STD and XBT data (Maul and Herman, 1984), and from satellite altimeter crossovers (Marsh, et. al., 1984). The 20 Sverdrups upper and 10 Sverdrups lower layer distribution of inflow transport in Experiment 40 gave rise to a variability map very similar to that obtained from the satellite (Figure 4); these maps agree more closely with each other than with the map from hydrographic data (Figure 5). Based on the agreement of variability maps, the mean sea surface from Experiment 40 (Figure 6) may well be the best mean available for the Gulf (Thompson, 1986). Experiment 40 became the baseline port-forced experiment from the Year 1 project. The model parameters were:

- upper layer inflow transport = 20 x 10^6 m^3 sec^{-1} (= 20 Sv),
- lower layer inflow transport = 10 x 10^6 m^3 sec^{-1} (= 10 Sv),
- wind stress = 0,
- horizontal eddy viscosity, A = 300 m^2 sec^{-1}
- grid spacing = 20 by 22 km (0.2 by 0.2 degrees),
- upper layer reference thickness, H1 = 200m
- lower layer reference thickness, H2 = 3300m,
- minimum depth of bottom topography = 500m,
- beta, df/dy = 2 x 10^{-11} m^{-1} sec^{-1},
- Coriolis parameter at the southern boundary, f = 4.5 x 10^{-5} sec^{-1},
- gravitational acceleration, g = 9.8 m sec^{-2},
- reduced gravity, g' = .03(H1+H2)/H2 m sec^{-2},
- interfacial stress = 0,
- coefficient of quadratic bottom stress = .003;
- time step = 1.5 hours.

Experiment 68 is identical to experiment 40 except for the addition of wind-forcing after the port-forced circulation has fully spun up. The winds used were from the Navy Corrected Geostrophic Wind data set for the Gulf of Mexico which is based on the Navy's twelve hourly surface pressure analysis from 1967 to 1982. Wind input was every 12 hours; at first 1967 winds were used repeatedly to spin-up the wind-driven flow and then winds from 1967 to 1977 were applied in sequence. Figures 7 to 10 show upper layer currents (i.e., vertically averaged currents above the thermocline) every 60 to 120 days for 300 days. Vectors are only drawn at every second point (i.e., every 0.4 degrees) to improve readability. Figure 7 shows the furthest northward penetration of the Loop Current ever attained by the ocean model, similar configurations have been seen in the Gulf. After the eddy breaks off, the Loop Current intrudes onto the Florida Shelf and some of the flow splits off to the north for a brief time (Figure 8). Similar intrusions have been observed in the Gulf, but the model's inadequate representation of shelf topography makes it likely that the simulated currents in shallow areas (say less than 100 m) are too high. A persistent anticyclonic gyre in the northwest Gulf has been a feature of almost all Gulf simulations performed to date. The addition of wind forcing in Experiment 68 has increased its average size and its effect on incoming Loop Current eddies (Figure 9). The presence of a gyre in this position is explainable by the northward migration of anti-cyclonic eddies along the coast of Mexico until the continental slope bends eastward and they can go no further; the effect is magnified because the winds also tend to produce an anticyclon-ic gyre at the same spot. However, in the Gulf the gyre probably dissipates relatively rapidly against the shallow shelf area.

Simulated surface currents from Experiment 68 have been delivered to MMS as representing the best simulation data available at the end of Year 1. They consist of velocity com-ponent (u and v) fields on a 0.2 degree rectangular grid covering the Gulf area, sampled every three days for 3780 model days (10.3 years).

III. YEAR 2 WIND-FORCED EXPERIMENTS

Simulations forced by winds based on a seasonal climatology from ship observations (Elliott, 1979), see Figures 11(c,d) to 14(c,d), had been performed before this project started, and will be briefly described below. Such wind fields are not ideal for driving ocean models since they contain very little of the total wind variability and mean wind strengths are in general far weaker than instantaneous winds. Recognizing this deficiency, NORDA funded JAYCOR to produce a wind set for the Gulf based on the Navy's twelve-hourly surface pressure analysis, which is available from 1967 to 1982 (Rhodes et. al., 1986). The geostrophic winds, corrected geostrophic winds, and wind stresses (all on a one degree grid covering the Gulf) every 12 hours from 1967 to 1982 are on magnetic tape. These are available through the MMS Gulf of Mexico Regional Office.

Figure 15 shows the wind stress and wind stress curl from this data set for 0000 and 1200 GMT on 14 January and 0000 GMT on 15 January 1976. There is large temporal variability of the wind field during this period, as general easterly flow gives way to strong northerly flow after a frontal passage in just a 24 hour period. The wind stress curl field also shows the rapid change, from a relatively weak field to a very strong field with strong horizontal gradients. Figure 16 shows similar plots for 14 and 15 July 1976. Even in the summer, when flow is generally weaker, very significant differences can be seen in a short time period. These strong variations and very rapid changes in the wind field indicate why the modeling of Gulf circulation requires wind data on short temporal scales.

Figures 11(a,b) to 14(a,b) show the seasonal climatologies averaged over the period 1967-1982. The wind stress and wind stress curls are much stronger in the winter season than the summer season as would be expected. There are persistent areas of positive curl over the Yucatan and negative curl in the southwest Gulf that are present for all seasons, which have not been seen in any previous study of Gulf wind stresses. Although not present at all time periods (Figures 15 and 16), these are also the dominant features of the instantaneous curl fields.

Experiment 31 was performed before this project started. It is identical to Experiment 40 except that it has a slightly smaller coefficient of quadratic bottom stress (0.002 rather than 0.003) and is wind forced by the seasonal climatology from ship observations shown in Figures 11 to 14 with no port forcing. After spinup the experiment exhibits an annual repeat cycle; Figures 17(a) to 20(a) show the interface deviation for each season with a 12.5 meter (rather than the more usual 25 meter) contour interval.

Experiment 202/11.0 was performed in year 2 of the project. It uses a bottom topography that is (before smoothing) a projection of the 0.1 degree topography onto a 0.2 degree grid. It all other respects it is similar to experiment 31 except that the initial wind forcing is the monthly climatology from the Navy Corrected Geostrophic Wind data set, i.e., it uses the wind stresses in Figure 11(c) to 14(c) except there are twelve monthly fields instead of four seasonal (three-monthly) fields. As in all wind-forced cases, the winds are linearly interpolated in time between wind inputs so that the winds change slightly at each timestep and the model is not shocked by a large sudden change in wind stress. After spin up this experiment also exhibits an annual repeat cycle, Figures 17(b) to 20(b) show the interface deviation for each season with a 12.5 meter contour interval. The two wind sets (seasonal ship winds in 31; monthly modeled winds in 202/11.0) give rise to qualitatively similar circulation patterns everywhere except in the southwest Gulf in the winter and spring. However, 202/11.0 has interface deviations that are about two to three times greater than experiment 31, which is consistent with the generally higher wind stress and wind stress curl values in the corrected geostrophic wind data set. In general ship observation-based wind fields tend to underestimate wind strengths, moreover the geostrophic winds have been corrected to agree closely with winds reported from the three National Data Buoy Center (NDBC) buoys in the central Gulf. Therefore, the circulation strength in 202/11.0 is likely to be more realistic than in experiment 31. In the southwest Gulf experiment 31 has very strong upwelling in the winter and spring, but experiment 220/11.0 exhibits relatively weaker downwelling at this time. Again, this is consistent with the very different wind stress curl patterns of the two data sets in the region, but in this case it is difficult to judge which is more nearly correct because independent data are very sparse in this region. In the northwest Gulf both experiments show a wind-induced west Texas coastal current, as was predicted by Sturges and Blaha (1976) from calculations of wind stress curl based on wind data tabulated by Hellerman (1967). Note that Loop Current eddy remnants often end up at about the same place as the wind-induced anticyclonic gyre, and it would be very difficult to distinguish some phases of wind-driven and Loop Current-driven circulation in the southwest Gulf without a fairly long time history of the feature in question.

Experiment 202/11.0 was continued after it reached a quasi-steady state with monthly averaged winds for each year, i.e., 12 wind sets per year, starting in 1967. Figures 21 to 24 show interface deviation plots for each season of 1971 and 1972. The effects of interannual wind variability are clearly seen, however the strength of the circulation does not appear to be significantly different than for the monthly climatology.

Unlike port-forced experiments, simulations with wind forcing only do not provide realistic Gulf wide circulation patterns. This is because wind induced flows in the Eastern Gulf, except over the continental shelf, are very small relative to the dominant, port-forced, Loop Current system. However, in the Western Gulf wind forcing is very significant, perhaps as important as the large Loop Current eddies that migrate westward from the Loop Current. The simulations with both port and wind forcing, described later, demonstrate that the effects of winds and Loop Current are not additive; for example, the Loop Current variability is significantly increased over port-forced only cases, despite the relative weakness of winds in the Eastern Gulf.

IV. YEAR 2 PORT-FORCED EXPERIMENTS

The bottom topography used in all 0.1 degree simulations is shown in Figure 25. It is derived from the SYNBAPS data base (Van Wyckhouse, 1973), but there is a flat shelf between the 500-m isobath and the coast and the topography has been smoothed by two applications of a 9-point real smoother to filter out features that could cause 2-grid point numerical noise in the model. One advantage of the 0.1 degree grid over the 0.2 degree version is that the required smoothing has significantly less effect on the steepness of the continental slope in the finer grid model. The model boundary is approximately at the position of the original 10-m isobath, but the position of the plotted coastline in all figures follows the actual coastline as closely as possible, i.e., the model boundary is often several points seaward of the plotted coastline boundary. The section of the Caribbean shown is treated as land by the model, and the position of the inflow port is marked by the termination of contour lines in the Yucatan Strait. In the 0.1 degree model the inflow port is 16 grid points wide, compared to 8 grid points in the 0.2 degree model. This allows the inflow velocity profile to be better resolved, i.e., the velocities at the core of the inflow jet can be higher in the 0.1 degree case for the same inflow transport. In all cases described here, the upper layer inflow is exactly normal to the port and has a cubic velocity profile with the maximum about one third of the way from the west end of the port and zero velocities at both ends, and the lower layer inflow is exactly normal to the port and has a linear velocity profile with the velocity at the western end of the port twice that at the eastern end. In last year's 0.2 degree experiments, such as experiments 40 and 68, the profile in both layers was parabolic with the maximum at the center and zero velocites at both ends of the port. In all experiments to date the inflow transport has been spun up from rest to its required value of 30 Sv in the first 300 days and has then been held constant for the duration of the simulation. A mean transport of about 30 Sv, with a seasonal cycle of about 4 Sv, and with highly energetic variations on shorter time scales, is the generally accepted characterization of the transport through the Florida Straits (Niiler and Richardson, 1973; Brooks, 1979, Schott and Zantopp, 1985). A further advantage of the 0.1 degree grid model is that it allows the use of a lower horizontal eddy viscosity. Eddy viscosity is used to paramatarize sub-grid scale processes, i.e., in practice to damp out all scales which are too small to be represented by the model's finite difference dynamics. Eddy viscosity can be lower on a fine grid because smaller scales are resolved. It is usual to run several simulations with different eddy viscosities (with the largest value two or three times the smallest), because very low values might allow significant circulation features that are only marginally resolved by the model dynamics.

Experiment 201/13.0 is the baseline port-forced 0.1 degree experiment. The model parameters are very similar to the 0.2 degree, experiment 40, except for the new inflow profiles and the lower eddy viscosity made possible by the finer grid. The parameters are:

- upper layer inflow transport = 20 x 10^6 m^3 sec^{-1} (= 20 Sv),
- lower layer inflow transport = 10 x 10^6 m^3 sec^{-1} (= 10 Sv),
- wind stress = 0,
- horizontal eddy viscosity, A = 100 m^2 sec^{-1}
- grid spacing = 10 by 11 km (0.1 by 0.1 degrees),
- upper layer reference thickness, H1 = 200m,
- lower layer reference thickness, H2 = 3450m,
- minimum depth of bottom topography = 500m,
- beta, df/dy = 2 x 10^{-11} m^{-1} sec^{-1},
- Coriolis parameter at the southern boundary, f = 4.5 x 10^{-5} sec^{-1},
- gravitational acceleration, g = 9.8 m sec^{-2},
- reduced gravity, g' = .03 m sec^{-2},
- interfacial stress = 0,
- coefficient of quadratic bottom stress = .002,
- time step = 1.0 hour.

Figures 26 to 28 show upper layer velocities every 90 days for a complete eddy cycle, as is usual for port-forced (only) cases all eddy cycles are similar after spin up. In these and all subsequent current plots the velocity is shown every 0.2 degrees, i.e., only half the model grid resolution is plotted, and all currents higher than 50 cm sec^{-1} are drawn as 50 cm sec^{-1}. In areas where the current is low and in the same direction over several grid points the plotted vectors are further thinned by a factor of two, this situation occurs infrequently in upper layer plots but is noticeable in the lower layer. In Figure 26(a) the Loop Current has repenetrated into the Gulf after shedding an eddy about 120 days previously. This anticyclonic eddy has reached the coast of

Mexico and has split into two, and is bracketed by two cyclonic gyres with the gyre in the southwest Gulf being particularly large. There is a cyclonic eddy on the wall of the Loop Current over the Florida Shelf; if the model included the true shelf depth this feature would probably dissipate very rapidly. In Figure 26(b), 90 days later, the eddies in the western Gulf are smaller, the Loop Current is penetrating further into the Gulf and is encroaching less onto the Florida Shelf. In Figure 27(a) the Loop Current is about to break off an eddy; the previous Loop Current eddy is now quite small and has started to move north along the coast of Mexico. In Figure 27(b) the eddy has detached from the Loop Current, surrounded by smaller cyclonic eddies; the previous eddy has migrated to the Texas coast and is very small. In Figure 28(a) the Loop Current eddy has migrated westward and is about to split into two, the Loop Current has started to repenetrate into the Gulf, and there is a cyclonic eddy just above it. In Figure 28(b) the situation is similar to Figure 26(a) and the cycle is complete, the small remnant of the previous Loop Current eddy appears to have been absorbed into the larger of the two pieces of the latest eddy.

Experiment 201/17.0 is similar to experiment 201/13.0 except that it has a lower eddy viscosity ($A=50\ m^2\ sec^{-1}$), and a larger coefficient of quadratic bottom friction (0.003). Simulated surface currents from this experiment, sampled every 3 days for 2 complete eddy-shedding cycles, have been delivered to MMS as representing the best port-forced experiment to date. Figures 29 to 34 show upper and lower layer currents every 90 days for one complete eddy cycle. In Figure 29 an anticyclonic eddy has just detached from the Loop Current, and it has a large associated anticyclonic deep water eddy at its leading edge. Figure 30, 90 days later, shows that the Loop Current eddy moving into the western Gulf has generated a counter-rotating vortex pair in the lower layer, with the anticyclone leading and the cyclone trailing the upper layer eddy. In Figure 31 the Loop Current eddy has reached the Mexican coast, and the leading deep water anticyclone has dissipated against the continental slope. The deep water cyclone has strengthened and a cyclone has formed in the upper layer, i.e., an anticyclone in the upper layer has become, in 90 days, a cyclone in the lower layer with a vortex pair in the upper layer. The Loop Current is repenetrating into the Gulf, and there are some signs of a northward counter current in the lower layer along the Florida slope. In Figure 32 the old Loop Current eddy system (two anticyclonic and one cyclonic eddy in the upper layer and a cyclonic eddy in the lower layer) is dissipating on the Mexican coast, and the leading anticyclonic component has started to move northward. A new Loop Current eddy is forming and small cyclonic meanders can be seen moving around the wall of the Loop Current. In the lower layer the northward counter current has intensified as part of a cyclonic circulation below the Loop Current. In Figure 33 a new Loop

Current eddy has just separated from the Loop Current. In Figure 34 it is moving into the central Gulf, but the previous Loop Current eddy (that formed more than 400 days previously) is still strongly in evidence to its southwest. The longevity of the first Loop Current eddy appears to be related to its breaking into two parts and then recoalescing.

Port-forced experiments provide realistic Gulf wide circulation patterns. However, there is usually very little variability from one Loop Current eddy cycle to the next. The Loop Current eddy shedding period is usually approximately constant for each experiment, although it varies from experiment to experiment. Almost all port-forced simulations have Loop Current eddies following the same south of west path across the Gulf. This is probably the preferred path for actual Loop Current eddies in the Gulf. Overall, port-forced simulations provide a very good realization of a typical Loop Current eddy cycle, and they demonstrate almost everything that was known about Gulf circulation up until the mid to late 1970's. Since then, however, the observational data base has been greatly expanded, and it is now recognized that the Gulf circulation has far more variability than these simulations allow. For example, the Loop Current eddy shedding period can be anything from 6 to 18 months, and Loop Current eddies can follow a westerly, rather than south westerly, path across the Gulf.

V. YEAR 2 PORT AND WIND FORCED EXPERIMENTS

Great difficulty was experienced in obtaining a long term simulation with both port and wind forcing. The basic strategy was as for experiment 68 of Year 1, i.e., spin up to statistical equilibrium with port forcing only and then to add wind forcing. As in Year 1 it was found that the port-forced simulation with the lowest eddy viscosity, in this case experiment 201/17.0, could not accept wind forcing. The reason is that the range of possible eddy viscosities depends on the maximum current speed, which is increased by about 50% when winds are added. Therefor, experiment 201/13.0 was selected as the base port-forced experiment. But even in this case the addition of wind forcing gave rise to strong upwelling in the very small region between an anticyclonic eddy and the coast of Texas. This upwelling was so strong that the layer interface surfaced, thus stopping the simulation. The usual method for controlling such episodic upwelling in the hydrodynamic model is to introduce layer thickness-dependent interfacial friction, i.e., friction that varies in time and space depending on the instantaneous upper layer thickness. For example, if the e-folding time (the time to reduce velocities by half) of the friction were set at 16 years for a layer thickness of 200 m, then the e-folding time would be 1 year (still quite small) anywhere with a layer thickness of 100 m, but it would decrease to 22 days for a 50-m layer, and to only 1.5 days for a 25-m thick layer. The basic idea is that the friction should have little effect providing the layer thickness stays in its normal range, say from 100 m to 400 m, but be sufficiently strong to prevent strong upwelling events to surface. A more correct way to handle upwelling is to add thermodynamics to the model. Upwelling events can then effectively 'surface' (without the layer interface's surfacing) by entraining mass from the lower layer until the densities of the two layers become equal. Thermodynamics will be added to the model in Year 3 of this program.

Unfortunately, to perform the subject simulation, experiment 201/16.0, the interfacial friction's e-folding time had to be set to 115 days at 200 m (7 days at 100 m) to prevent surfacing, and this is sufficiently strong to modify the evolution of desired upwelling events such as the cyclonic eddies that move around the wall of the Loop Current. Experiment 201/16.0 applies monthly averaged winds from 1967, 1968, and so on, to experiment 201/13.0 after 6 years of port-forced spin up. It has an interfacial friction e-folding time that is 115 days at a layer thickness of 200 m in the far west of the basin, but this increases to an e-folding time of about 3 years for the same thickness in the eastern Gulf. Figures 35 to 39 show upper layer currents every 90 days for two Loop Current eddy shedding cycles with winds from 1968 and 1969. The

maximum currents lie between 110 and 165 cm sec^{-1}, against 95 to 110 cm sec^{-1} for the port-forced experiment 201/13.0, see Figures 26 to 29. The two, eddy-shedding cycles take about 360 and 450 days respectively and overall there is more variability than in the port only case. The anticyclonic gyre off the Texas coast is generally larger than in 201/13.0, as would be expected from the presence of a similarly positioned gyre in the wind forced case, see Figures 21 to 24. Simulated surface currents from experiment 201/16.0, sampled every 3 days for more than 10 years, have been delivered to MMS as representing the best Gulf simulation to date.

VI. LAYERED MODELS AND BOTTOM TOPOGRAPHY

Bottom topography is very important for realistic simulations of Gulf circulation. Although the NORDA/JAYCOR model has an excellent representation of bottom topography, it still suffers from the fundamental drawback of layered formulations: topography must be confined to the lowest layer at all times. A layered formulation was chosen for the ocean model because alternatives that represent shelf topography more accurately do so by increasing the vertical resolution by a factor of 5 to 10. This leads to corresponding increases in computer time and memory that make realistic simulations of Gulf circulation impractical (i.e., prohibatively expensive) using such models on even the fastest existing supercomputers.

In all of JAYCOR's two layer Gulf of Mexico simulations to date the minimum depth of the bottom topography is set at 500 m. The layer interface is initially at 200 m, and can deepen at the center of Loop Current eddies to about 450 m, so there is no danger of the interface intersecting the topography. Figure 25 shows the topography used by the 0.1 degree model. There are broad areas near the coast where the model topography has been unrealistically set to 500 m. The experiments performed to date demonstrate that topography limited to 500 m is sufficient to realistically simulate circulation in the deep water of the Gulf. For example, Loop Current eddies show evidence of topographic steering, even though there is no direct interaction between the eddy in the upper layer and the topography in the lower layer.

Continental slope and shelf areas cannot be adequately represented by existing layered models since the shelf water should be entirely from the upper layer. Apart from the obvious problems this causes for flow on the shelf, the artificial deepening of the shelf in these models has at least two possibly unrealistic effects on deep water circulation. It allows deep water phenomena, such as mesoscale eddies, to encroach on 'shallow' shelf areas, and it drastically reduces the potentially very large energy dissipation over the shelf. In particular, the Loop Current tends to encroach on the West Florida Shelf in the model (although limited encroachments have been observed in the Gulf, the present model cannot be expected to simulate them realistically), and a Loop Current eddy remnant off the Texas coast which is a semi-permanent feature of all simulations to date would almost certainly dissipate, or move further offshore, in a model that had a better representation of the shelf area.

In order to quantify how well the ocean model is performing in shelf areas a comparison has been made, by Evans Waddell at Science Applications International Corporation, between three years of hydrograhic data obtained at fixed moorings on the Florida Shelf as part of a MMS sponsored Gulf of Mexico Physical Oceanography Study (Waddell, 1986) and 1080 days of

TABLE 1

3-YEAR JAYCOR MODEL SIMULATION
& OBSERVED DATA STATISTICS
UPPER LAYER

ID	LAT	LONG	INST. DEPTH	WATER DEPTH	U-MEAN	U-MAX	U-MIN	U-VARIANCE	V-MEAN	V-MAX	V-MIN	V-VARIANCE	PRINCIPAL AXES (DEGREES TRUE)
MJX1	25:48.00	84:12.00	100	505	26.6	81.0	-19.3	758.9	-23.9	18.5	-77.9	567.3	130.0
MJC2	25:53.20	84:19.20	100	180	0.6	36.8	-27.8	53.7	-4.1	33.0	-81.8	224.6	176.0
MJX1	25:48.00	84:12.00	100	505	26.6	81.0	-19.3	758.9	-23.9	18.5	-77.9	567.3	130.0
MJE2	27:25.20	84:37.50	100	180	0.5	20.8	-26.5	18.7	-3.2	36.1	-43.5	104.8	179.0
MJZ1	26:12.00	83:00.00	100	500	3.2	37.7	-34.4	139.3	3.5	47.2	-22.0	118.4	129.0
MJF2	26:14.50	83:13.30	40	50	0.0	13.7	-29.8	6.0	-1.0	21.1	-20.1	12.3	152.0
MJY1	26:00.00	83:36.00	100	500	6.2	46.8	-41.5	235.1	-9.6	21.1	-54.1	277.7	139.0
MJA2	26:05.00	83:42.00	50	75	1.1	23.9	-14.7	27.4	-4.0	28.1	-43.4	139.4	171.0

- Instrument and water depth in meters.

- All speeds in cm s^{-1}.

- Instrument depth on model moorings = ½(200 m).

- Model data has been truncated to match observed data.

TABLE 2

3-YEAR JAYCOR MODEL SIMULATION
& OBSERVED DATA STATISTICS
LOWER LAYER

ID	LAT	LONG	INST. DEPTH	WATER DEPTH	U-MEAN	U-MAX	U-MIN	U-VARIANCE	V-MEAN	V-MAX	V-MIN	V-VARIANCE	PRINCIPAL AXES (DEGREES TRUE)
MJW2	25:24.00	85:24.00	1723	3246	-2.1	0.3	-4.5	1.3	0.4	3.1	-1.4	1.1	50.0
MJC4	25:36.03	85:29.97	1565	3200	1.0	39.9	-33.5	92.1	1.8	33.8	-24.4	86.6	129.0
MJW2	25:36.00	84:48.00	1172	2143	0.0	3.2	-3.4	2.9	-0.5	8.0	-7.2	15.9	157.0
MJW4	25:42.90	84:53.10	1100	1697	-0.6	8.5	-11.7	6.8	3.4	38.5	-33.5	78.6	173.0

- Instrument and water depth in meters.

- All speeds in cm s^{-1}.

- Instrument depth on model moorings = 200 + ½(lower layer depth).

- Model data has been truncated to match observed data.

simulated current meter data at approximately the same locations from the 0.1 degree port-forced experiment 201/13.0. Figure 40 shows the locations of the moorings; moving eastward from deep to shallow water the simulated data sets V, W, X, Y, Z correspond to moorings G, A, C, D (DA), F, respectively. Since the ocean model is a simulation, rather than a prediction, it is not possible to make a day by day comparison of the data sets. However, a realistic simulation should behave similarly to the actual Gulf and, therefore, it is appropriate to compare various statistics from the observations and the simulation. The major limitations of the comparison are that the ocean model does not have wind forcing, and the observational data covers less than two eddy cycles with gaps due to instrument failures. Another possible limitation of comparisons at a small number of locations is that relatively minor errors in the position of a simulated circulation feature might lead to large differences from the observations; however, that does not appear to be the case in this instance.

Table 1 summarizes the statistics at the three moorings (C, DA, F) and three simulated locations (X, Y, Z) on the shelf, and at mooring E which is north of mooring C. In all cases the currents are significantly stronger in the simulation than in the observations. Figures 41 and 42 are a comparison of observed and simulated kinetic energy spectra at moorings C and F, but note that the use of a linear rather than the more usual logarithmic scale for variance tends to magnify the differences between the data sets. The simulation at C, M0X1, has a very strong signal at a period of about 400 days and very little energy at periods less than 30 days. A port-driven experiment should not have much energy at short time scales, since wind forcing is dominant at these scales. But the energy variance peak indicates that the Loop Current, with an eddy shedding cycle of about 400 days, acts directly at M0X1. The observations at C, M0C2, have a comparatively level spectra with a minor peak at about 85 days and with energy at periods down to 5 days. The Loop Current clearly does not reach location C in the Gulf, the minor peak in the spectra might, however, be due to the passage of filaments that are often observed on the wall of the Loop Current. The simulation at F, M0Z1, is far too energetic and still shows a strong influence from the Loop Current. In fact, M0Z1 is a better fit than M0X1 to M0C2 on the shelf edge. Data from the corresponding observational location, M0F1, produce a very flat spectrum and very little energy variance, as is expected in water that is only 50 m deep. Overall the ocean model exhibits a very strong Loop Current effect over the shelf area, an effect that is not present in the observations.

Table 2 summarizes the statistics at the two moorings (G, A) in deeper water and at the cooresponding simulated locations (V, W). Only deep currents are included, this is

unfortunate since the ocean model would probably show good agreement with the observations at about 100 m depth. The simulated deep currents are significantly weaker than those observed in the Gulf, particularly at mooring G which is in 3,000 m of water directly in the path of the Loop Current. The deep currents for experiment 201/17.0 are quite similar to those for 201/13.0, and Figures 29 to 34 indicate that the simulated currents are probably stronger between V and W than they are at these locations, and that the strongest simulated deep currents under the Loop Current are further south. However, even if it is assumed that the ocean model is producing the same deep water circulation features as those observed, but with a shift to the south, there would still be a factor of 2 to 3 difference in current speed ranges. The simulated deep currents are very sensitive to the amount of deep transport through the Yucatan Strait, but there is little data available on the vertical distribution of flow through the Strait. Many of the initial simulations of the Gulf had only 4 Sv inflow in the deep water, more recent simulations use 10 Sv. The data at moorings G and A suggest that an even larger deep transport might be appropriate. One of the main reasons for locating moorings at G and A, in deep water, was the need for data that could be used to tune the ocean model's deep flow characteristics. This is a good example of cooperation between the physical oceanography and ocean modeling programs at MMS. Simulations in Year 3 of the modeling program may use a larger deep inflow transport, however surface currents are more important that deep flow so these simulations will only be delivered to MMS if they give rise to more realistic upper layer currents.

In Year 3 of the modeling study, now in progress, an effort will be made to develop an efficient layered ocean model that will allow layer interfaces to effectively intersect the bottom topograhy. It is likely that more than one workable solution to this problem can be found if computer cost is not taken into account. In fact, the major difficulty will be in finding a practical solution that does not impose too high an overhead for its use. When intersection occurs in a coventional layer model the layer thickness becomes negative which is clearly unphysical, leading to unrealistic results and, if the situation persists, catastrophic failure of the run due to undamped instabilities. The obvious solution of setting a minimum layer thickness at or about zero does not work because, (a) it leads to loss of mass, and (b) clamping the layer thickness induces dispersive ripples in the interface at the intersection point (i.e., we have an unresolved boundary layer). One promising approach to the layer intersection problem is to insure positive layer thicknesses via 'Flux Corrected Transport', a technique that was originally developed for fluid problems with shocks (Book et. al., 1981). In this method the continuity equation is solved for layer thickness using two different sets of transports, one obtained via a low

order (highly dispersive) scheme guaranteed to give monotonic results and the other via a standard (ripple prone) high order scheme. The low order scheme used alone would prevent layer intersection, but it very rapidly damps out circulation features and therefore would not produce realistic simulations. Instead, the final layer thickness at each point is a linear combination of the two solutions, chosen to be as close as possible to the high order solution. Away from areas of layer intersection the high order scheme will dominate, but near intersections just sufficient contribution from the low order scheme will be used to ensure overall positivity. In other words, bottom topography is still confined to the lowest layer, but that layer can get very thin so there is effectively no contribution from the deep layer over the shelf and no limit on how shallow the bottom topography can be. This method has been used with some success for interfaces that intersect the surface (Bleck et. al., 1983), but is usually implemented in fully explicit models. Explicit free surface ocean models are not used for long term simulations because they require very short time-steps. To be practical, therefore, flux-corrected transport must be modified to work with the present semi-implicit time stepping scheme, or perhaps a split-explicit version of the model must be developed.

In order to demonstate the viability of using flux-corrected transport for layer intersection problems, a two dimensional explicit version of the ocean model for flux-corrected transport was developed by JAYCOR for NORDA in the summer of 1985. The goal of the project was to run a numerical experiment that is simple to describe but very difficult to perform with any kind of conventional ocean model. Two basins are separated by a sloping wall, i.e. a seamount, and at time zero the first basin is partially full of water with the second empty. As the experiment progresses more water is added to the first basin until it overflows the seamount and the second basin starts to fill with water, eventually both basins are full of water. Conventional layered ocean models cannot even simulate the first stage of the experiment, which requires the air-sea layer interface to intersect the sloping seamont topography. No conventional ocean model can simulate the second stage of the experiment, in which the second basin fills with water. In order to run the simulation in a reasonable amount of time, the experiment was performed in a parameter space quite different from a typical ocean basin. For example, the water was only 100 m deep with a very gently sloping seamount. Moreover, the simulation only indicates that the method can allow layer interfaces to intersect topography to be practical flux-corrected transport must be extended to allow longer timesteps than those use in explicit models.

Figures 43 to 51 show layer depth every 6 hours for the full 2 days of the experiment described above. At time zero the air-sea interface is defined across the entire region, but

the layer is very thin in the second basin. Water is added slowly at the center of the first basin and the water level rises. At 12 hours (Figure 45) the level is about 15 m above the top of the seamount, and water has started to run down its opposite side into the second basin. At later times the level in the first basin continues to rise because the water is being added more quickly than is allowed to run into the second basin, but the pressure head directly above the seamount continues to be about 15 m. At 42 hours (Figure 50) the water level in both basins is above the seamounts, but there is still a notch in the air-sea interface above the seamount. In Figure 51 the levels in the two basins are almost equal. The reason for the fairly large pressure head above the seamount and the slowness of the flow into the second basin is that flux corrected transport requires that velocities in a layer tend to zero as the layer thickness goes to zero. This is achieved by using layer thickness dependent bottom friction that goes to infinity as the layer thickness tends to zero. In practice this means that thin layers become thicker only slowly; however, this happens quickly enough for layer interface to move up (and down) the topography in the first layer at a reasonable rate. The notch seen in the interface is Figure 50 is an artifact of the flux corrected transport method, it illustrates that the method may not produce realistic results near the point at which the interface intersects topography. This will almost certainly be true for any method that allows layers to intersect topography. In the Gulf of Mexico, therefore, velocities will be questionable at the shelf break (particularly in the lowest layer) but realistic over the shelf and over deep water.

VII. REFERENCES

1. Bleck, R.C., Rooth, D.B., Boudra 1983. "Wind-Driven Spinup in Eddy-Resolving Ocean Models Formulated in Isopycnic and Isobaric Coordinates". Rosenstiel School of Marine and Atmos. Sci., U of Miami, Florida.

2. Book, D.L., J.P. Boris, S.T. Zalesak 1981: "Flux-Corrected Transport" in D.L. Book (ed), Finite Difference Techniques for Vectorized Fluid Dynamics Calculations, Springer-Verlag.

3 Brooks, I.H. 1979. Fluctuations in the Transport of the Florida Current at Periods Between Tidal and Two Weeks. J. Phys. Oceanogr. 9:1048-1053.

4. Elliott, B.A. 1979. Anticyclonic Rings and the Energetics of the Circulation in the Gulf of Mexico. Ph.D. Dissertation, Texas A&M University, 188 p.

5. Hellerman, A. 1967. An Updated Estimate of the Wind Stress of the World Ocean. Mon. Wed. Rev. 95:607-628.

6. Hurlburt, H.E. and Thompson, J.D. 1980. A Numerical Study of Loop Current Intrusions and Eddy Shedding. J. Phys. Oceanogr. 10:1611-1651.

7. Leipper, D.F. 1970. A Sequence of Current Patterns in the Gulf of Mexico. J. Geophys. Res. 75:637-657.

8. Marsh, J.G., Cheney, R.E., McCarthy, J.J. and T.V. Martin. 1984. Regional Mean Sea Surfaces Based on GEOS-3 and SEASAT Altimeter Data. Marine Geodesy 8:385-402.

9. Maul, G.A. and Herman, A. 1984. Mean Dynamic Topography of the Gulf of Mexico with Application to Satellite Altimetry. Marine Geodesy (to appear).

10. Merrell, W.J. and Morrison, J.M. 1981. On the Circulation of the Western Gulf of Mexico, with Observations from April 1978. J. Geophys. Res. 86:4181-4185.

11. Niiler, P.P. and Richardson, W.S. 1973. Seasonal Variability of the Florida Current. J. Mar. Res. 31:144-167.

12. Rhodes, R.C., Thompson, J.D. and Wallcraft, A.J. 1986. The Navy Corrected Geostrophic Wind Data Set for the Gulf of Mexico. NORDA tech. rep. (to appear).

REFERENCES (Cont.)

13. Schott, F.A. and Zantopp, R.J. 1985. On the Seasonal and Interannual Variability of the Florida Current. Science 227:308-311.

14. Sturges, W. and Blaha, J.P. 1976. A Western Boundary Current in the Gulf of Mexico. Science 192:367-369.

15. Thompson, J.D. 1986. Altimeter Data and Geoid Error in Mesoscale Ocean Prediction: Some Results from a Primitive Equation Model. J. Geophys. Res. 91:2401-2417.

16. Wyckhouse, R.J. 1973. Synthetic Bathymetric Profiling System (SYNBAPS). Naval Oceangraphic Office Tech. Rep. TR-233.

17. Vukovitch, F.M. and Maul, G.A. 1984. Cyclonic Eddies in the Eastern Gulf of Mexico. J. Phys. Oceanogr. (in press).

18. Waddell, E. 1986. Gulf of Mexico Physical Oceanography Program Final Report: Years 1 and 2. (Final Report in two volumes by SAIC submitted to Minerals Management Service, Metairie, LA. Contract No. 14-12-0001-29158).

19. Wallcraft, A.J. 1985. Gulf of Mexico Circulation Modeling Study Annual Progress Report: Year 1. (Progress report by JAYCOR submitted to Minerals Management Service, Metairie, LA. Contract No. 14-12-0001-30073).

FIGURES

FIGURE 1: (a) Instantaneous view of the interface deviation in a two-layer simulation of the Gulf of Mexico driven from rest to statistical equilibrium solely by inflow through the Yucatan Straits (Experiment 9). The contour interval is 25 m, with solid contours representing downward deviations. (b) Depth of the 22 degree isothermal surface, 4-18 August 1966 (Alaminos cruise 66-A-11), from Leipper (1970). The contour interval is 25 m.

FIGURE 1

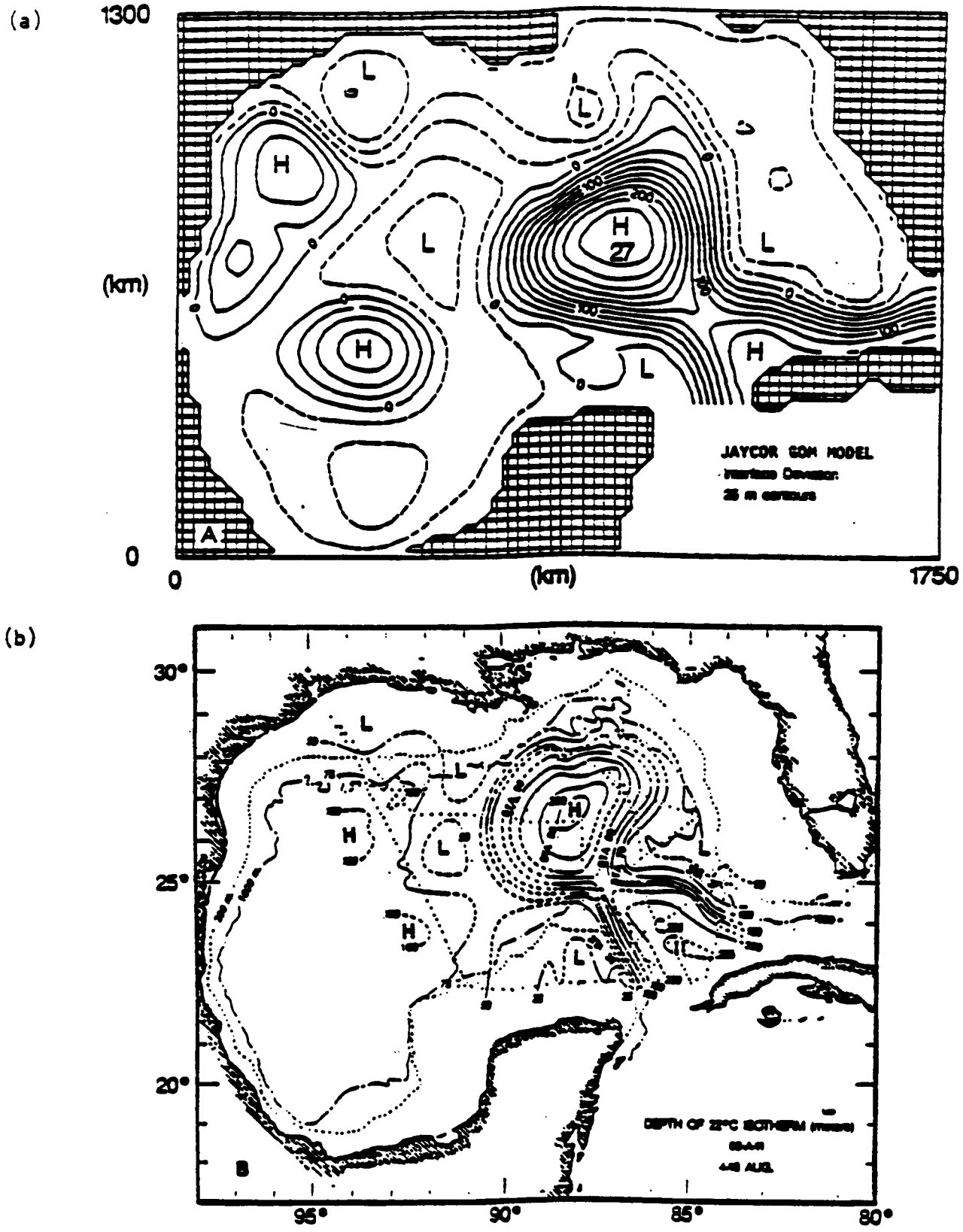
(a)
1300
(km)
0
0
(km)
1750
L
H
27
JAYCOR EOM MODEL
A
(b)
30°
25°
20°
95°
90°
85°
80°
B

FIGURE 2: (a) Interface deviation from the Gulf of Mexico simulation at model day 1970 after an eddy has separated from the Loop Current and propagated westward. (b) Ninety days later the major anticyclonic eddy has developed into a counter-rotating vortex pair in the western Gulf. The cyclonic vortex is to the north and the anticyclonic to the south.

FIGURE 2

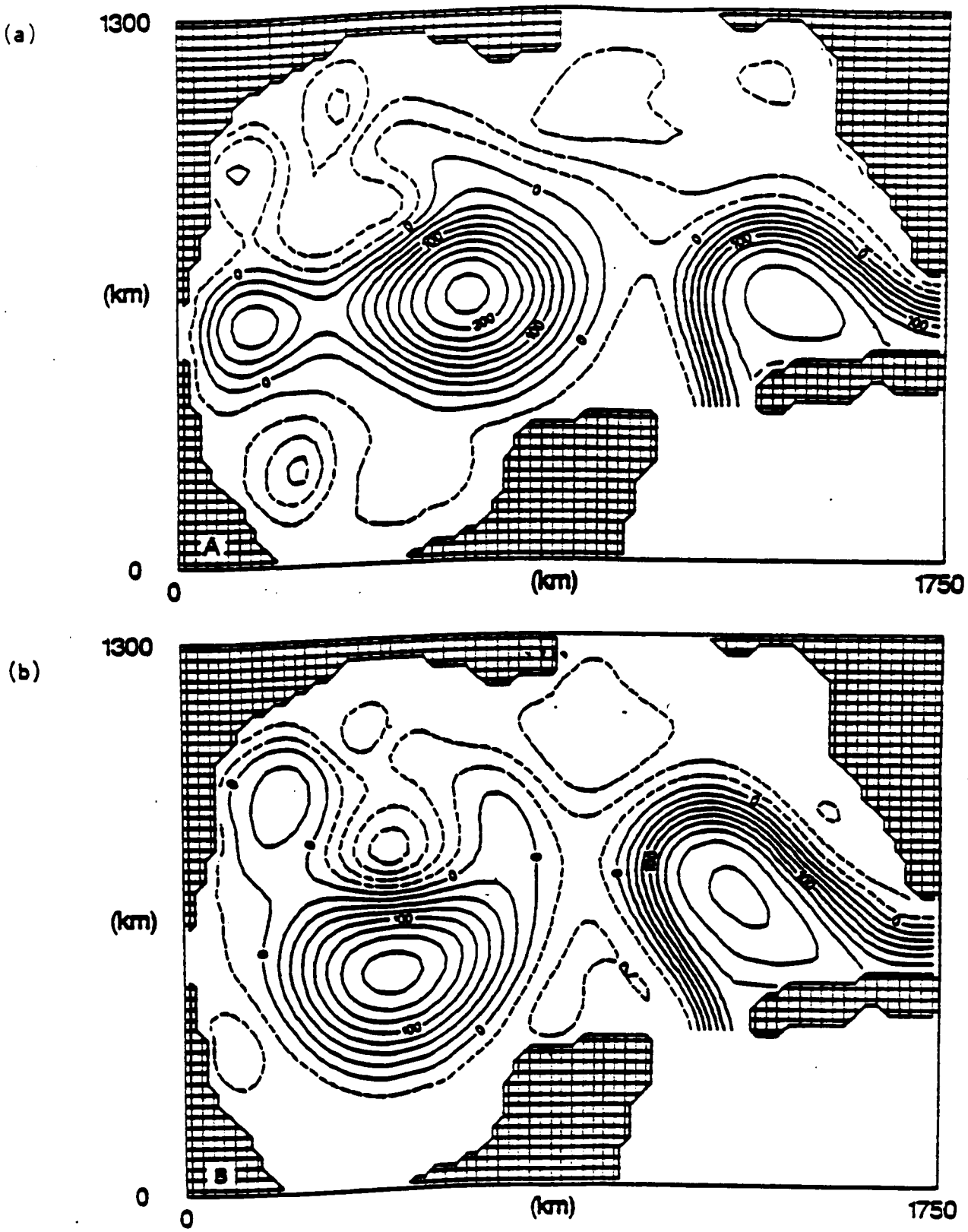

FIGURE 3: Counter-rotating vortex pair in the western Gulf of Mexico as shown by the depth of the 15 degree isotherm (in meters), observed in April 1978. The cyclonic vortex is to the north and the anticyclonic to the south (from Merrell and Morrison, 1981).

FIGURE 3

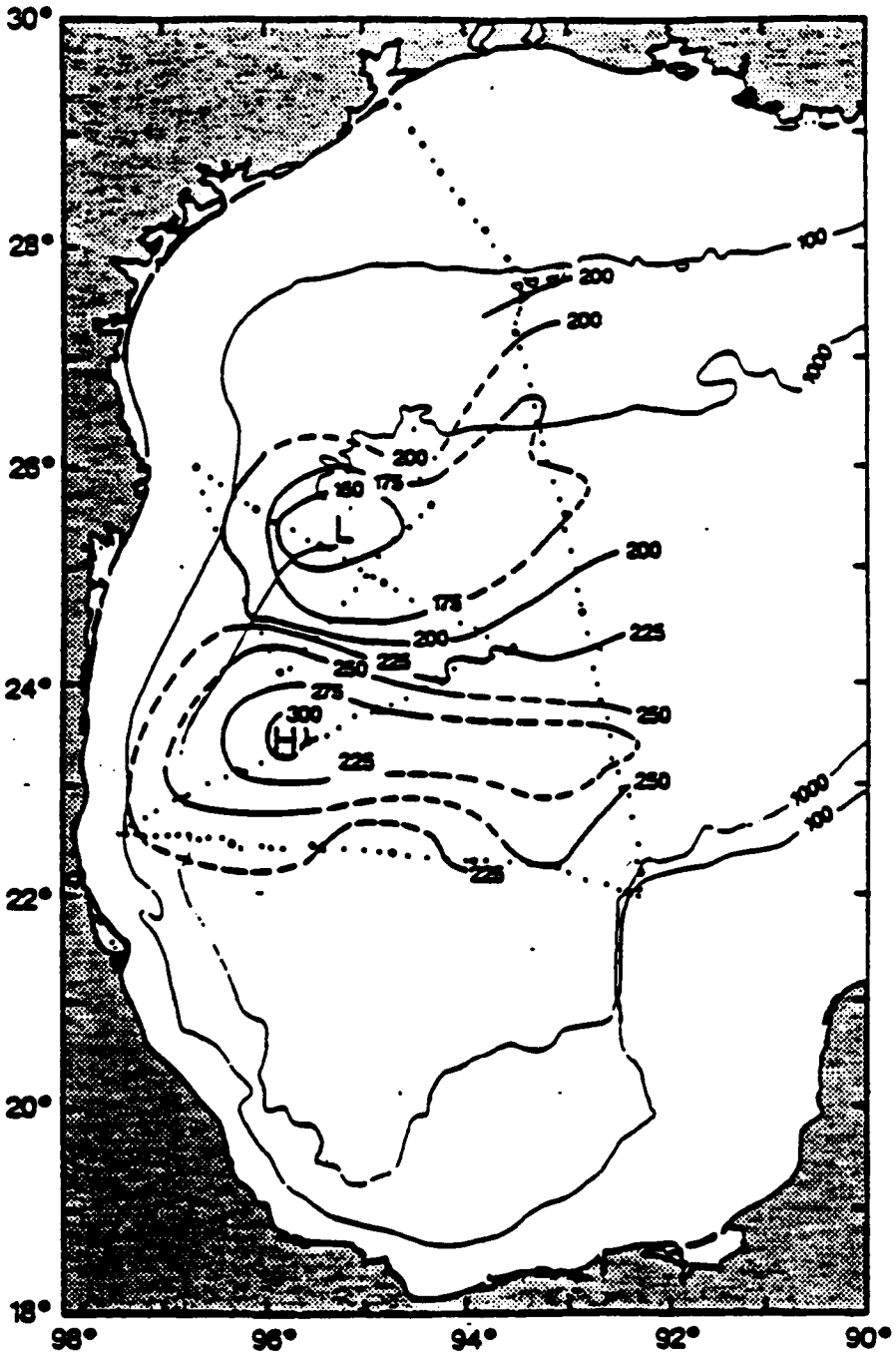
30°
28°
26°
24°
22°
20°
18°
98°
96°
94°
92°
90°
100
200
200
1000
200
175
150
L
200
175
200
225
225
250
275
300
H
225
250
1000
100
225

FIGURE 4: Sea surface height variability for the Gulf of Mexico. (a) Based on about 16,000 GEOS-3 and SEASAT cross-overs, spanning nearly four years (from Marsh et. al., 1984). (b) Based on an ocean model simulation with port forcing only (Experiment 40), measured over three eddy cycles at statistical equilibrium with the free surface sampled every ten days for a total of over 300,000 "observations".

FIGURE 5: Sea surface height (a) variability and (b) mean, for the Gulf of Mexico. Based on all available hydrographic, STD and XBT data at over 16,000 stations, with substantial filtering (from Maul and Herman, 1984).

FIGURE 6: Mean sea surface height for the Gulf of Mexico. Based on an ocean model simulation with port forcing only (Experiment 40), measured over three eddy cycles at statistical equilibrium. The contour interval is 5 cm.

FIGURE 4

SEA SURFACE VARIABILITY FROM GEOS-3 AND SEASAT CROSS OVERS (CM)

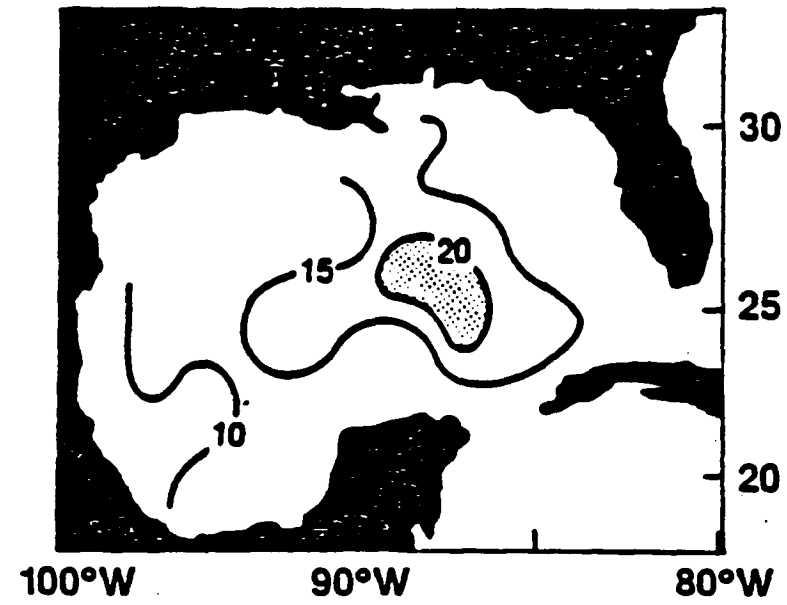

SEA SURFACE VARIABILITY (CM) FROM NORDA MODEL

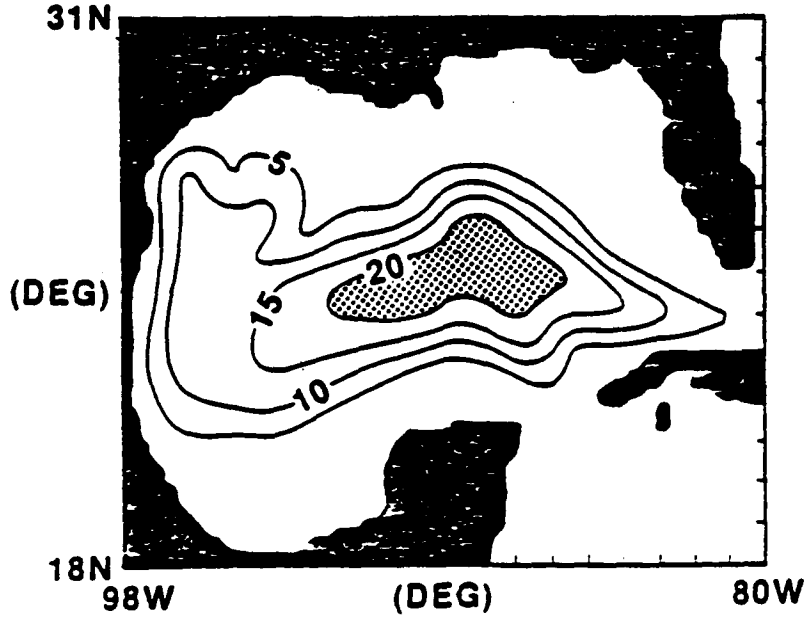

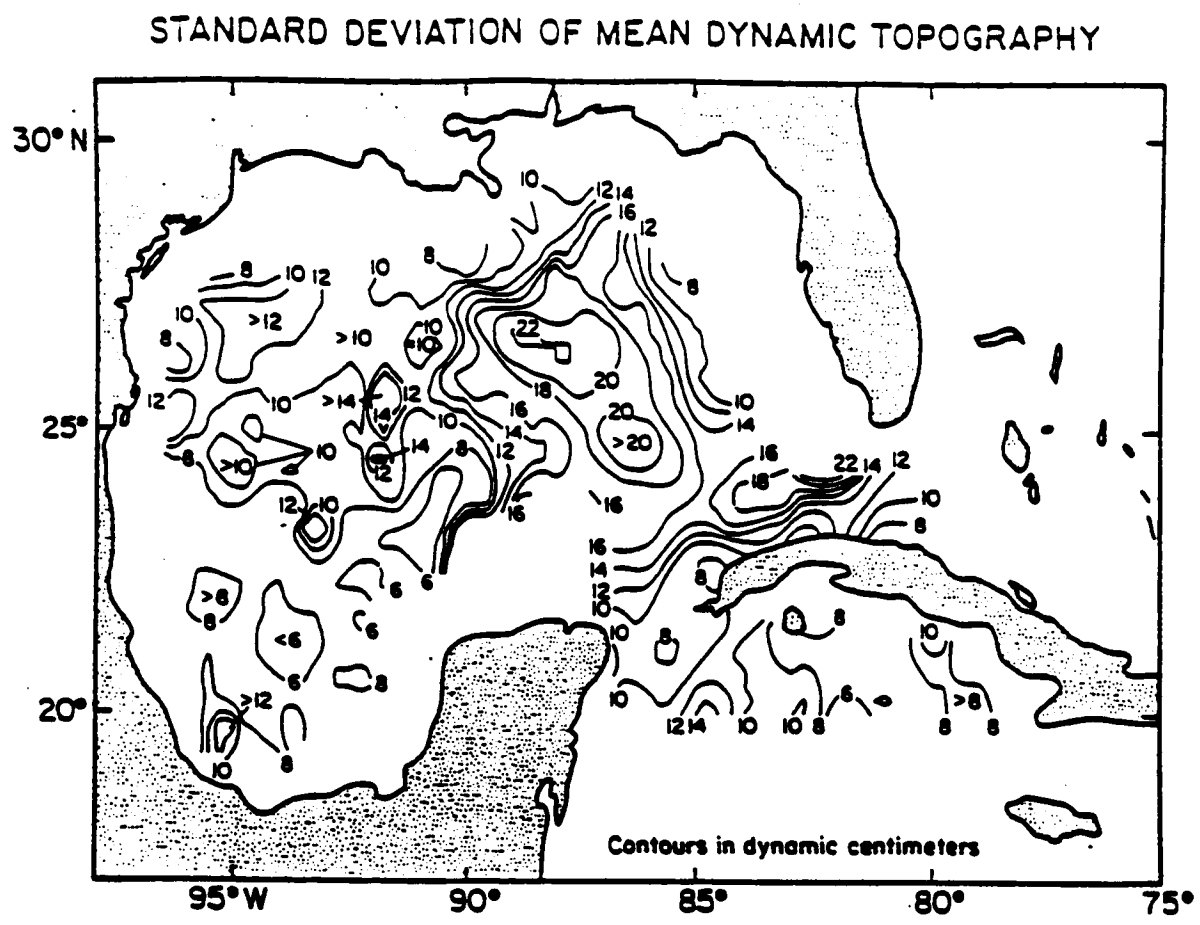
STANDARD DEVIATION OF MEAN DYNAMIC TOPOGRAPHY
30° N
25°
20°
95° W
90°
85°
80°
75°
Contours in dynamic centimeters

FIGURE 5

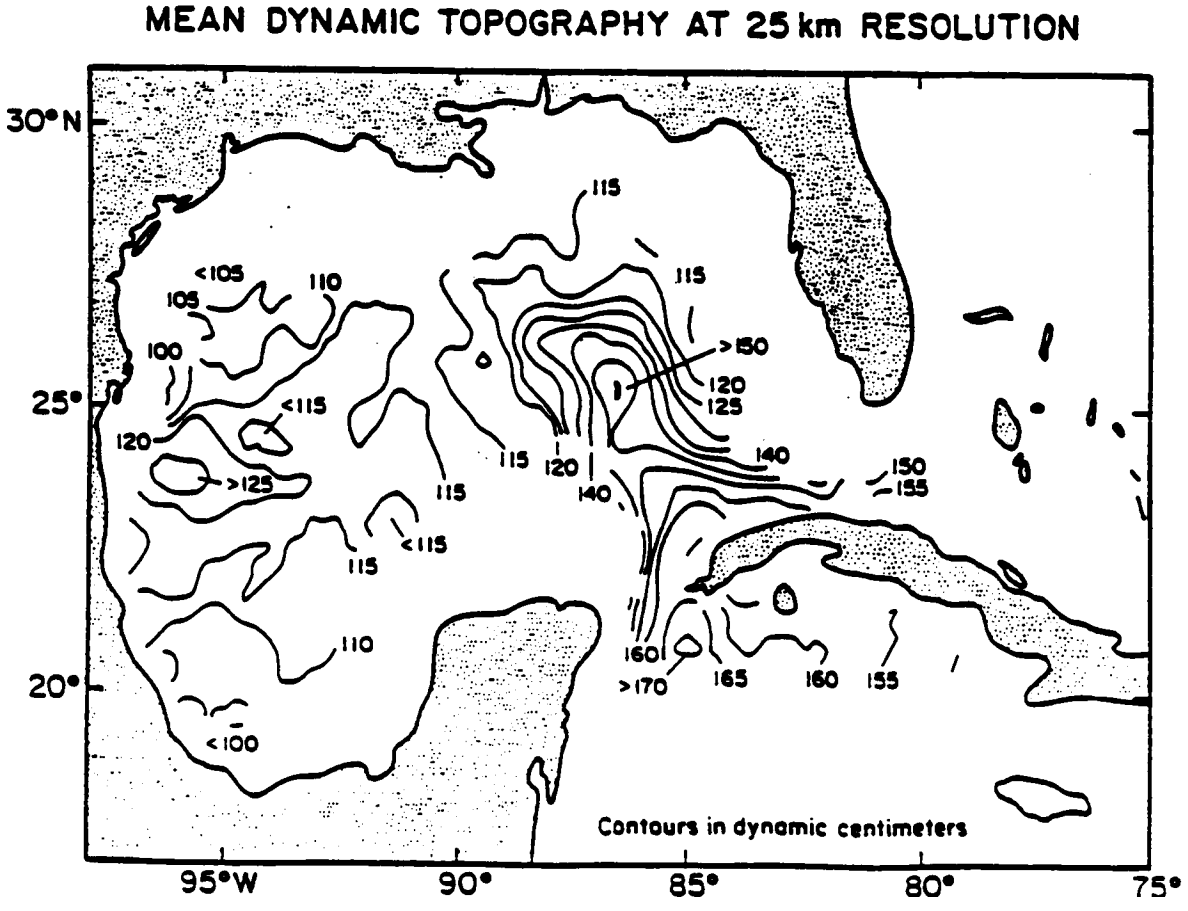
MEAN DYNAMIC TOPOGRAPHY AT 25 km RESOLUTION
30° N
25°
20°
95° W
90°
85°
80°
75°
Contours in dynamic centimeters

FIGURE 6

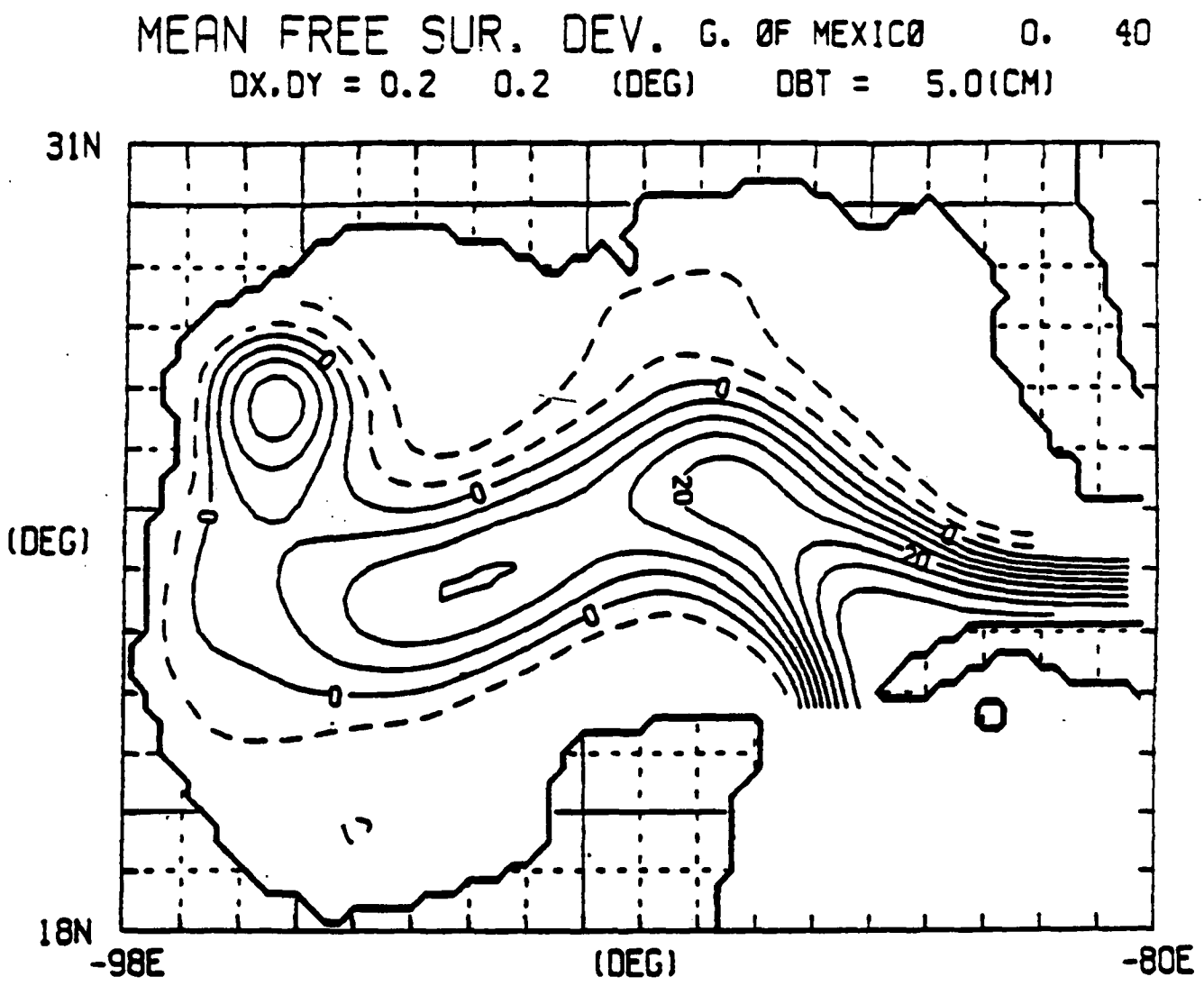
MEAN FREE SUR. DEV. G. ØF MEXICØ 0. 40
DX.DY = 0.2 0.2 (DEG) DBT = 5.0(CM)
31N
(DEG)
18N
-98E
(DEG)
-80E
0
20

FIGURE 7: Instantaneous view of upper layer averaged velocities from Experiment 68 on model day 3918. Vectors are only plotted at every second model grid point, i.e., every 0.4 degrees.

FIGURE 8: Instantaneous view of upper layer averaged velocities from Experiment 68 on model day 4038. Vectors are only plotted at every second model grid point, i.e., every 0.4 degrees.

FIGURE 9: Instantaneous view of upper layer averaged velocities from Experiment 68 on model day 4158. Vectors are only plotted at every second model grid point, i.e., every 0.4 degrees.

FIGURE 10: Instantaneous view of upper layer averaged velocities from Experiment 68 on model day 4218. Vectors are only plotted at every second model grid point, i.e., every 0.4 degrees.

FIGURE 7

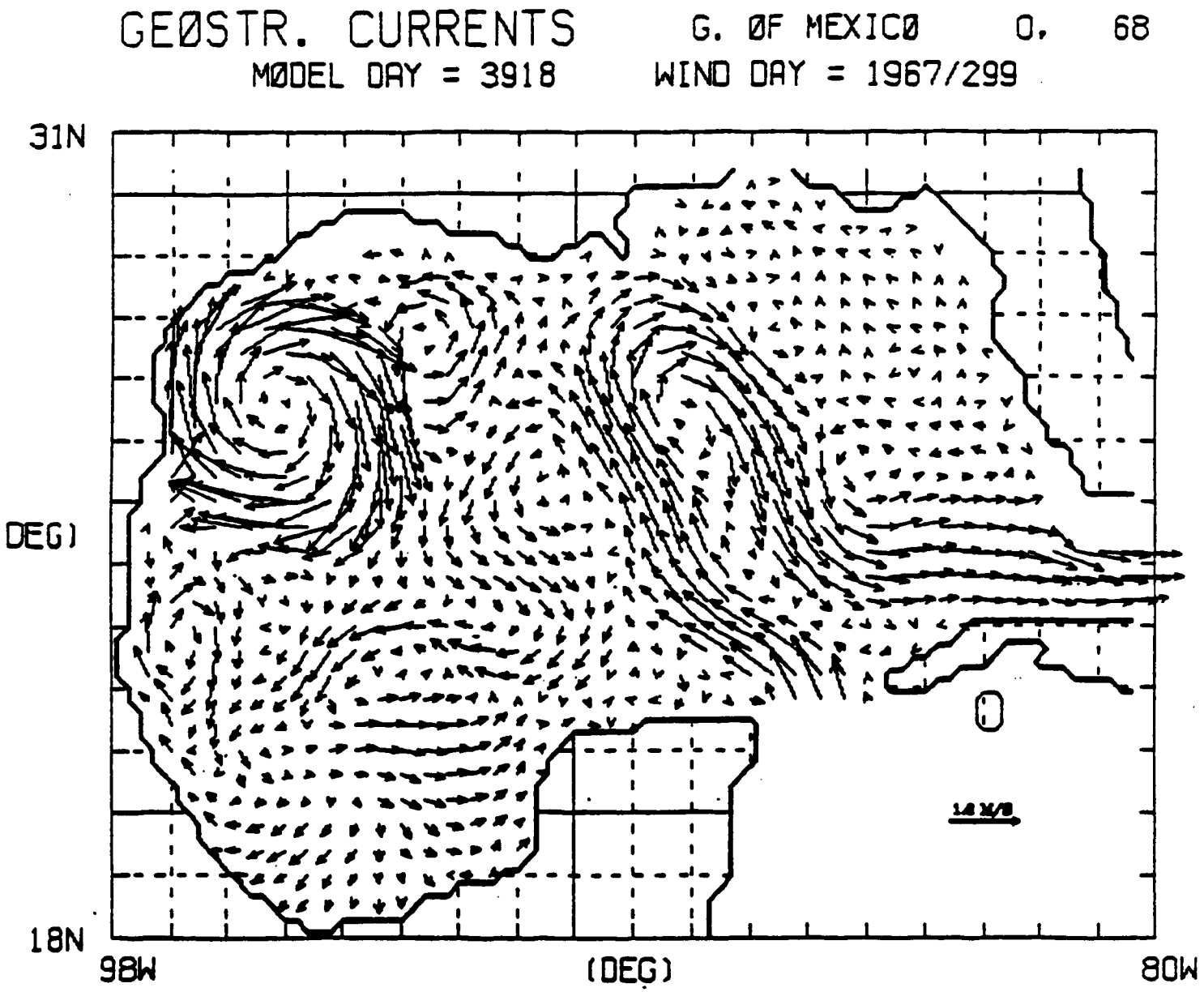
GEØSTR. CURRENTS
G. ØF MEXICØ
0. 68
MØDEL DAY = 3918
WIND DAY = 1967/299
31N
DEG)
18N
98W
(DEG)
80W
MAX PLØTED VECTØR = 1.29 (M/SEC)

FIGURE 8

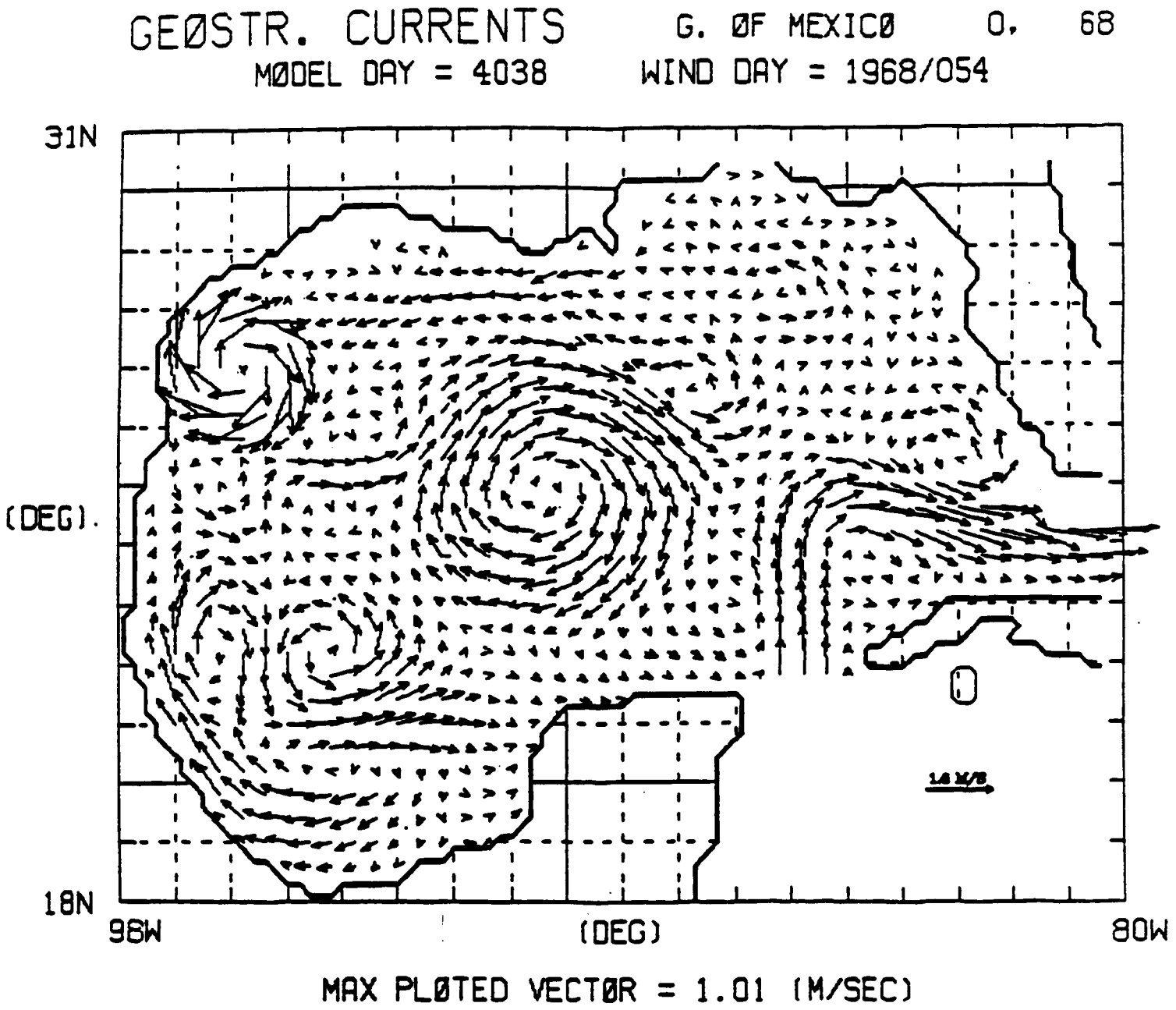
GEØSTR. CURRENTS
G. ØF MEXICØ
0. 68
MØDEL DAY = 4038
WIND DAY = 1968/054
31N
(DEG).
18N
98W
(DEG)
80W
MAX PLØTED VECTØR = 1.01 (M/SEC)

FIGURE 9

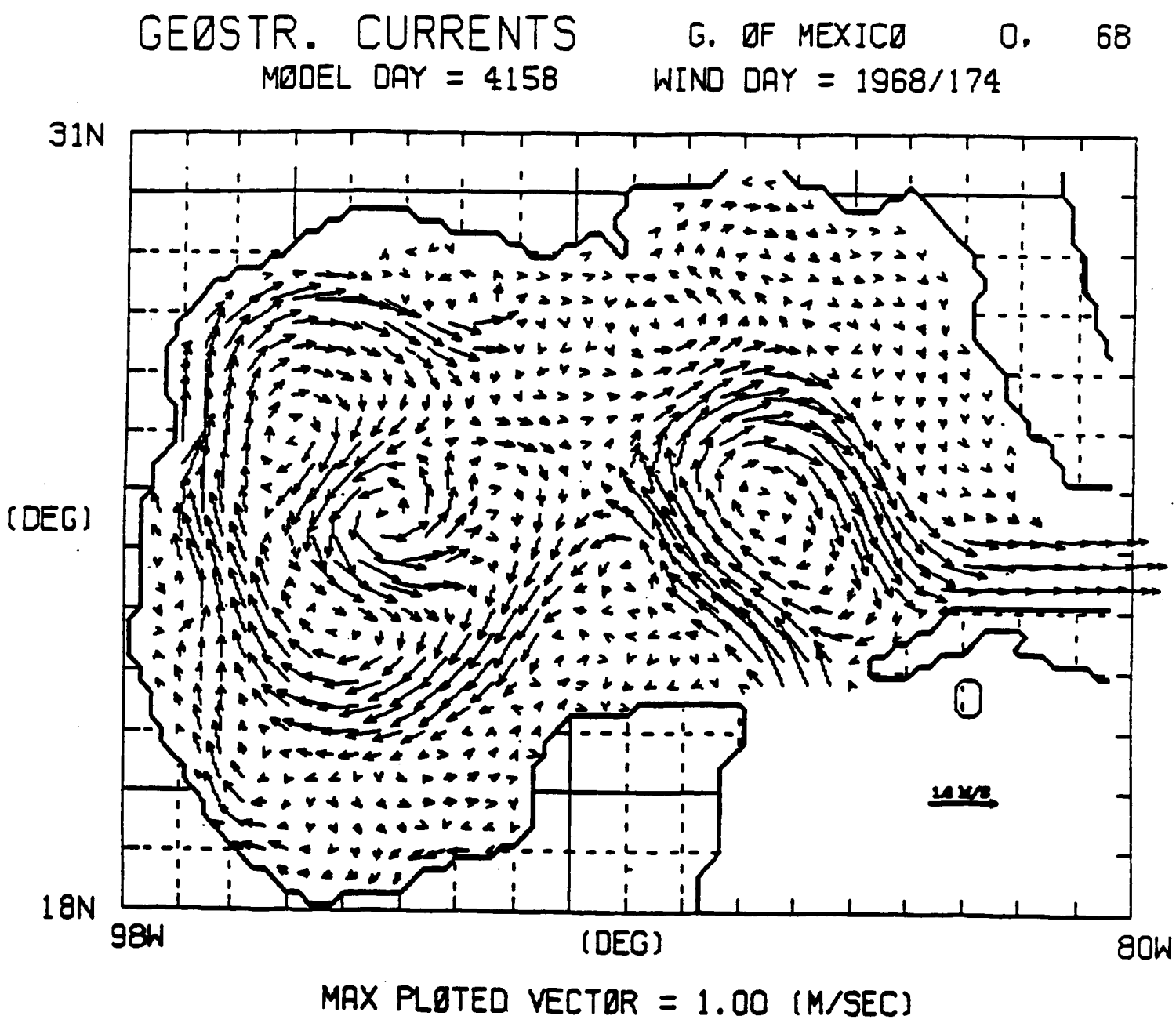
GEØSTR. CURRENTS
G. ØF MEXICØ
0. 68
MØDEL DAY = 4158
WIND DAY = 1968/174
31N
(DEG)
18N
98W
(DEG)
80W
MAX PLØTED VECTØR = 1.00 (M/SEC)

FIGURE 10

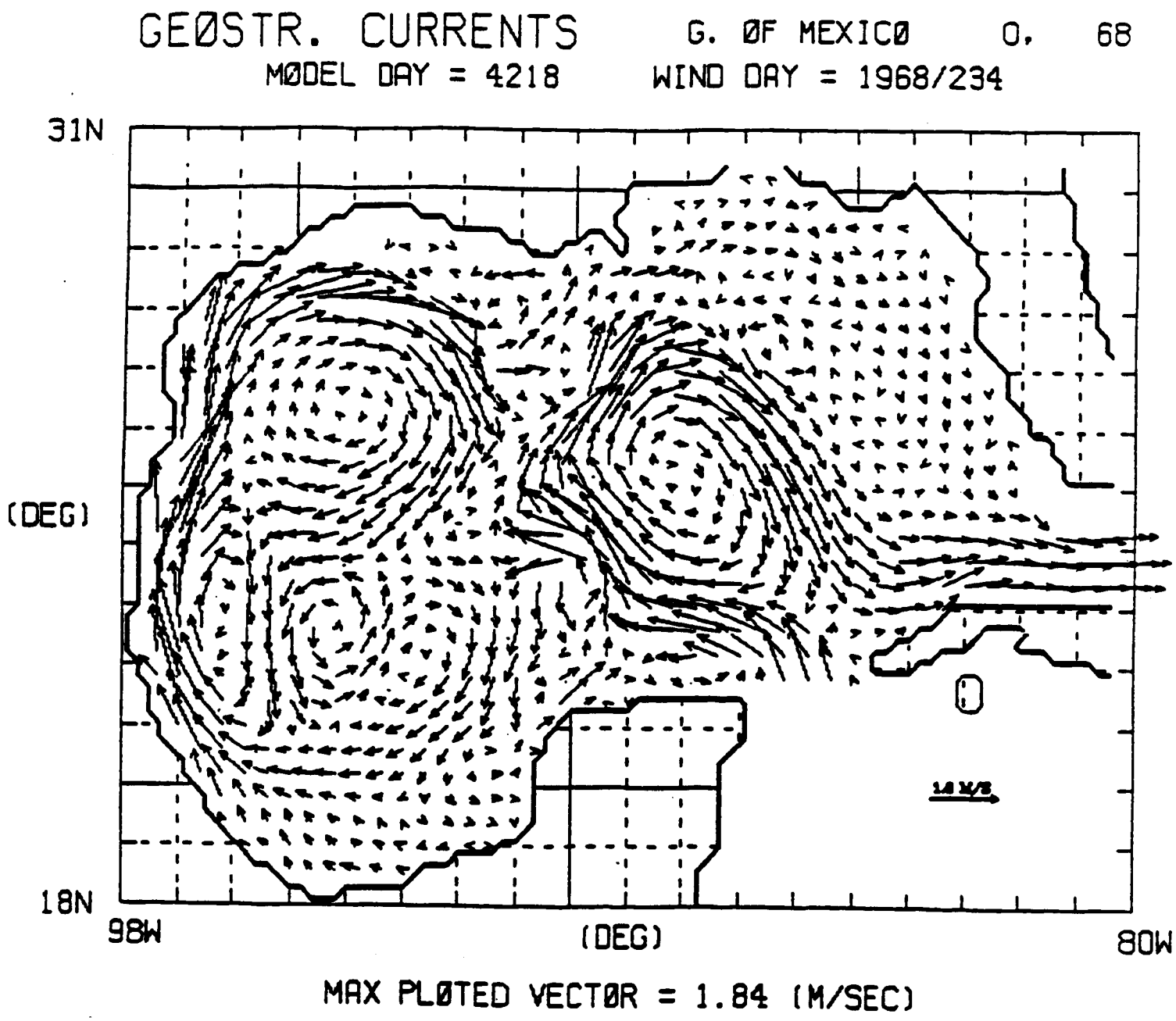

MAX PLØTED VECTØR = 1.84 (M/SEC)

FIGURE 11: Seasonal climatology for winter (Dec., Jan., Feb.) from ship observations (Elliott, 1979) and from the Navy Corrected Geostrophic Wind data set (1967-1982): (a) wind stress 1967-1982, (b) wind stress curl 1967-1982, (c) ship wind stress, and (d) ship wind stress curl.

FIGURE 12: Seasonal climatology for spring (March, April, May) from ship observations (Elliott, 1979) and from the Navy Corrected Geostrophic Wind data set (1967-1982): (a) wind stress 1967-1982, (b) wind stress curl 1967-1982, (c) ship wind stress, and (d) ship wind stress curl.

FIGURE 13: Seasonal climatology for summer (June, July, Aug.) from ship observations (Elliott, 1979) and from the Navy Corrected Geostrophic Wind data set (1967-1982): (a) wind stress 1967-1982, (b) wind stress curl 1967-1982, (c) ship wind stress, and (d) ship wind stress curl.

FIGURE 14: Seasonal climatology for fall (Sept., Oct., Nov.) from ship observations (Elliott, 1979) and from the Navy Corrected Geostrophic Wind data set (1967-1982): (a) wind stress 1967-1982, (b) wind stress curl 1967-1982, (c) ship wind stress, and (d) ship wind stress curl.

FIGURE 11

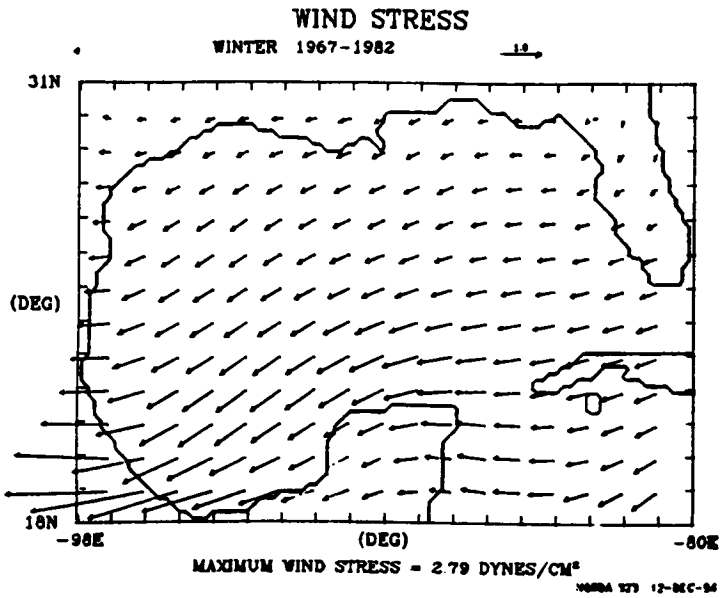
WIND STRESS
WINTER 1967-1982
31N
(DEG)
18N
-98E
(DEG)
-80E
MAXIMUM WIND STRESS = 2.79 DYNES/CM²

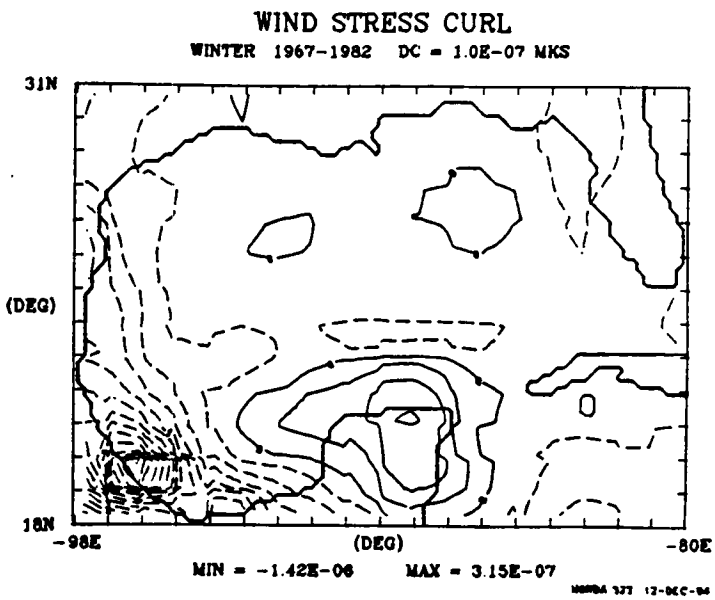
WIND STRESS CURL
WINTER 1967-1982 DC = 1.0E-07 MKS
31N
(DEG)
18N
-98E
(DEG)
-80E
MIN = -1.42E-06 MAX = 3.15E-07

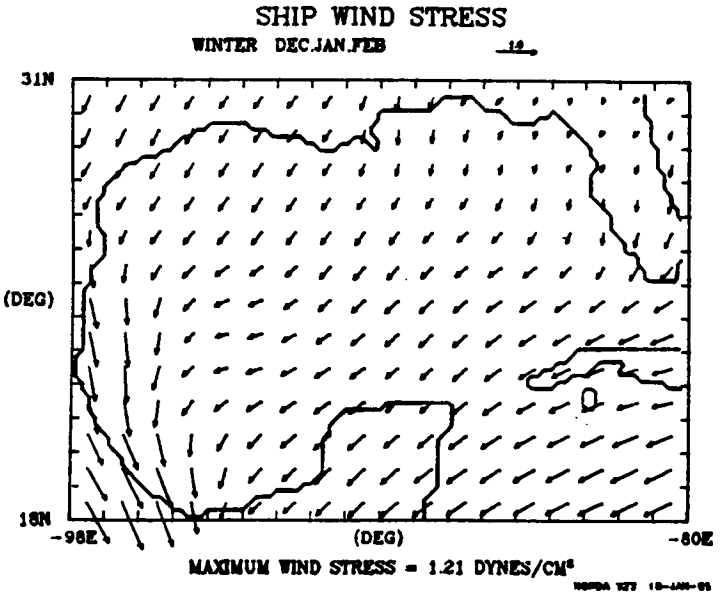
SHIP WIND STRESS
WINTER DEC.JAN.FEB
31N
(DEG)
18N
-98E
(DEG)
-80E
MAXIMUM WIND STRESS = 1.21 DYNES/CM²

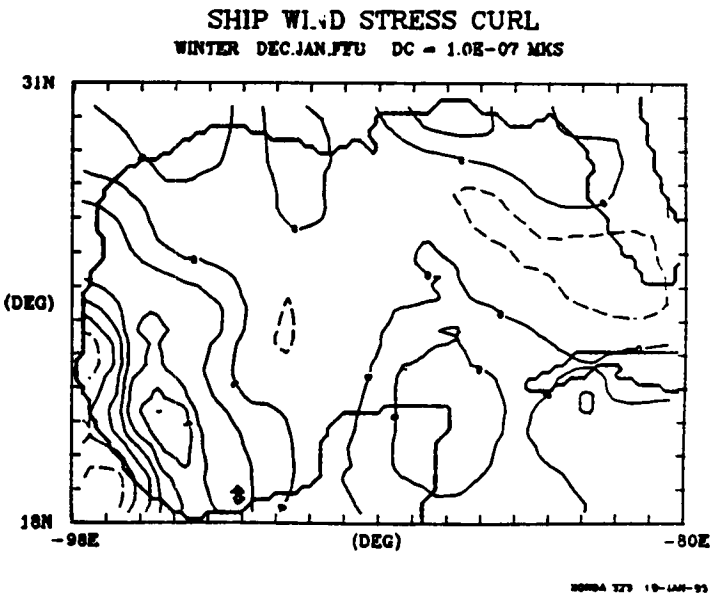
SHIP WIND STRESS CURL
WINTER DEC.JAN.FEB DC = 1.0E-07 MKS
31N
(DEG)
18N
-98E
(DEG)
-80E

FIGURE 12

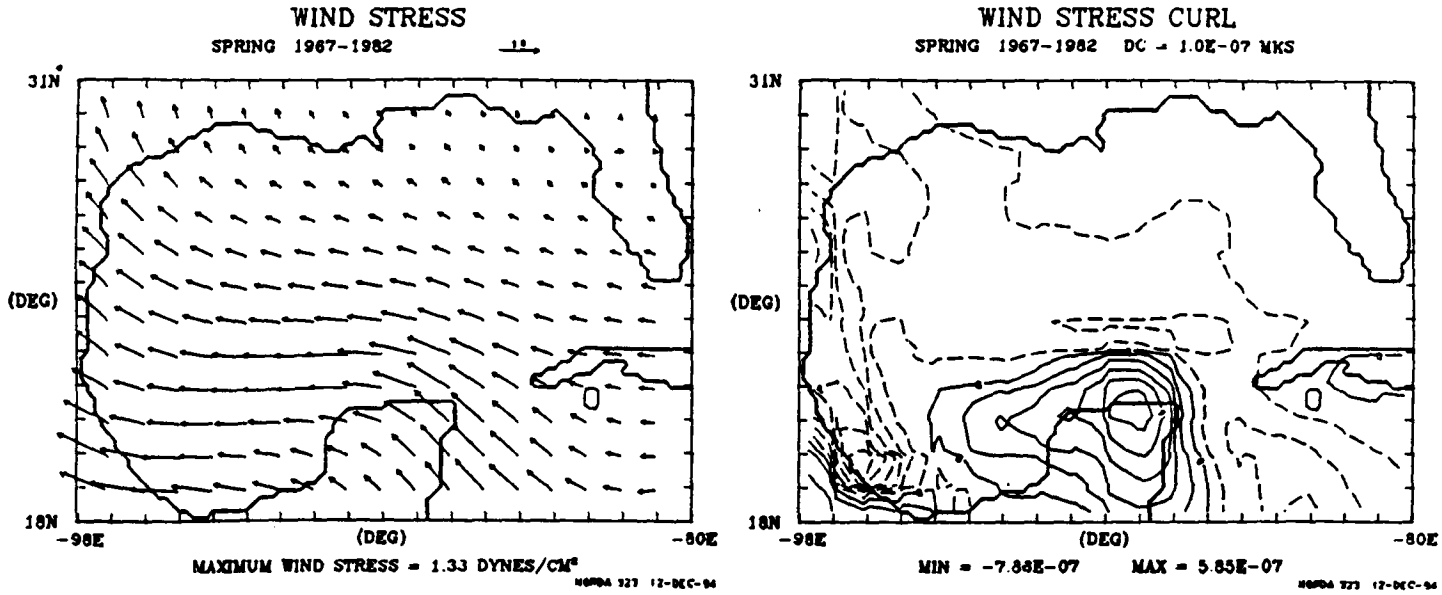
WIND STRESS
SPRING 1967-1982
31N
(DEG)
18N
-98E
(DEG)
-80E
MAXIMUM WIND STRESS = 1.33 DYNES/CM²
WIND STRESS CURL
SPRING 1967-1982 DC = 1.0E-07 MKS
31N
(DEG)
18N
-98E
(DEG)
-80E
MIN = -7.86E-07 MAX = 5.85E-07

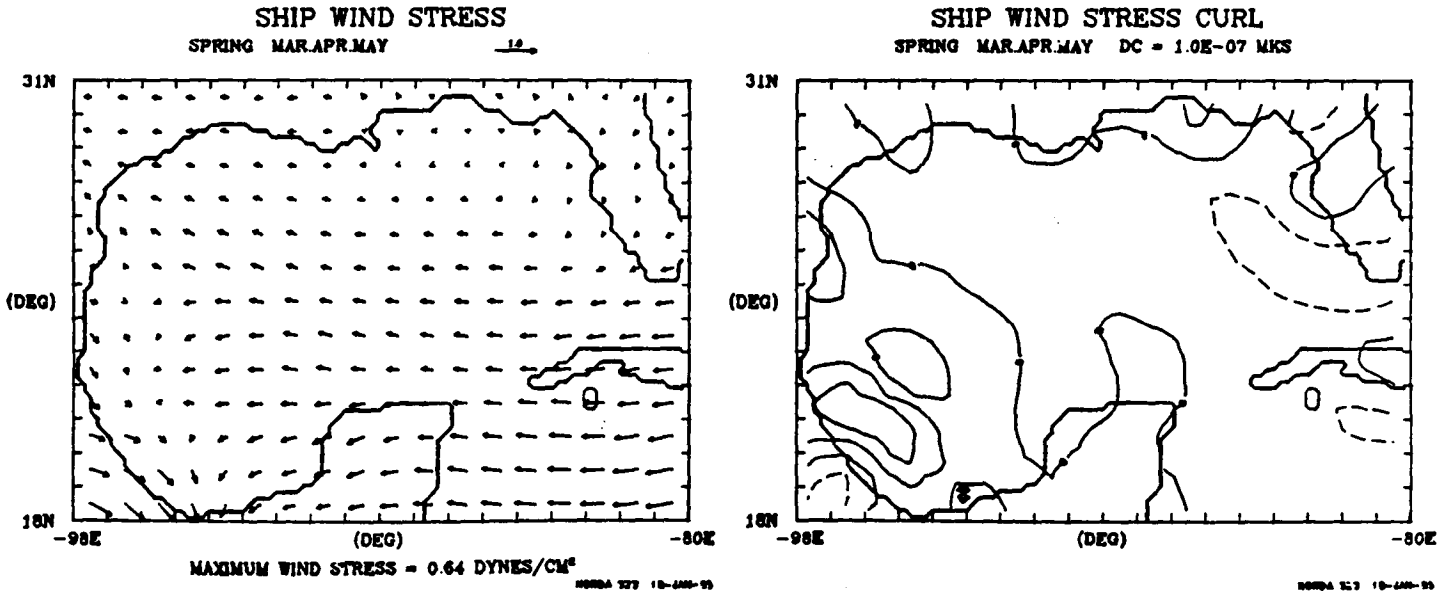
SHIP WIND STRESS
SPRING MAR.APR.MAY
31N
(DEG)
18N
-98E
(DEG)
-80E
MAXIMUM WIND STRESS = 0.64 DYNES/CM²
SHIP WIND STRESS CURL
SPRING MAR.APR.MAY DC = 1.0E-07 MKS
31N
(DEG)
18N
-98E
(DEG)
-80E

FIGURE 14

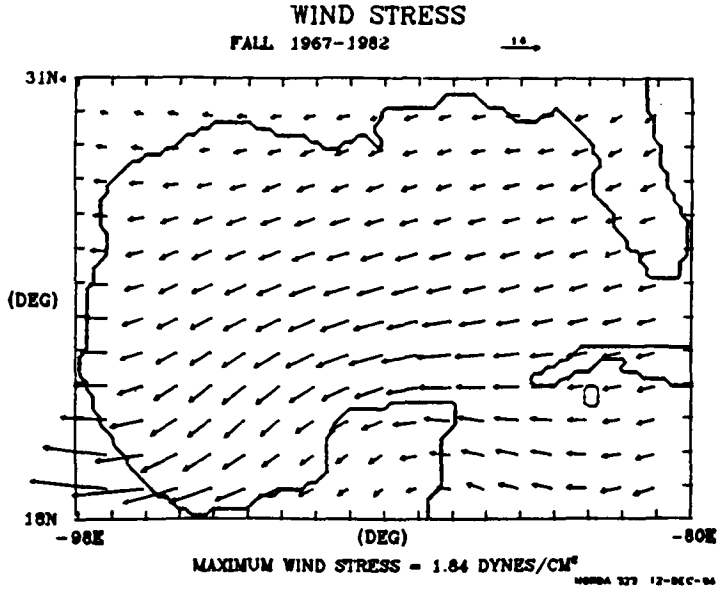
WIND STRESS
FALL 1967-1982
31N
(DEG)
18N
-98E
(DEG)
-80E
MAXIMUM WIND STRESS = 1.84 DYNES/CM²

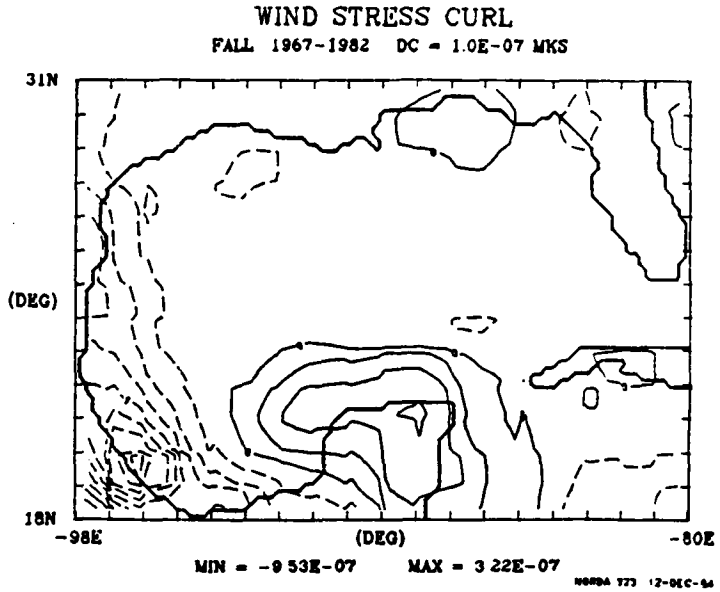
WIND STRESS CURL
FALL 1967-1982 DC = 1.0E-07 MKS
31N
(DEG)
18N
-98E
(DEG)
-80E
MIN = -9.53E-07 MAX = 3.22E-07

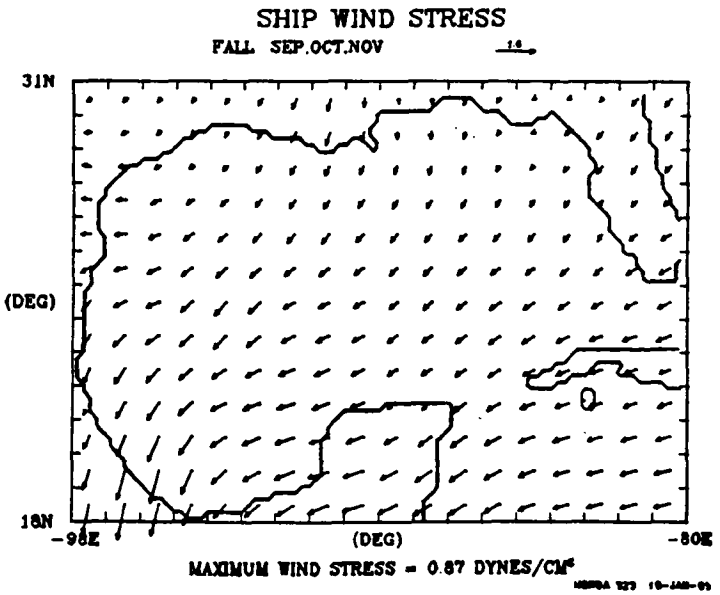
SHIP WIND STRESS
FALL SEP.OCT.NOV
31N
(DEG)
18N
-98E
(DEG)
-80E
MAXIMUM WIND STRESS = 0.87 DYNES/CM²

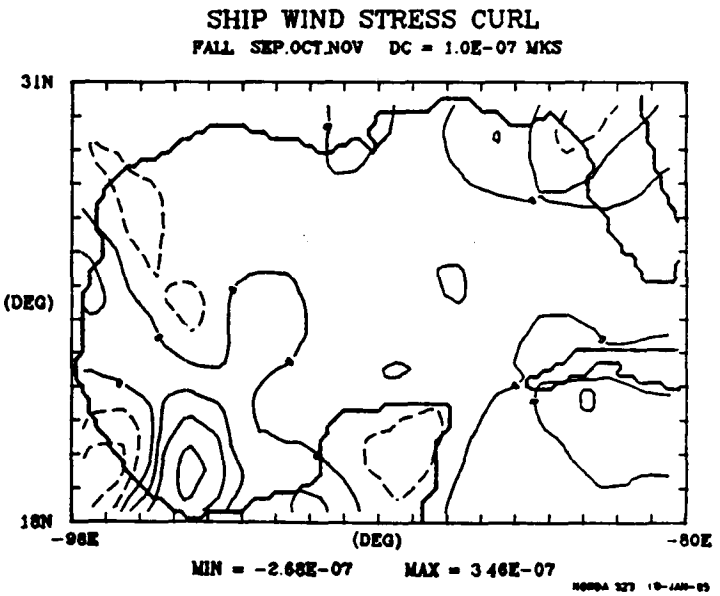
SHIP WIND STRESS CURL
FALL SEP.OCT.NOV DC = 1.0E-07 MKS
31N
(DEG)
18N
-98E
(DEG)
-80E
MIN = -2.68E-07 MAX = 3.46E-07

FIGURE 15: Instantaneous wind stress and wind stress curl from the Navy Corrected Geostrophic Wind data set, for 0000 and 1200 GMT on 14 January and 0000 GMT on 15 January 1976.

FIGURE 16: Instantaneous wind stress and wind stress curl from the Navy Corrected Geostrophic Wind data set, for 0000 and 1200 GMT on 14 July and 0000 GMT on 15 July 1976.

FIGURE 15

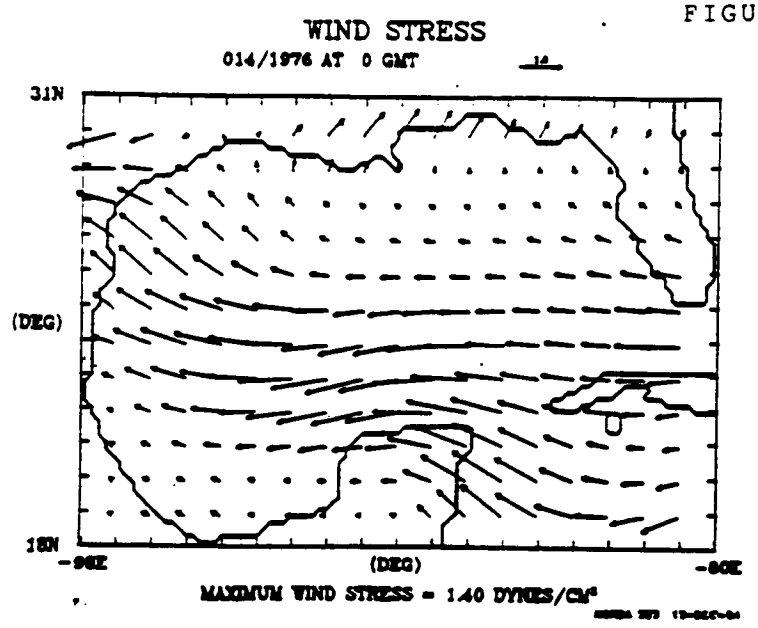
WIND STRESS
014/1976 AT 0 GMT
31N
(DEG)
18N
-98E
(DEG)
-80E
MAXIMUM WIND STRESS = 1.40 DYNES/CM²

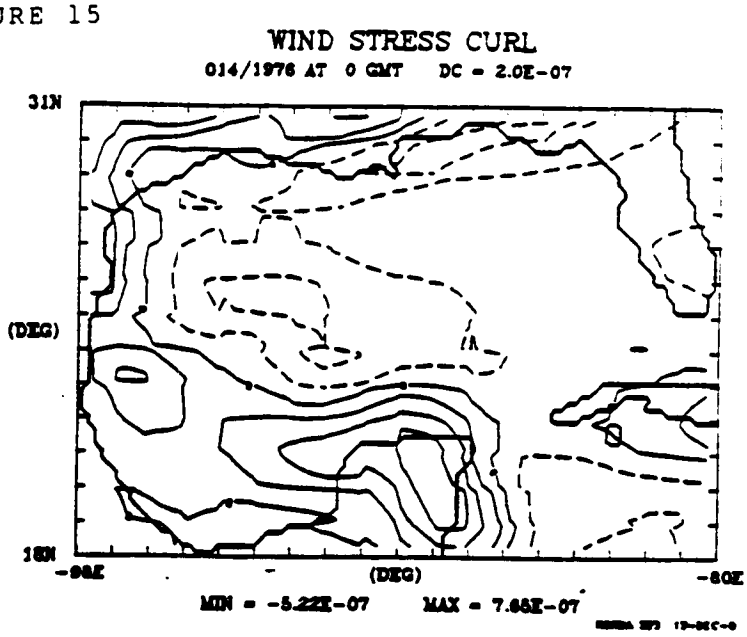
WIND STRESS CURL
014/1976 AT 0 GMT DC = 2.0E-07
31N
(DEG)
18N
-98E
(DEG)
-80E
MIN = -5.22E-07 MAX = 7.66E-07

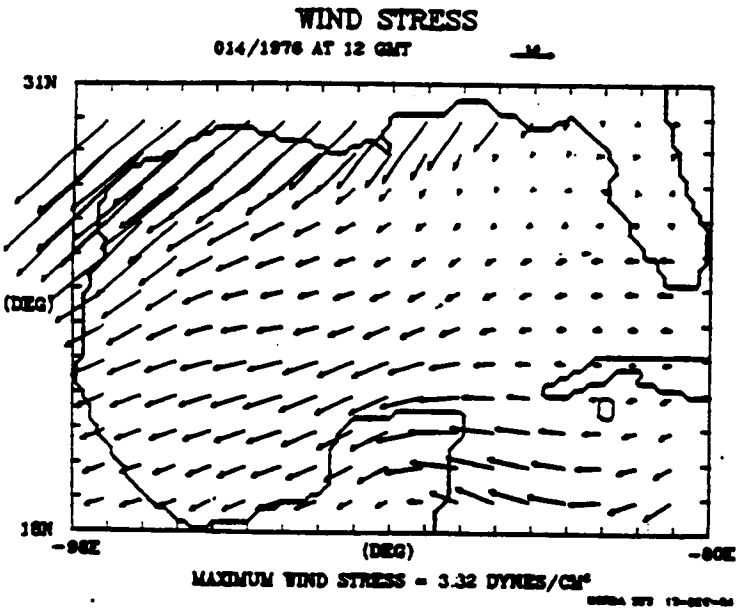
WIND STRESS
014/1976 AT 12 GMT
31N
(DEG)
18N
-98E
(DEG)
-80E
MAXIMUM WIND STRESS = 3.32 DYNES/CM²

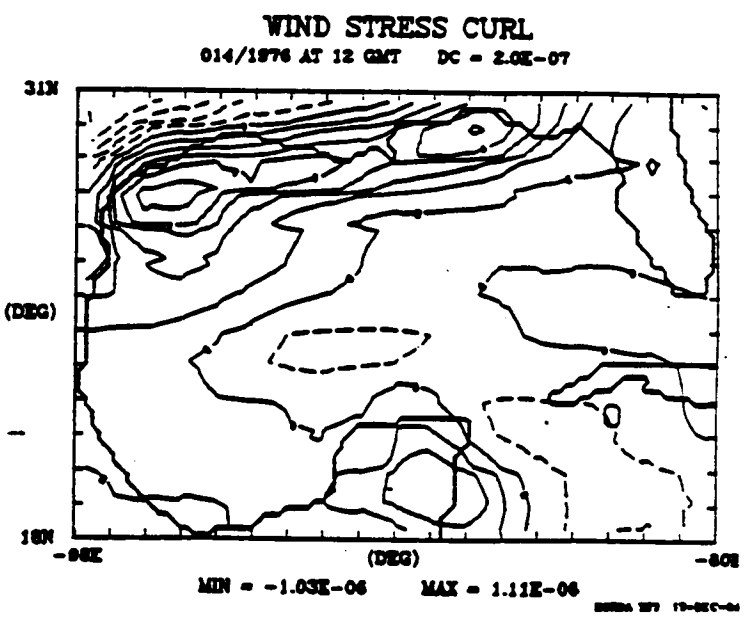
WIND STRESS CURL
014/1976 AT 12 GMT DC = 2.0E-07
31N
(DEG)
18N
-98E
(DEG)
-80E
MIN = -1.03E-06 MAX = 1.11E-06

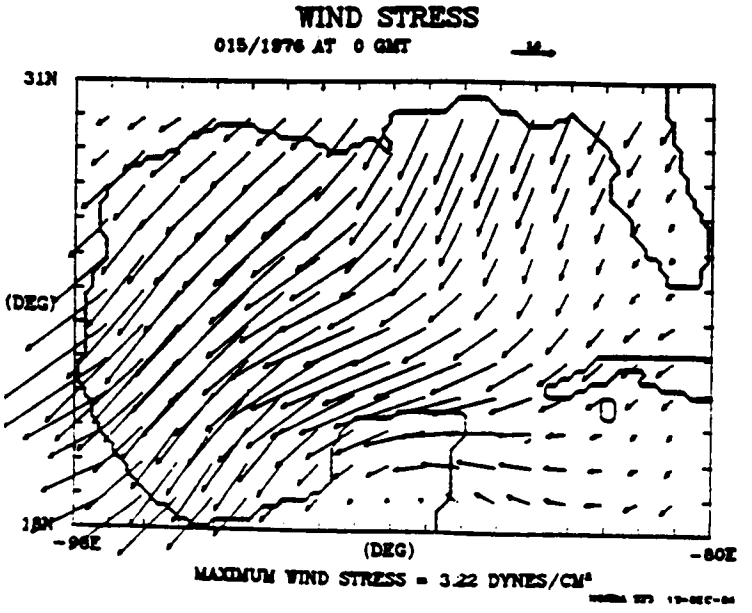
WIND STRESS
015/1976 AT 0 GMT
31N
(DEG)
18N
-98E
(DEG)
-80E
MAXIMUM WIND STRESS = 3.22 DYNES/CM²

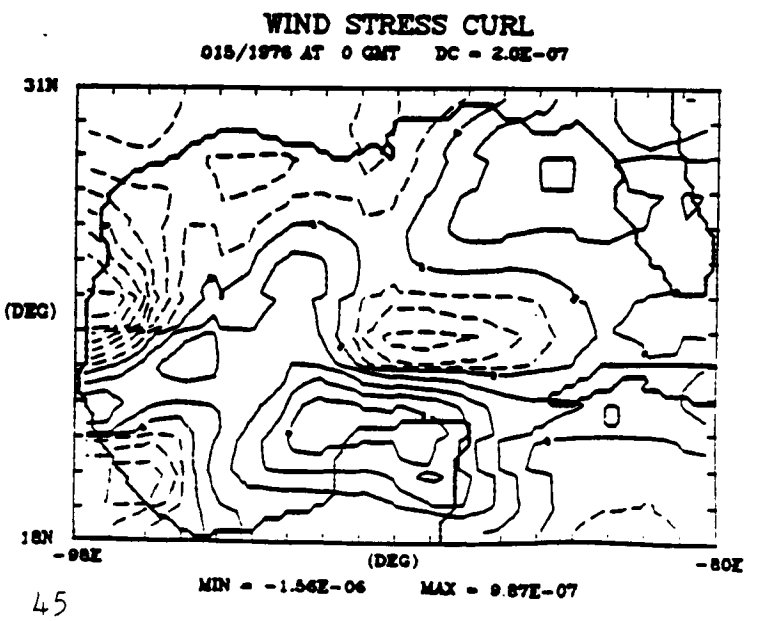
WIND STRESS CURL
015/1976 AT 0 GMT DC = 2.0E-07
31N
(DEG)
18N
-98E
(DEG)
-80E
MIN = -1.56E-06 MAX = 9.87E-07

FIGURE 16

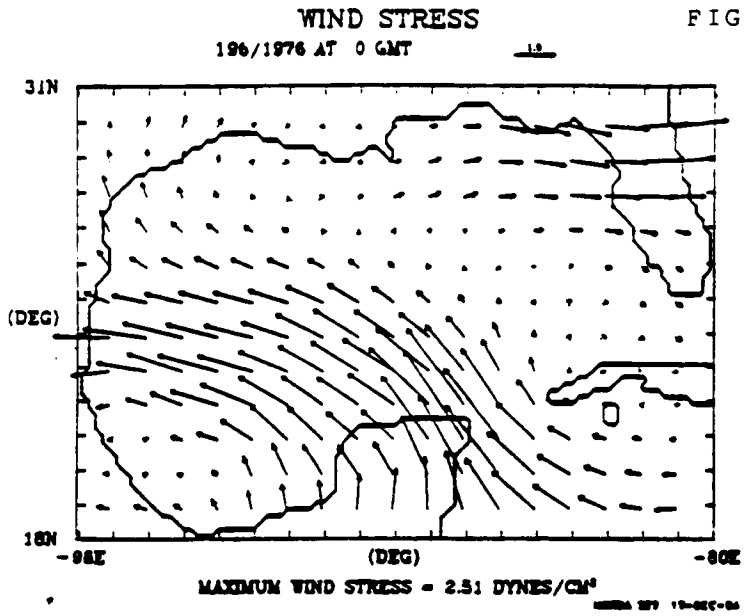
WIND STRESS
196/1976 AT 0 GMT
31N
(DEG)
18N
-98E
(DEG)
-80E
MAXIMUM WIND STRESS = 2.51 DYNES/CM²

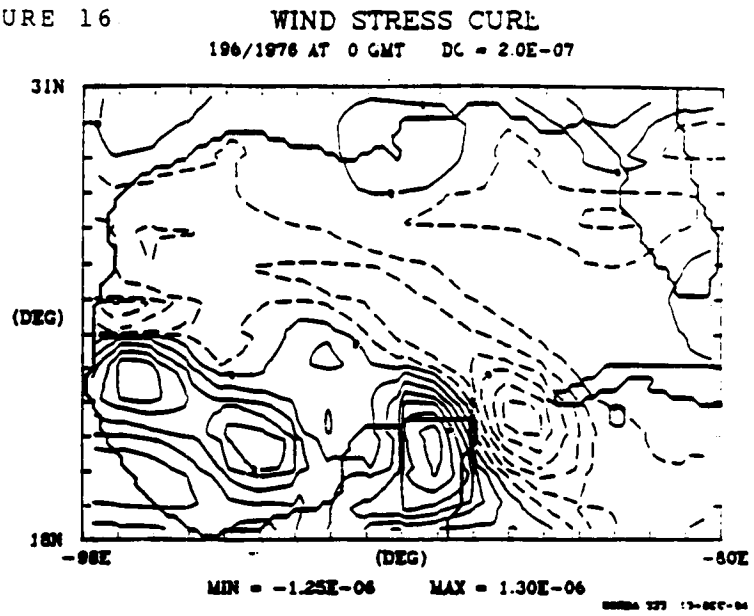
WIND STRESS CURL
196/1976 AT 0 GMT DC = 2.0E-07
31N
(DEG)
18N
-98E
(DEG)
-80E
MIN = -1.25E-06 MAX = 1.30E-06

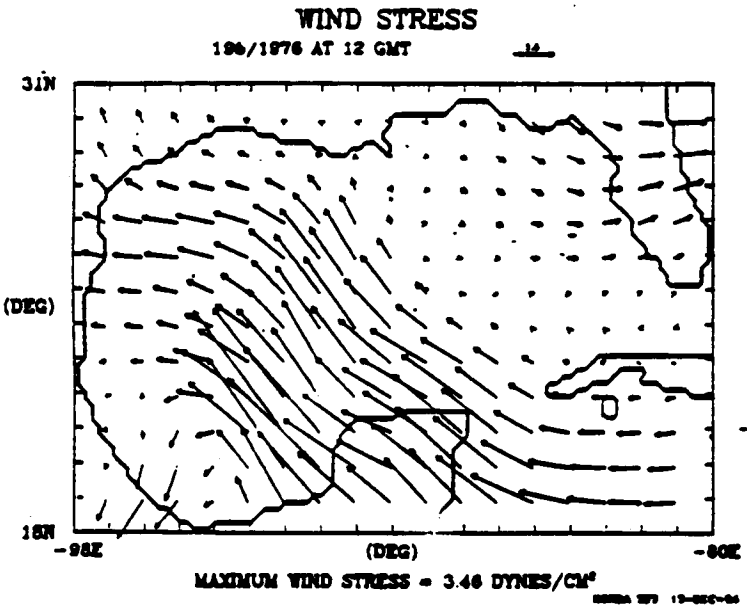
WIND STRESS
196/1976 AT 12 GMT
31N
(DEG)
18N
-98E
(DEG)
-80E
MAXIMUM WIND STRESS = 3.46 DYNES/CM²

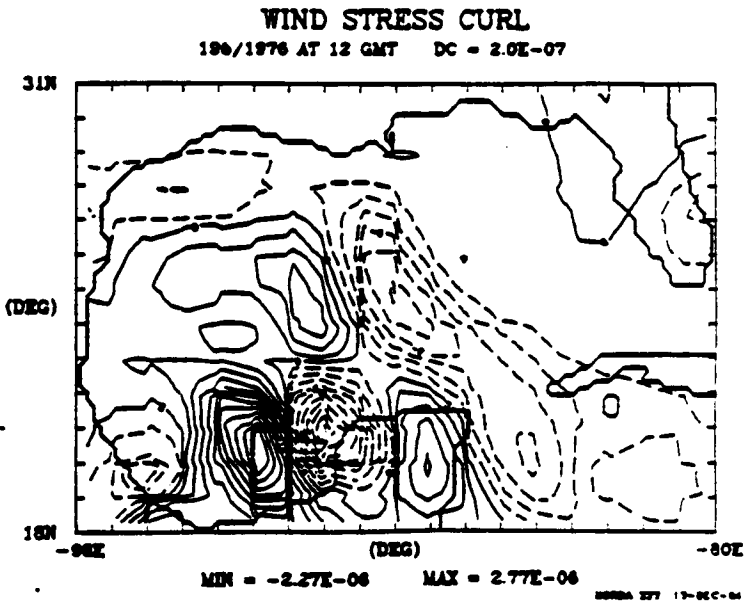
WIND STRESS CURL
196/1976 AT 12 GMT DC = 2.0E-07
31N
(DEG)
18N
-98E
(DEG)
-80E
MIN = -2.27E-06 MAX = 2.77E-06

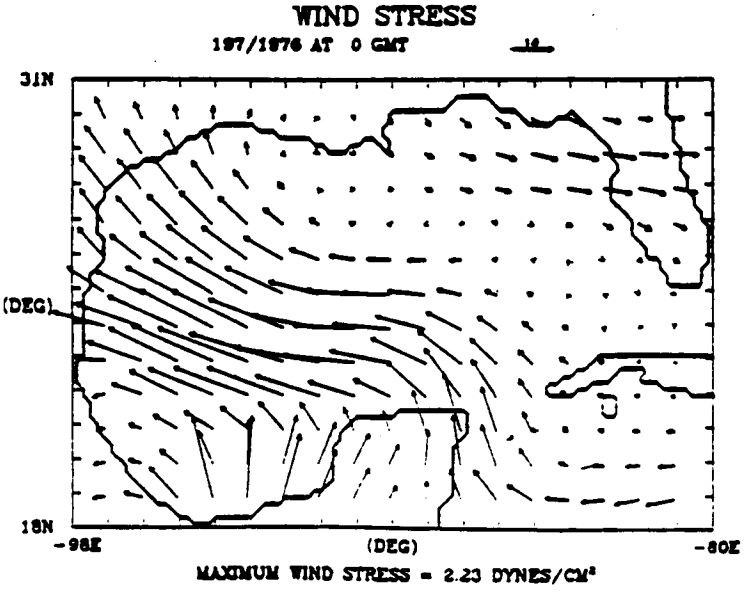
WIND STRESS
197/1976 AT 0 GMT
31N
(DEG)
18N
-98E
(DEG)
-80E
MAXIMUM WIND STRESS = 2.23 DYNES/CM²

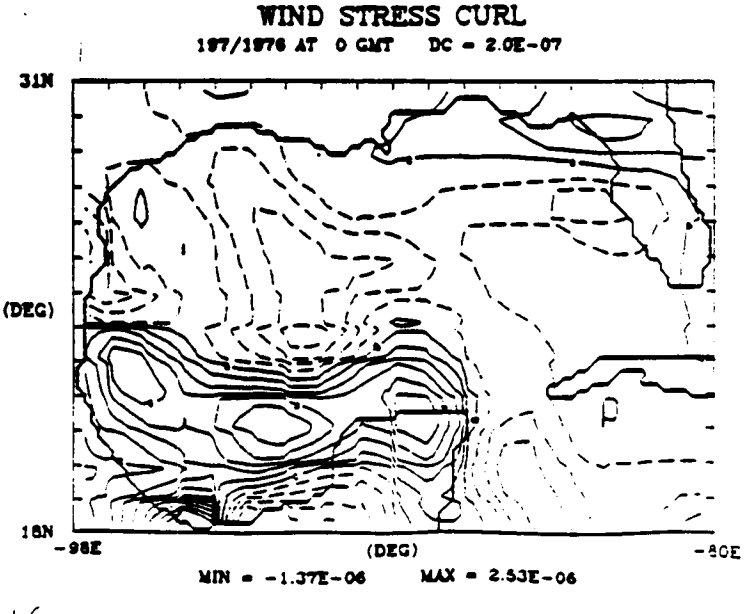
WIND STRESS CURL
197/1976 AT 0 GMT DC = 2.0E-07
31N
(DEG)
18N
-98E
(DEG)
-80E
MIN = -1.37E-06 MAX = 2.53E-06

FIGURE 17: Instantaneous view of the interface deviation in the winter from two simulations driven solely by climatological winds. (a) Experiment 31 driven by seasonal ship winds, and (b) Experiment 202/13.0 driven by monthly winds from the Navy Corrected Geostrophic Winds data set. The contour interval is 12.5m, with solid contours representing downward deviations.

FIGURE 18: Instantaneous view of the interface deviation in the spring from two simulations driven solely by climatological winds. (a) Experiment 31 driven by seasonal ship winds, and (b) Experiment 202/13.0 driven by monthly winds from the Navy Corrected Geostrophic Winds data set. The contour interval is 12.5m, with solid contours representing downward deviations.

FIGURE 19: Instantaneous view of the interface deviation in the summer from two simulations driven solely by climatological winds. (a) Experiment 31 driven by seasonal ship winds, and (b) Experiment 202/13.0 driven by monthly winds from the Navy Corrected Geostrophic Winds data set. The contour interval is 12.5m, with solid contours representing downward deviations.

FIGURE 20: Instantaneous view of the interface deviation in the fall from two simulations driven solely by climatological winds. (a) Experiment 31 driven by seasonal ship winds, and (b) Experiment 202/13.0 driven by monthly winds from the Navy Corrected Geostrophic Winds data set. The contour interval is 12.5m, with solid contours representing downward deviations.

FIGURE 17

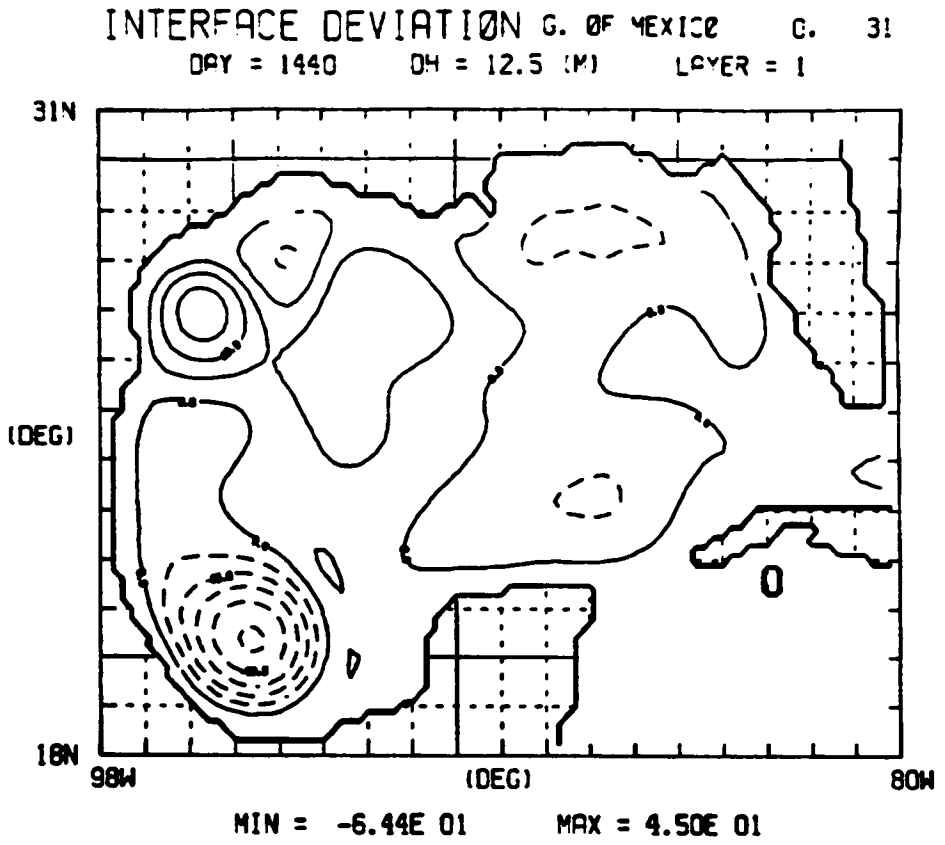
INTERFACE DEVIATIØN G. ØF MEXICØ C. 3!
DAY = 1440 DH = 12.5 (M) LAYER = 1
31N
(DEG)
18N
98W
(DEG)
80W
0
MIN = -6.44E 01 MAX = 4.50E 01

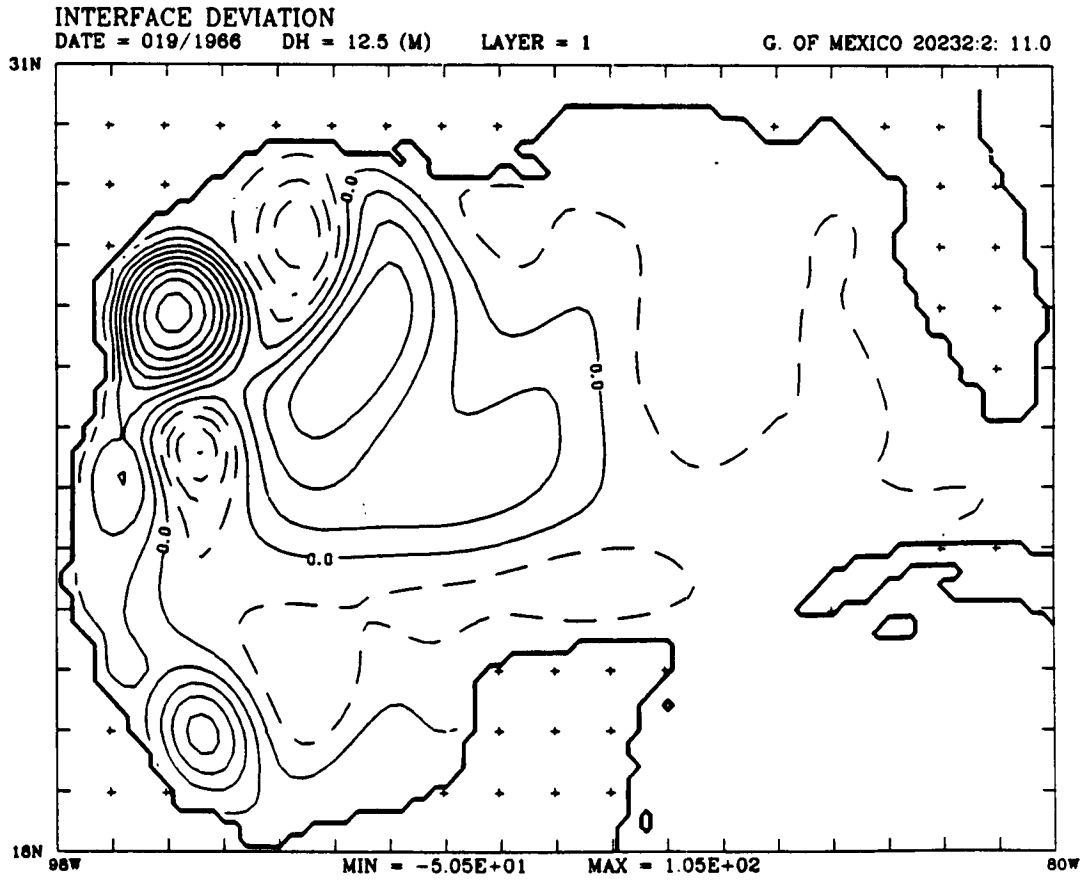
INTERFACE DEVIATION
DATE = 019/1966 DH = 12.5 (M) LAYER = 1
G. OF MEXICO 20232:2: 11.0
31N
18N
98W
80W
0.0
0.0
0.0
0.0
0
MIN = -5.05E+01 MAX = 1.05E+02
NORDA 323 02/21/86

FIGURE 18

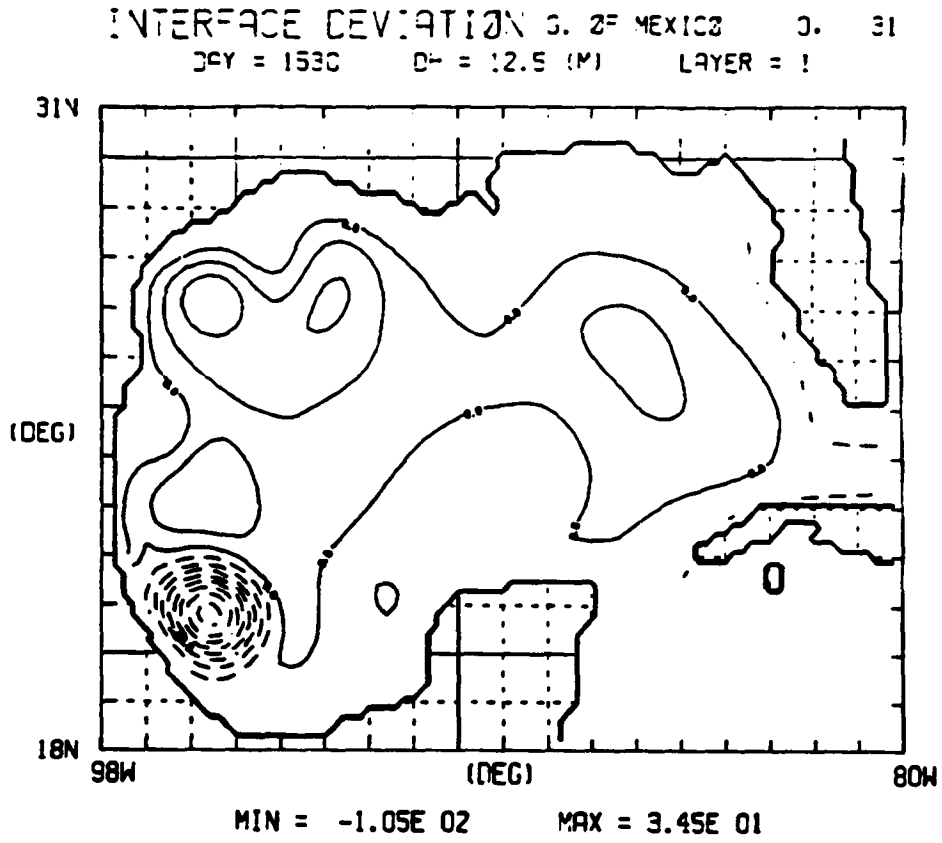
INTERFACE DEVIATION G. OF MEXICO 31
DAY = 153C DH = 12.5 (M) LAYER = 1
31N
(DEG)
18N
98W
(DEG)
80W
0
MIN = -1.05E 02 MAX = 3.45E 01

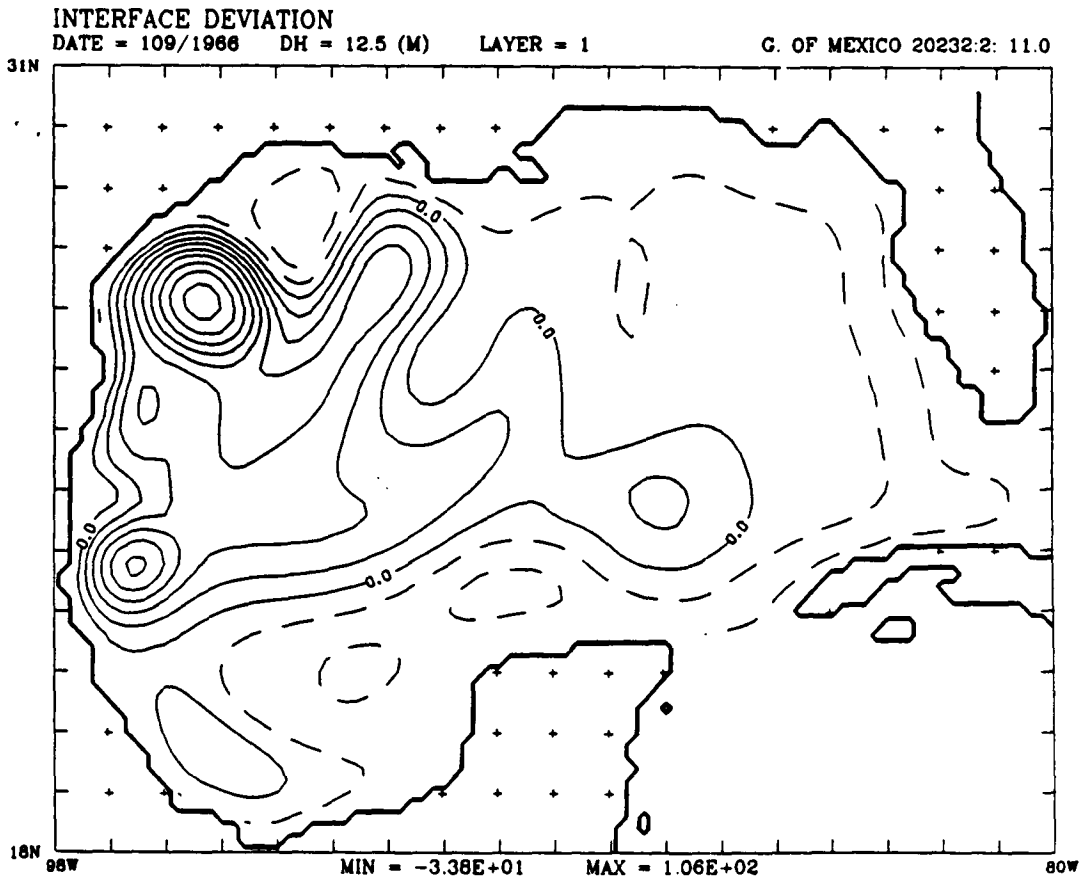
INTERFACE DEVIATION
DATE = 109/1966 DH = 12.5 (M) LAYER = 1
G. OF MEXICO 20232:2: 11.0
31N
0.0
0.0
0.0
0.0
0.0
0
18N
98W
MIN = -3.38E+01 MAX = 1.06E+02
80W
NORDA 323 02/21/86

FIGURE 19

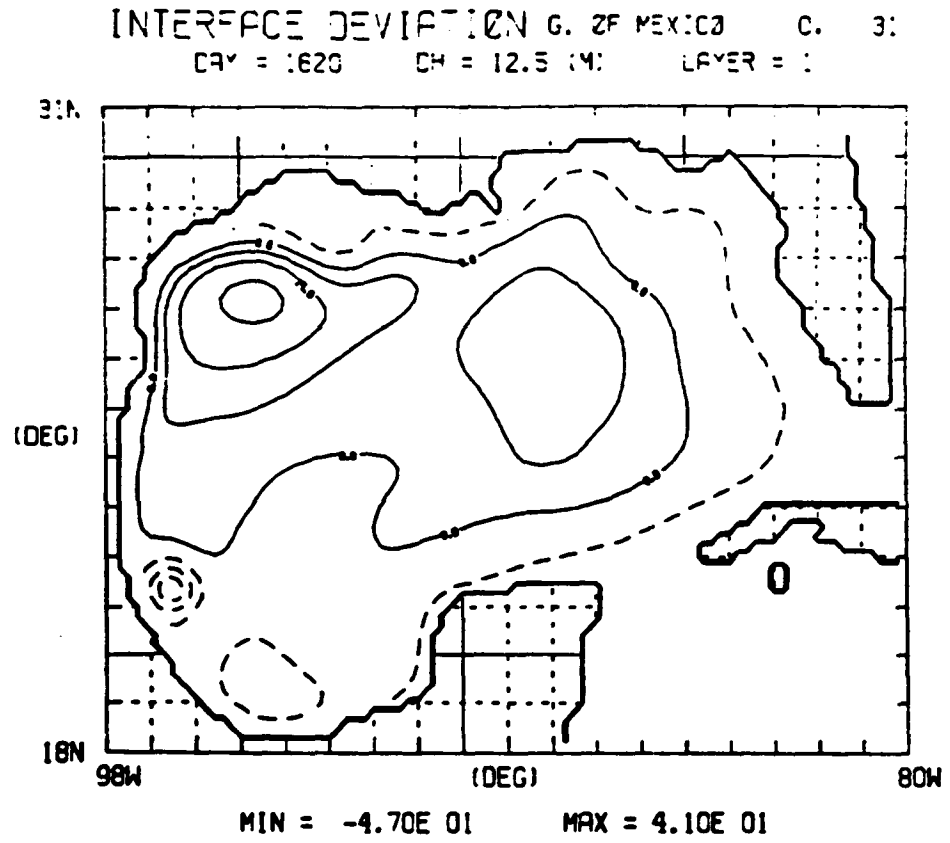
INTERFACE DEVIATION G. OF MEXICO
DAY = 1620 DH = 12.5 (M) LAYER = 1
31N
(DEG)
18N
98W
(DEG)
80W
0
MIN = -4.70E 01 MAX = 4.10E 01

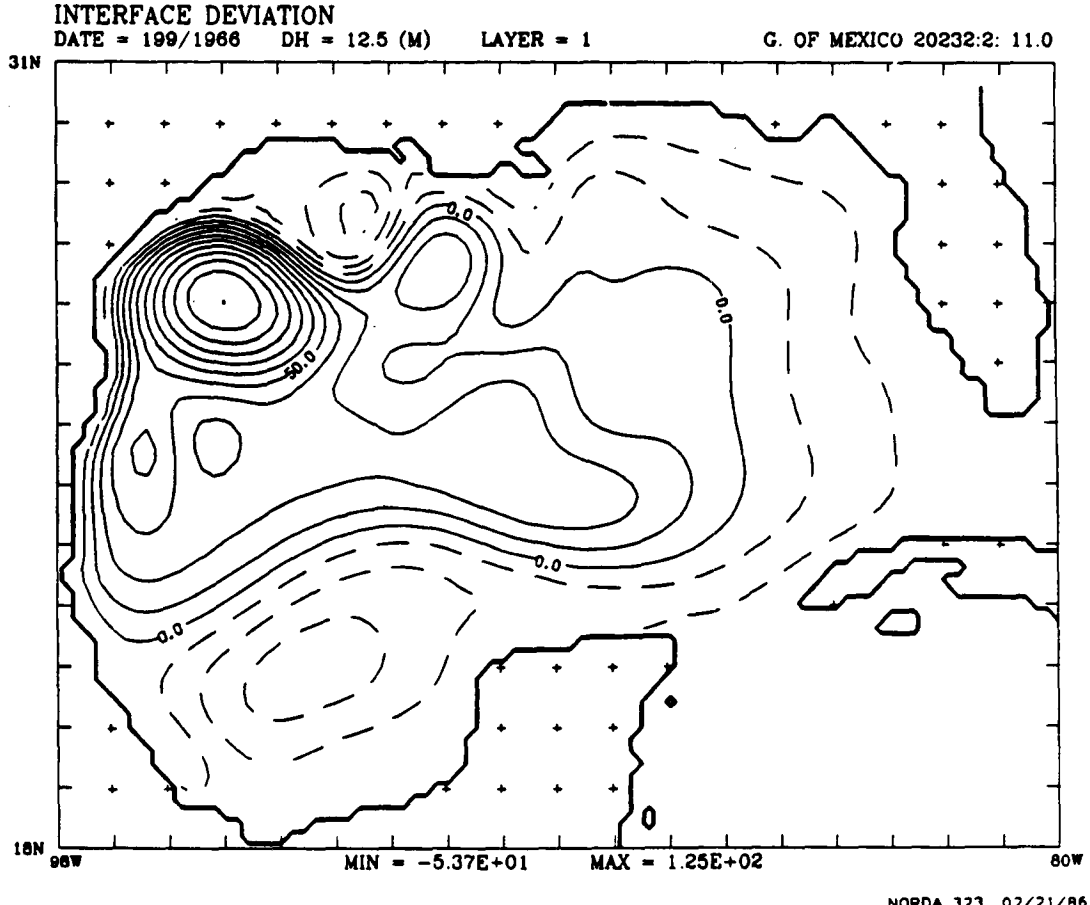
INTERFACE DEVIATION
DATE = 199/1966 DH = 12.5 (M) LAYER = 1
G. OF MEXICO 20232:2: 11.0
31N
18N
98W
80W
0.0
0.0
0.0
0.0
-50.0
0
MIN = -5.37E+01 MAX = 1.25E+02
NORDA 323 02/21/86

FIGURE 20

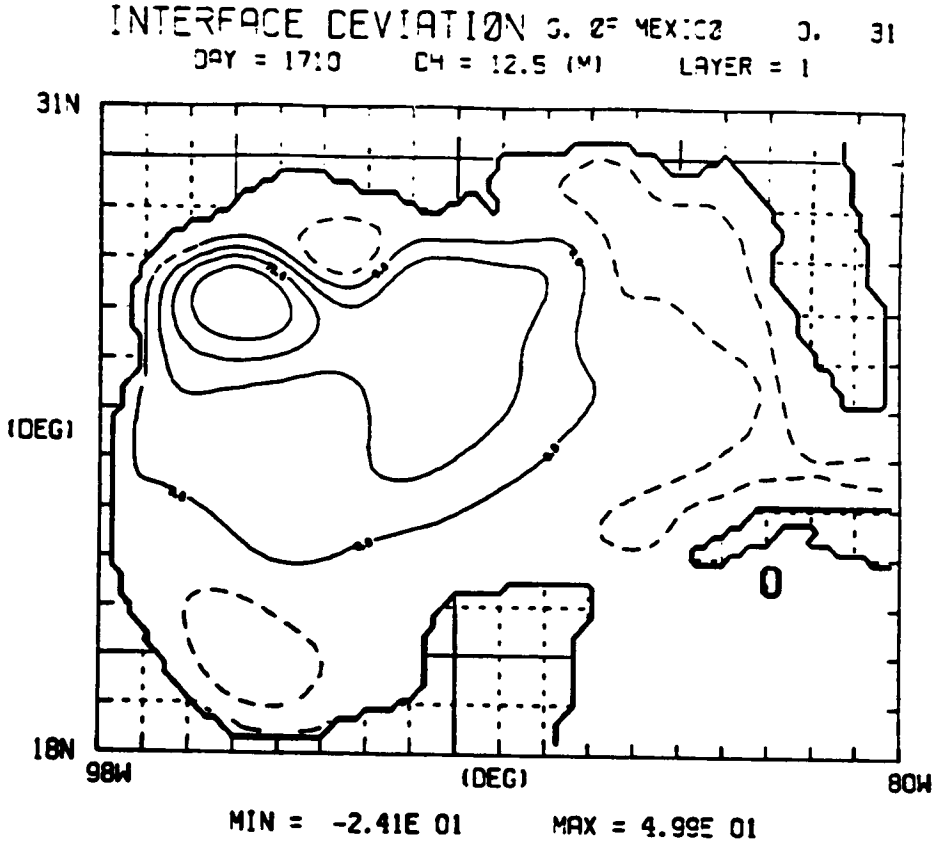
INTERFACE DEVIATION G. OF MEXICO 31
DAY = 170 DH = 12.5 (M) LAYER = 1
31N
(DEG)
18N
98W
(DEG)
80W
0
MIN = -2.41E 01 MAX = 4.99E 01

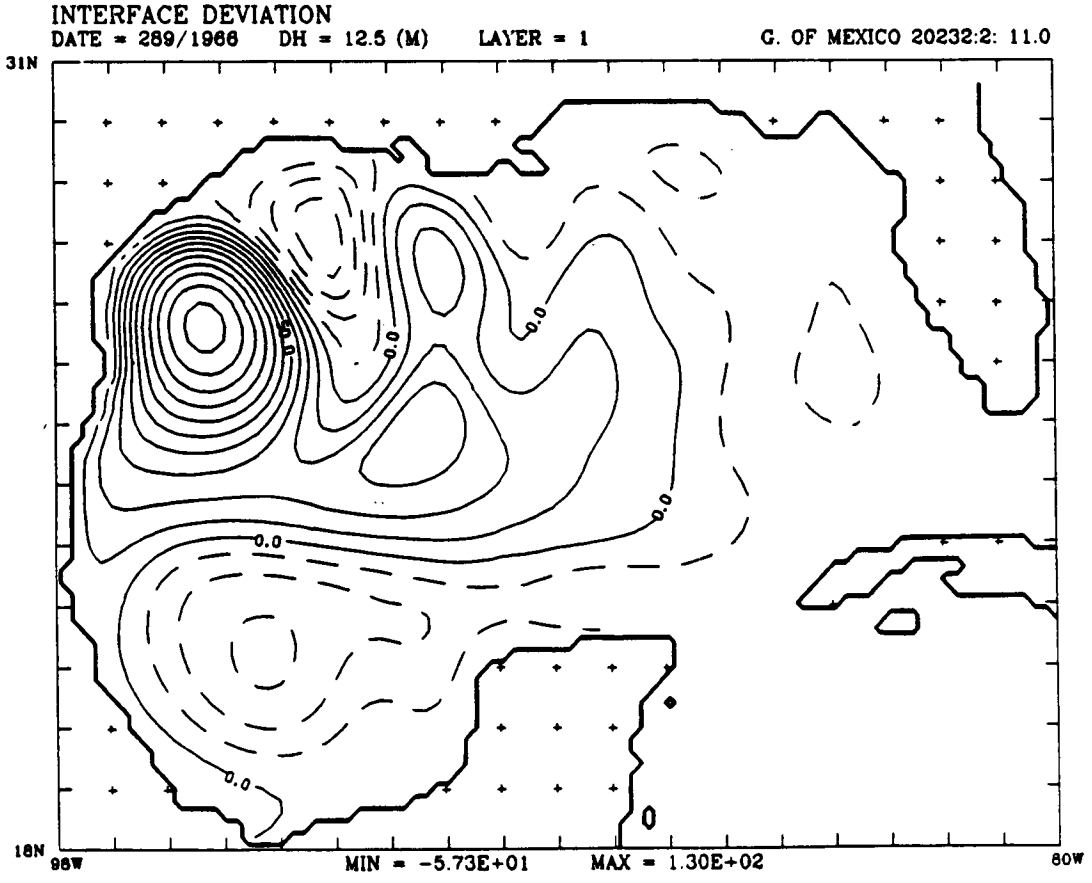
INTERFACE DEVIATION
DATE = 289/1966 DH = 12.5 (M) LAYER = 1
G. OF MEXICO 20232:2: 11.0
31N
18N
98W
80W
0.0
0
MIN = -5.73E+01 MAX = 1.30E+02
NORDA 323 02/21/86

FIGURE 21: Instantaneous view of the interface deviation in the winter from Experiment 202/13.0 driven solely by winds averaged by month from the Navy Corrected Geostrophic Winds data set. (a) winter of 1970/1971, and (b) winter of 1971/1972. The contour interval is 12.5m, with solid contours representing downward deviations.

FIGURE 22: Instantaneous view of the interface deviation in the spring from Experiment 202/13.0 driven solely by winds averaged by month from the Navy Corrected Geostrophic Winds data set. (a) spring of 1971, and (b) spring of 1972. The contours interval is 12.5m, with solid contours representing downward deviations.

FIGURE 23: Instantaneous view of the interface deviation in the summer from Experiment 202/13.0 driven solely by winds averaged by month from the Navy Corrected Geostrophic Winds data set. (a) summer of 1971, and (b) summer of 1972. The contour interval is 12.5m, with solid contours representing downward deviations.

FIGURE 24: Instantaneous view of the interface deviation in the fall from Experiment 202/13.0 driven solely by winds averaged by month from the Navy Corrected Geostrophic Winds data set. (a) fall of 1971, and (b) fall of 1972. The contour interval is 12.5m, with solid contours representing downward deviations.

FIGURE 21

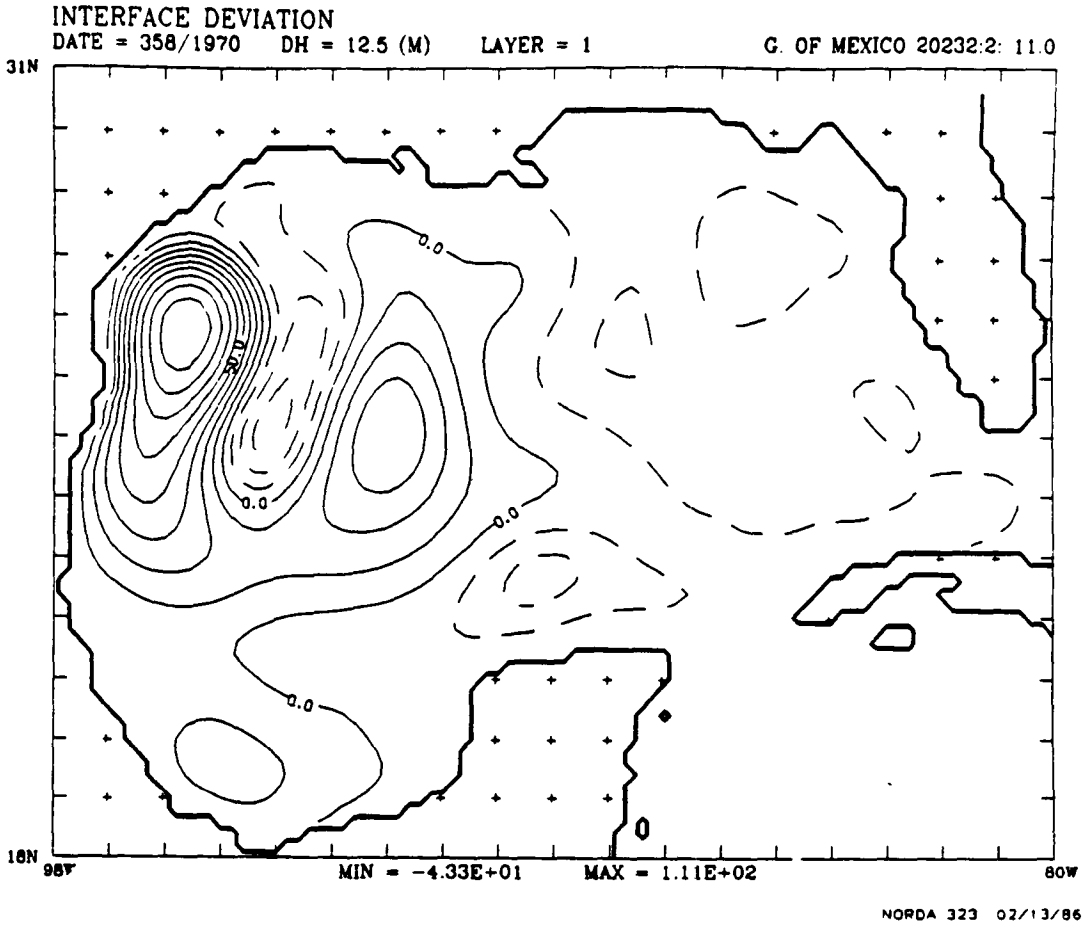
INTERFACE DEVIATION
DATE = 358/1970 DH = 12.5 (M) LAYER = 1
G. OF MEXICO 20232:2: 11.0
31N
18N
98W
80W
0.0
0.0
0.0
0.0
0
MIN = -4.33E+01 MAX = 1.11E+02
NORDA 323 02/13/86

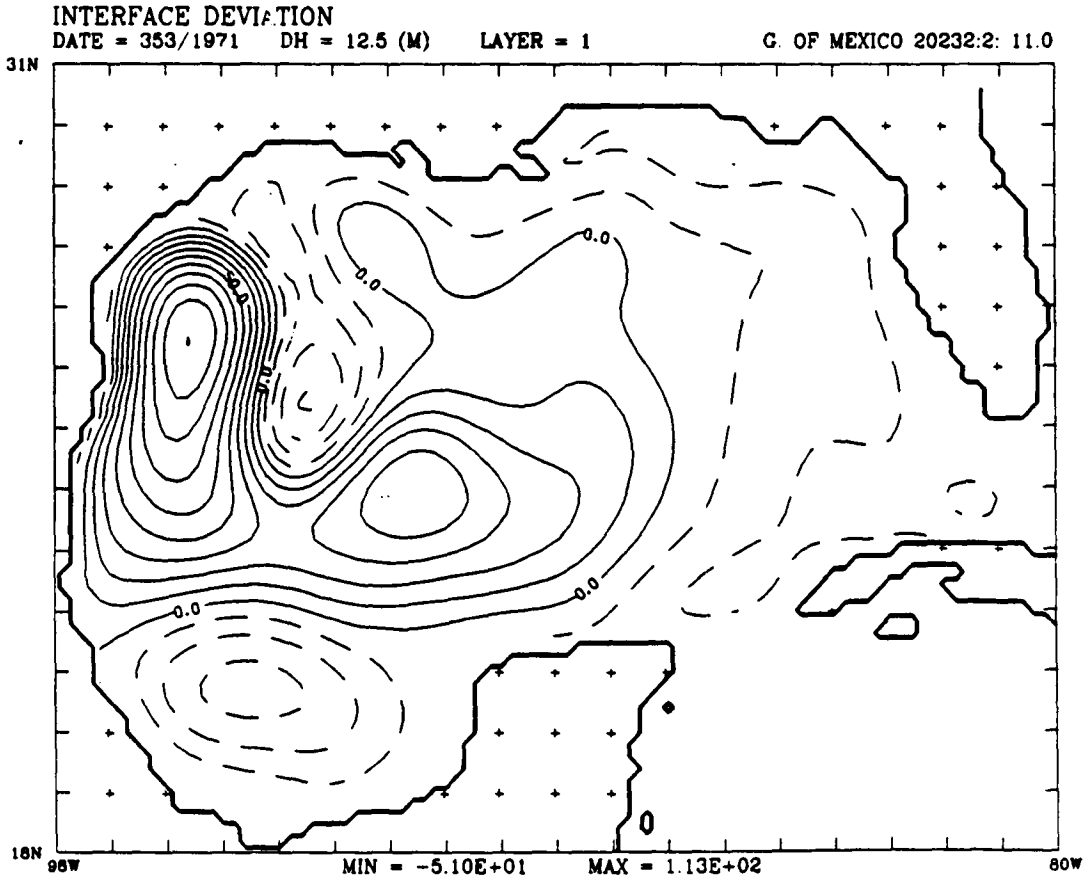
INTERFACE DEVIATION
DATE = 353/1971 DH = 12.5 (M) LAYER = 1
G. OF MEXICO 20232:2: 11.0
31N
18N
98W
80W
0.0
0.0
0.0
0.0
0.0
0
MIN = -5.10E+01 MAX = 1.13E+02
NORDA 323 02/13/86

FIGURE 22

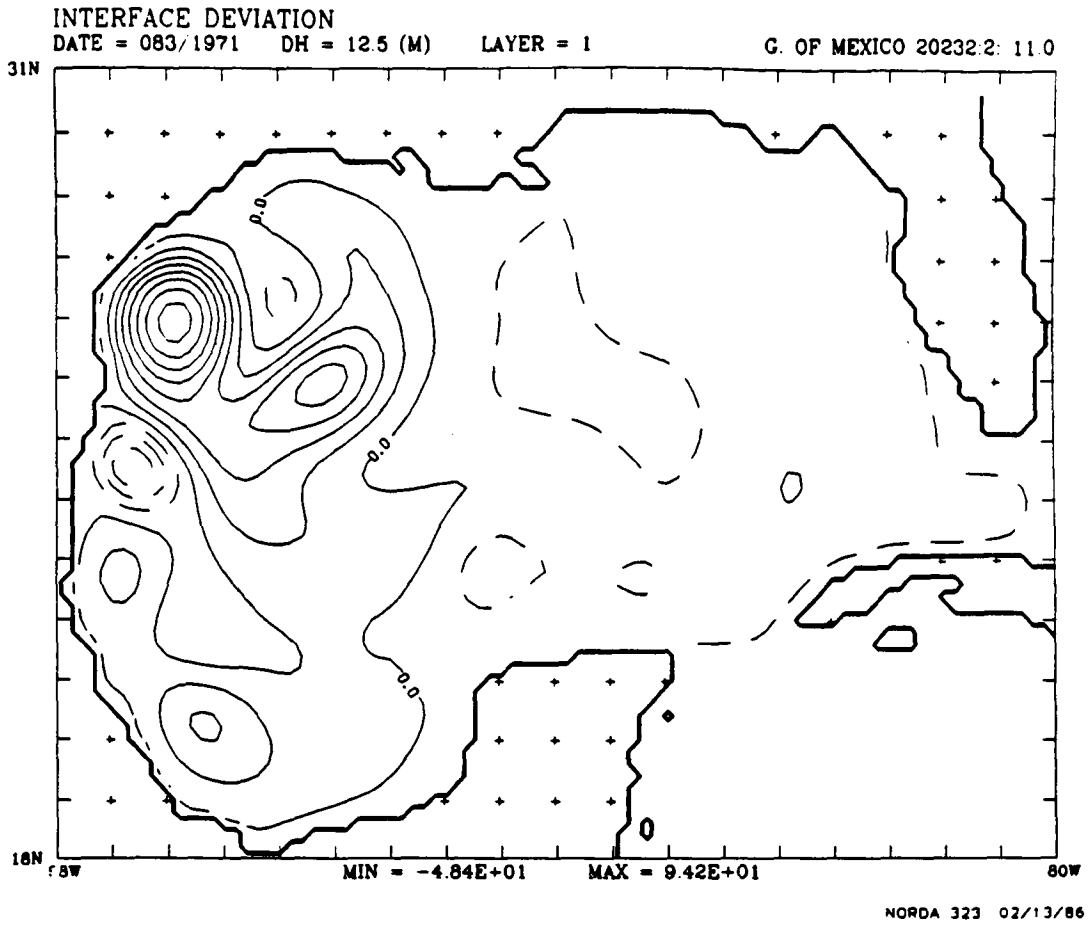
INTERFACE DEVIATION
DATE = 083/1971 DH = 12.5 (M) LAYER = 1
G. OF MEXICO 20232:2: 11.0
31N
18N
98W
80W
0.0
0.0
0.0
0
MIN = -4.84E+01 MAX = 9.42E+01
NORDA 323 02/13/86

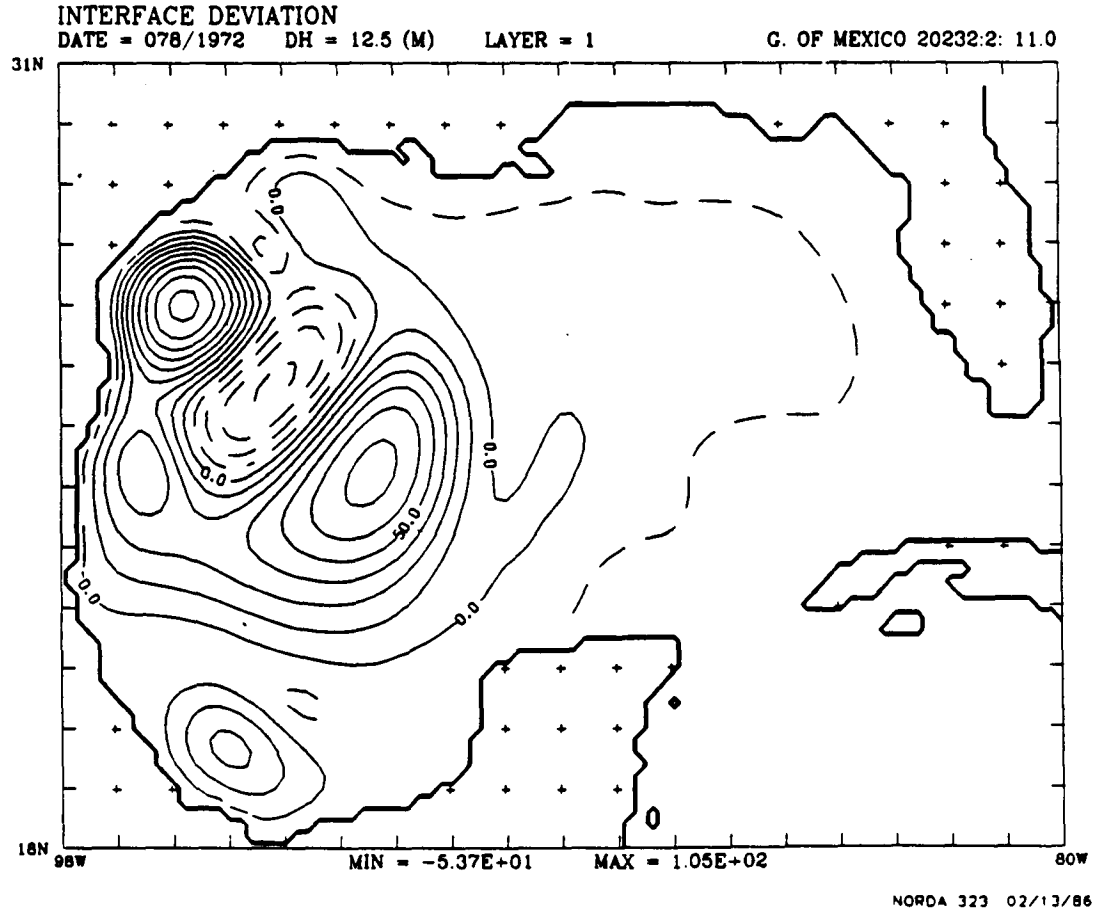
INTERFACE DEVIATION
DATE = 078/1972 DH = 12.5 (M) LAYER = 1
G. OF MEXICO 20232:2: 11.0
31N
18N
98W
80W
0.0
0.0
0.0
-50.0
0.0
0
MIN = -5.37E+01 MAX = 1.05E+02
NORDA 323 02/13/86

FIGURE 23

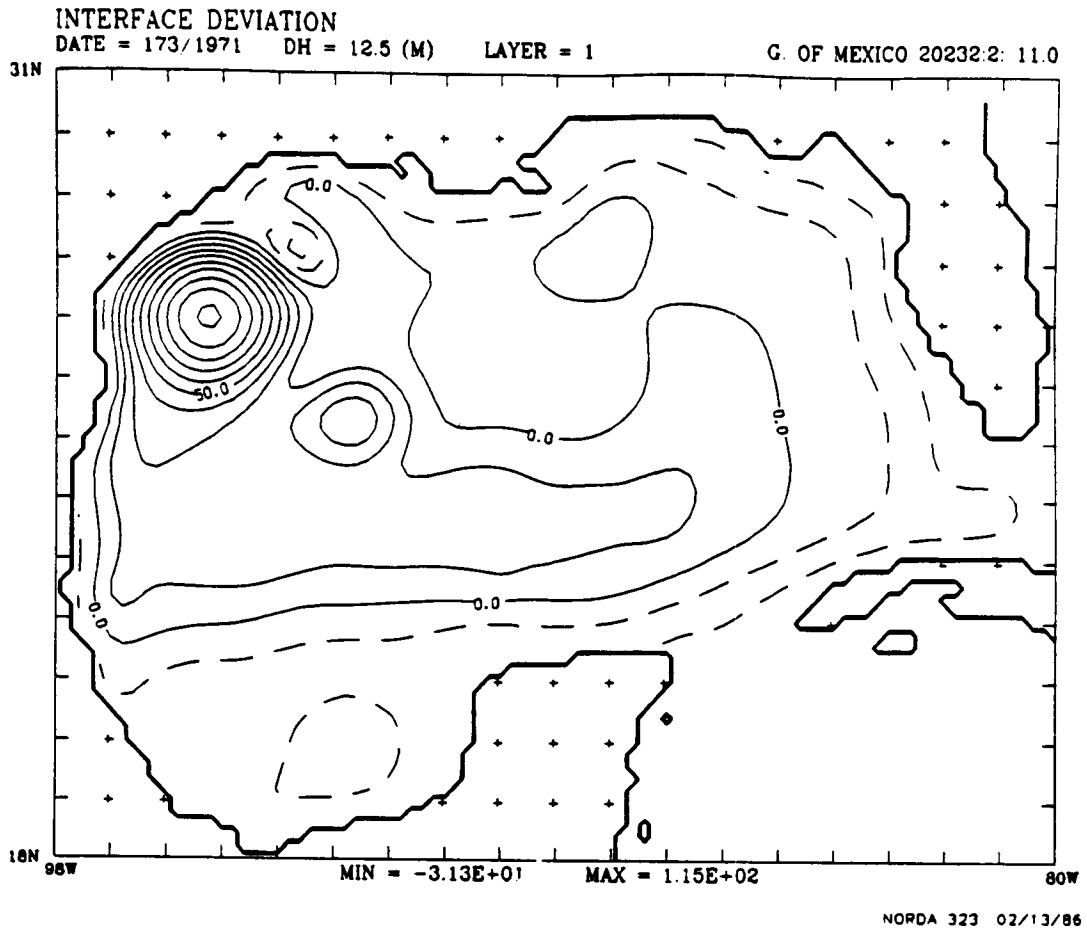
INTERFACE DEVIATION
DATE = 173/1971 DH = 12.5 (M) LAYER = 1
G. OF MEXICO 20232:2: 11.0
31N
18N
98W
80W
0.0
50.0
MIN = -3.13E+01
MAX = 1.15E+02
NORDA 323 02/13/86

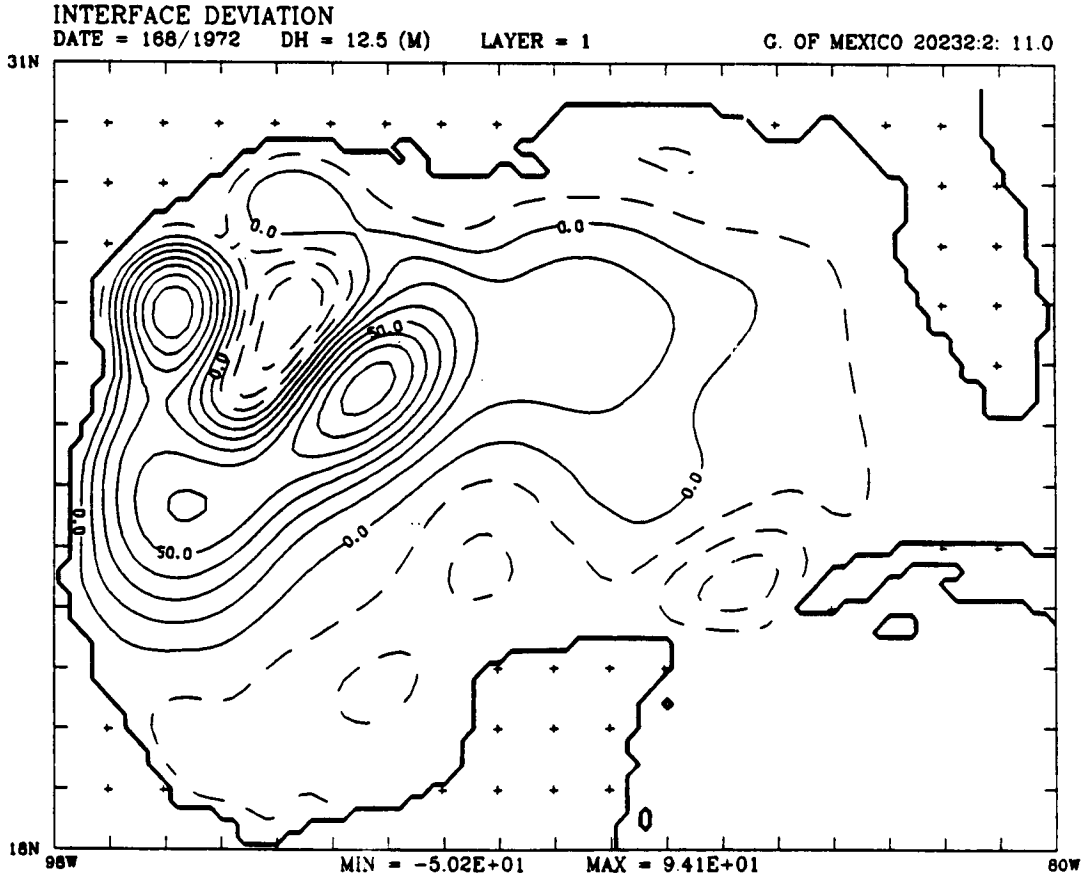
INTERFACE DEVIATION
DATE = 168/1972 DH = 12.5 (M) LAYER = 1
G. OF MEXICO 20232:2: 11.0
31N
18N
98W
80W
0.0
50.0
MIN = -5.02E+01
MAX = 9.41E+01
NORDA 323 02/13/86

FIGURE 24

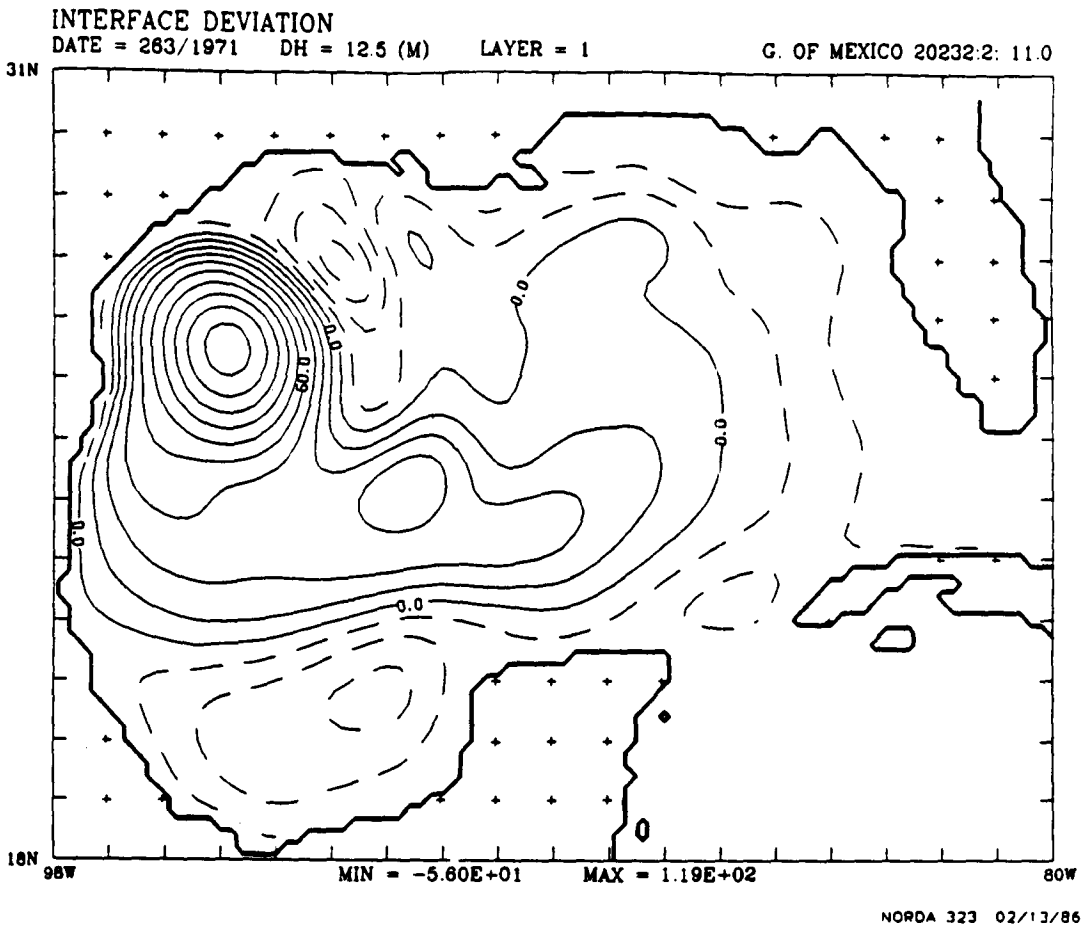
INTERFACE DEVIATION
DATE = 263/1971 DH = 12.5 (M) LAYER = 1
G. OF MEXICO 20232:2: 11.0
31N
18N
98W
80W
MIN = -5.60E+01 MAX = 1.19E+02
NORDA 323 02/13/86

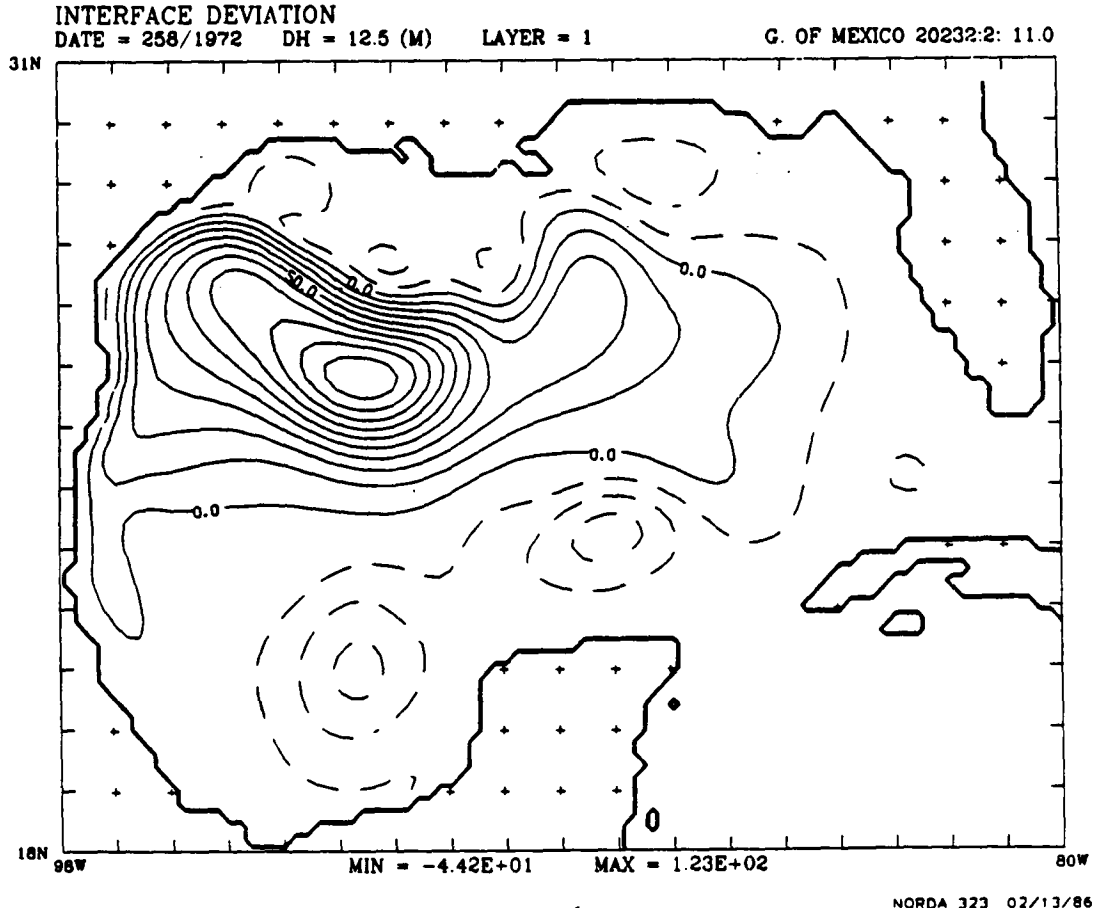
INTERFACE DEVIATION
DATE = 258/1972 DH = 12.5 (M) LAYER = 1
G. OF MEXICO 20232:2: 11.0
31N
18N
98W
80W
MIN = -4.42E+01 MAX = 1.23E+02
NORDA 323 02/13/86

FIGURE 25: Bottom topography and coastline geometry for Gulf of Mexico model on 0.1 degree grid. The contour interval is 500 m, and there is a flat shelf between the 500 m isobath and the coast. The section of the Caribbean shown is treated as land by the model, the position of the inflow port is marked by the termination of contour lines in the Yucatan Strait.

FIGURE 25

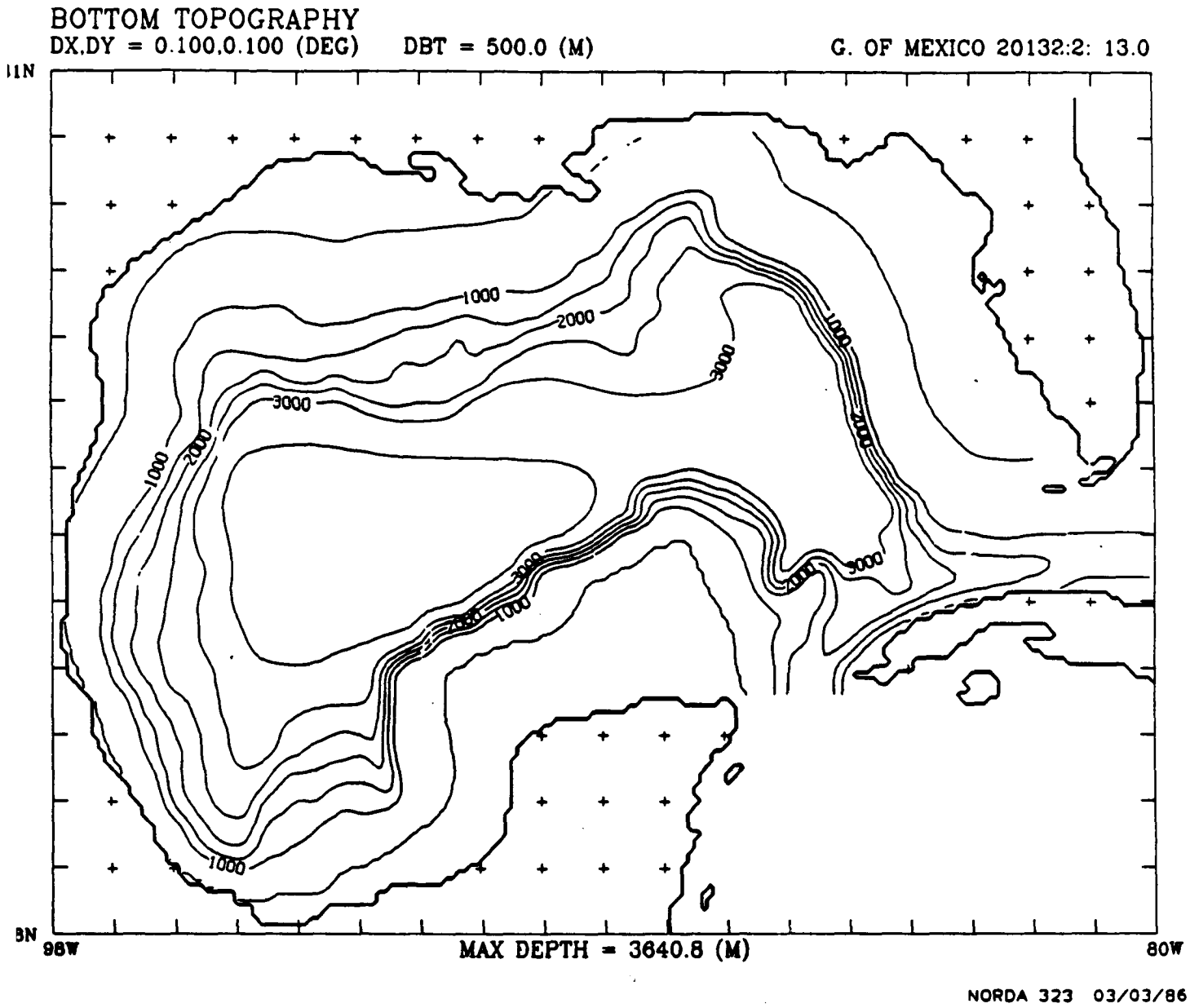
BOTTOM TOPOGRAPHY
DX,DY = 0.100,0.100 (DEG)
DBT = 500.0 (M)
G. OF MEXICO 20132:2: 13.0
11N
3N
98W
80W
MAX DEPTH = 3640.8 (M)
1000
2000
3000
NORDA 323 03/03/86

FIGURE 26

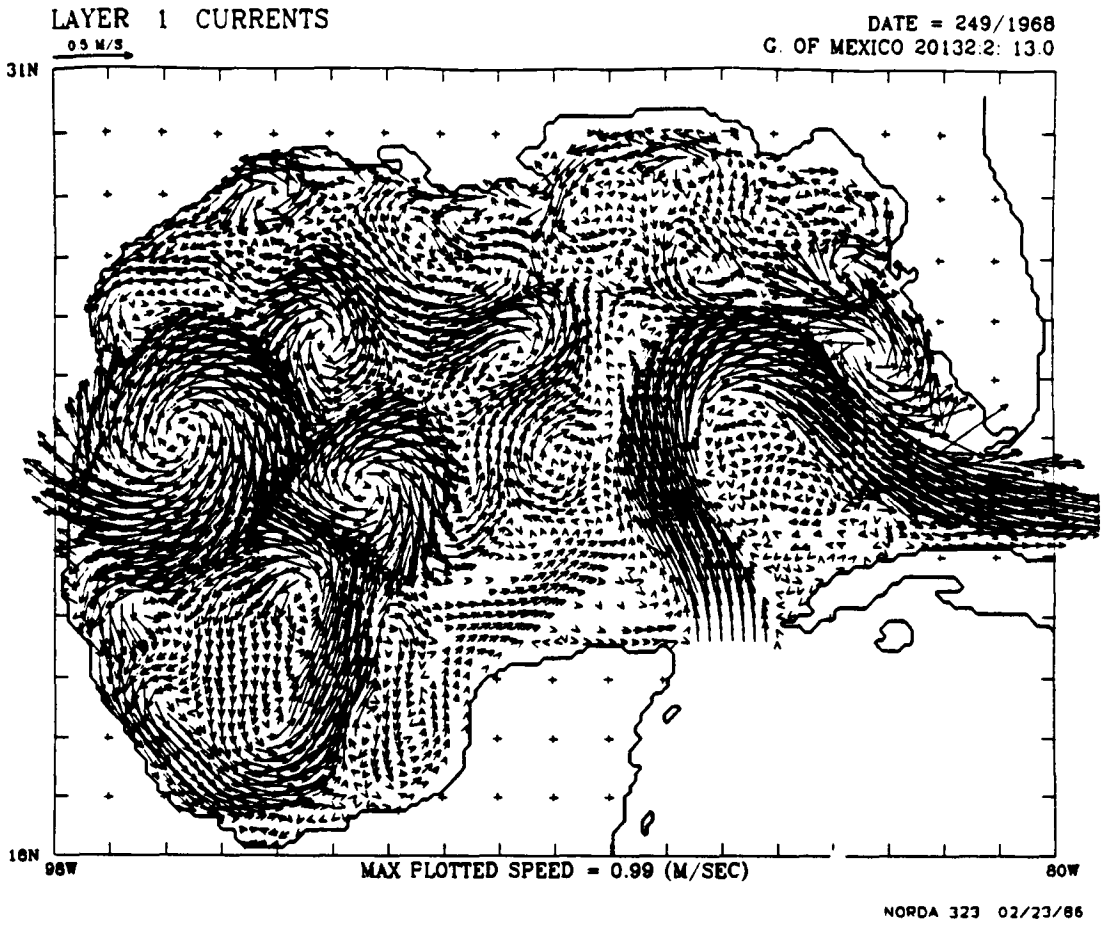
LAYER 1 CURRENTS
0.5 M/S
DATE = 249/1968
G. OF MEXICO 20132:2: 13.0
31N
18N
98W
80W
MAX PLOTTED SPEED = 0.99 (M/SEC)
NORDA 323 02/23/86

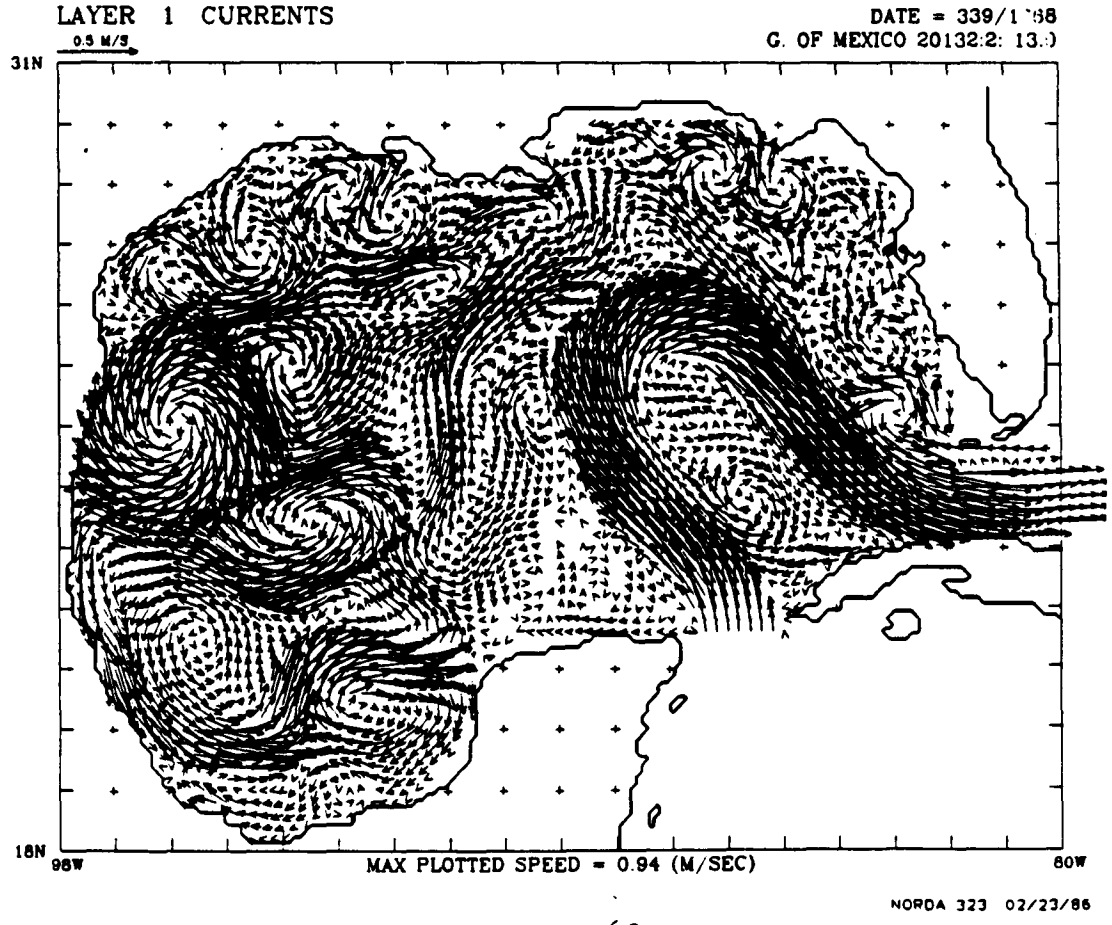
LAYER 1 CURRENTS
0.5 M/S
DATE = 339/1968
G. OF MEXICO 20132:2: 13.0
31N
18N
98W
80W
MAX PLOTTED SPEED = 0.94 (M/SEC)
NORDA 323 02/23/86

FIGURE 27

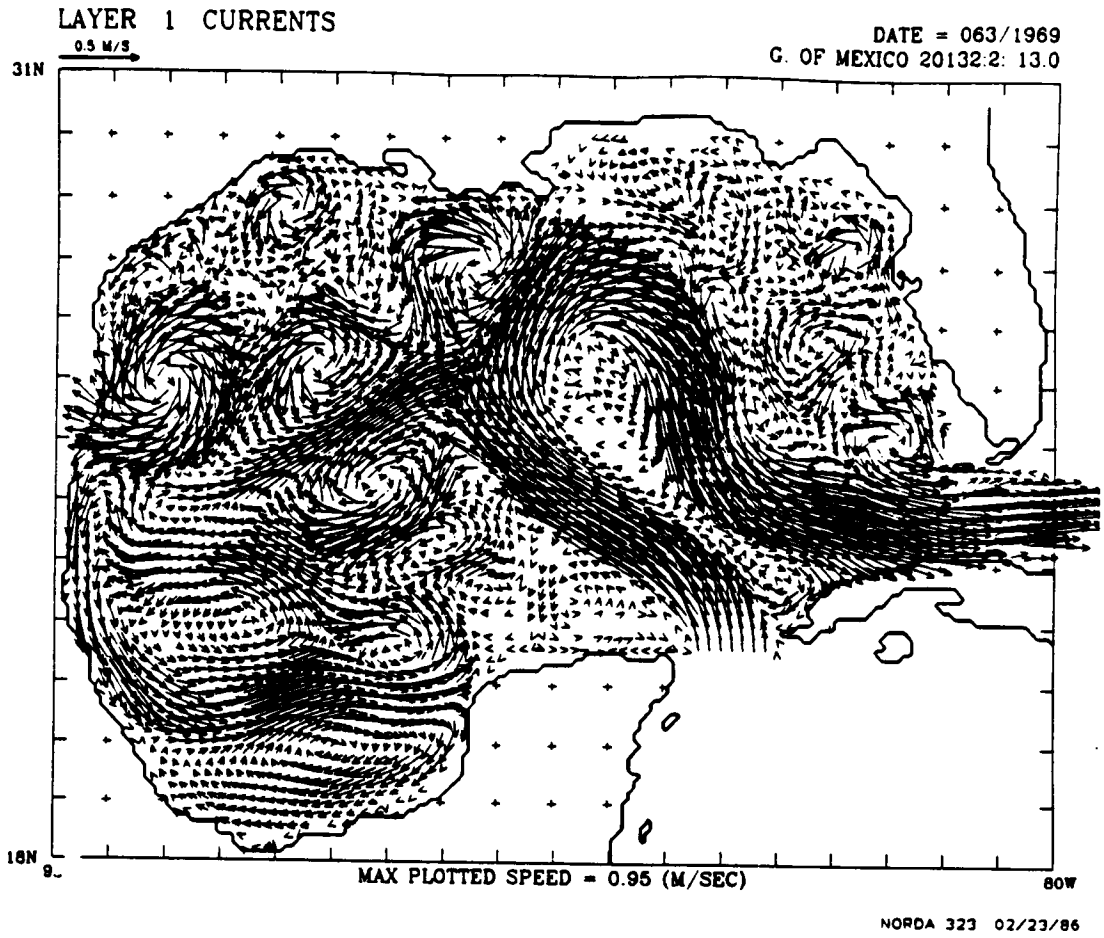
LAYER 1 CURRENTS
0.5 M/S
DATE = 063/1969
G. OF MEXICO 20132:2: 13.0
31N
18N
98W
MAX PLOTTED SPEED = 0.95 (M/SEC)
80W
NORDA 323 02/23/86

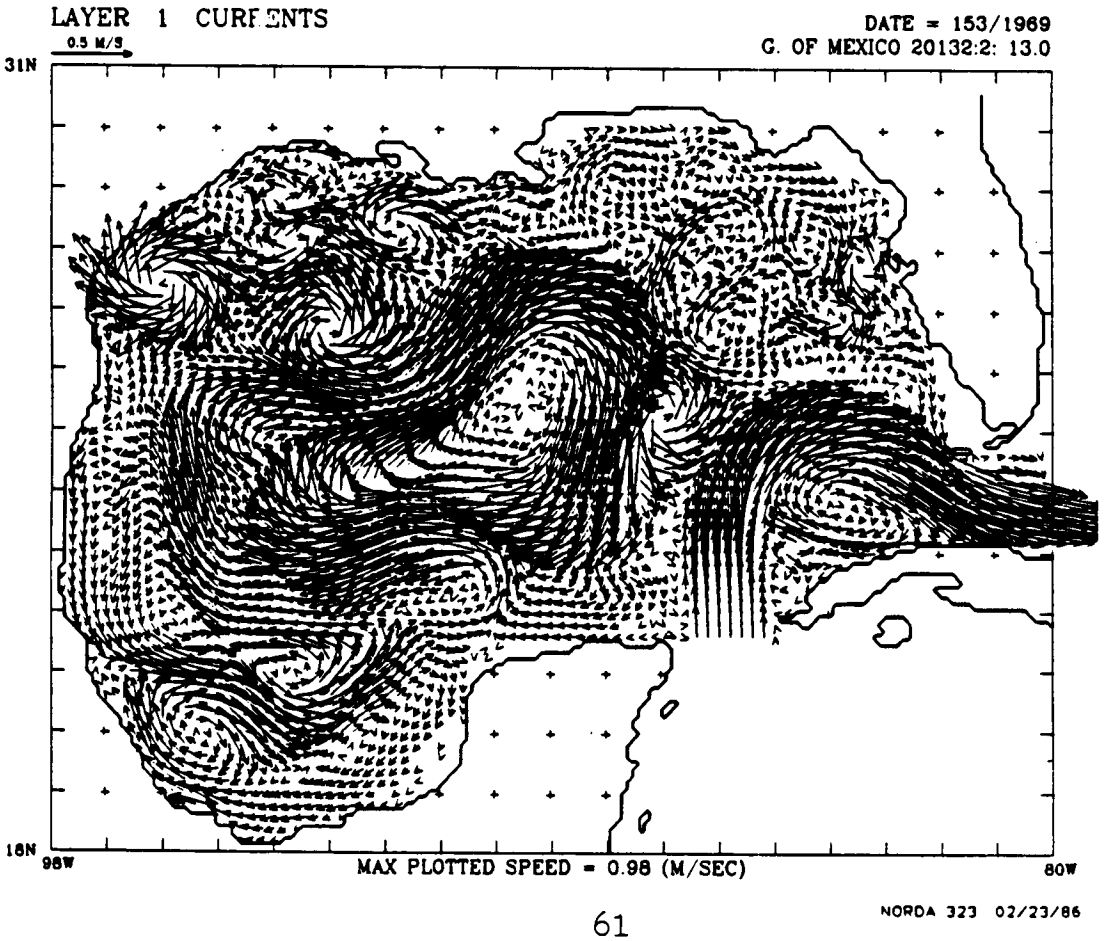
LAYER 1 CURRENTS
0.5 M/S
DATE = 153/1969
G. OF MEXICO 20132:2: 13.0
31N
18N
98W
MAX PLOTTED SPEED = 0.98 (M/SEC)
80W
NORDA 323 02/23/86

FIGURE 28

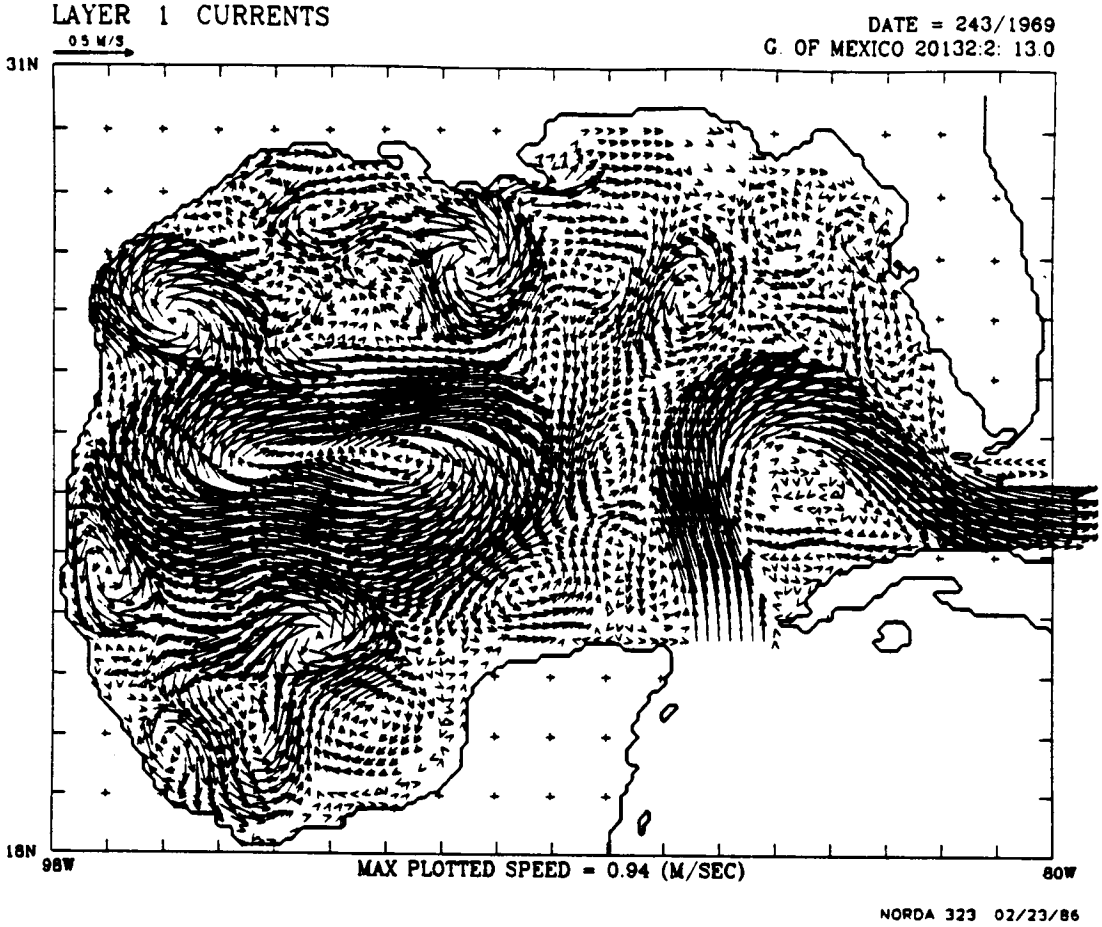
LAYER 1 CURRENTS
0.5 M/S
DATE = 243/1969
G. OF MEXICO 20132:2: 13.0
31N
18N
98W
80W
MAX PLOTTED SPEED = 0.94 (M/SEC)
NORDA 323 02/23/86

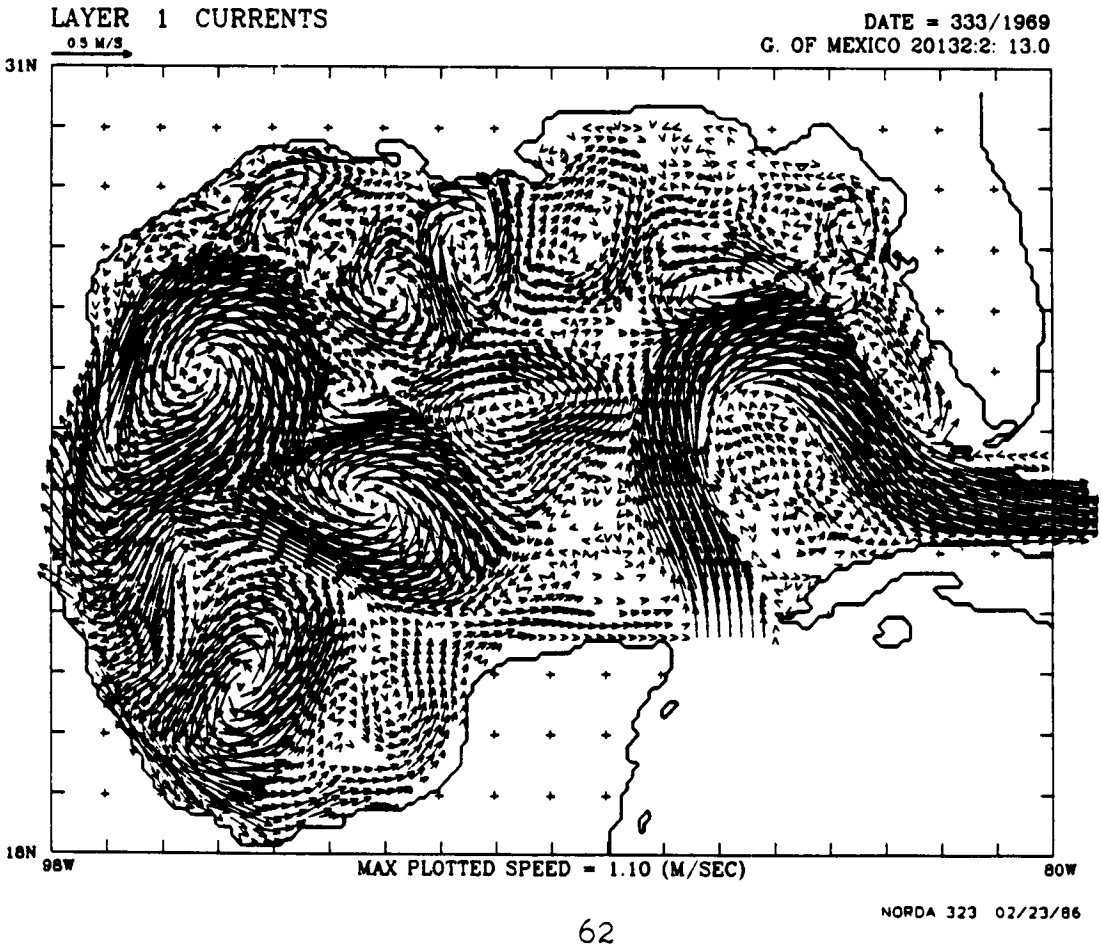
LAYER 1 CURRENTS
0.5 M/S
DATE = 333/1969
G. OF MEXICO 20132:2: 13.0
31N
18N
98W
80W
MAX PLOTTED SPEED = 1.10 (M/SEC)
NORDA 323 02/23/86

FIGURE 29: Instantaneous view of the (a) upper and (b) lower layer averaged velocities from Experiment 201/17.0 on model day 2070. Since this experiment has no wind forcing the assigned date (264/1965) is arbitrary. Vectors are only plotted at every second model grid point, i.e., every 0.2 degrees, and all velocities greater than 50 cm/sec are plotted as 50 cm/sec.

FIGURE 30: Instantaneous view of the (a) upper and (b) lower layer averaged velocities from Experiment 201/17.0 on model day 2160. Since this experiment has no wind forcing the assigned date (354/1965) is arbitrary. Vectors are only plotted at every second model grid point, i.e., every 0.2 degrees, and all velocities greater than 50 cm/sec are plotted as 50 cm/sec.

FIGURE 31: Instantaneous view of the (a) upper and (b) lower layer averaged velocities from Experiment 201/17.0 on model day 2250. Since this experiment has no wind forcing the assigned date (079/1966) is arbitrary. Vectors are only plotted at every second model grid point, i.e., every 0.2 degrees, and all velocities greater than 50 cm/sec are plotted as 50 cm/sec.

FIGURE 32: Instantaneous view of the (a) upper and (b) lower layer averaged velocities from Experiment 201/17.0 on model day 2340. Since this experiment has no wind forcing the assigned date (169/1966) is arbitrary. Vectors are only plotted at every second model grid point, i.e., every 0.2 degrees, and all velocities greater than 50 cm/sec are plotted as 50 cm/sec.

FIGURE 33: Instantaneous view of the (a) upper and (b) lower layer averaged velocities from Experiment 201/17.0 on model day 2430. Since this experiment has no wind forcing the assigned date (259/1966) is arbitrary. Vectors are only plotted at every second model grid point, i.e., every 0.2 degrees, and all velocities greater than 50 cm/sec are plotted as 50 cm/sec.

FIGURE 34: Instantaneous view of the (a) upper and (b) lower layer averaged velocities from Experiment 201/17.0 on model day 2520. Since this experiment has no wind forcing the assigned date (349/1966) is arbitrary. Vectors are only plotted at every second model grid point, i.e., every 0.2 degrees, and all velocities greater than 50 cm/sec are plotted as 50 cm/sec.

FIGURE 29

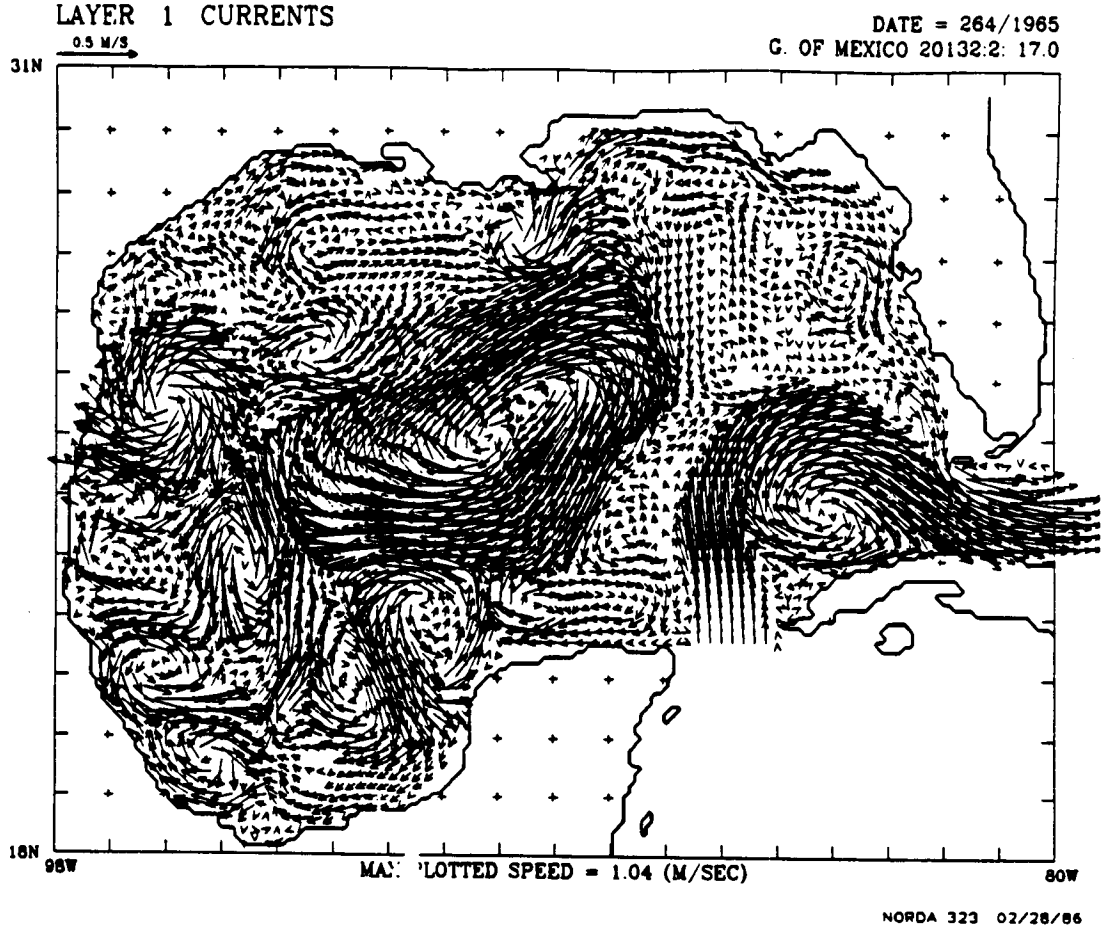
LAYER 1 CURRENTS
0.5 M/S
DATE = 264/1965
G. OF MEXICO 20132:2: 17.0
31N
16N
98W
80W
MAX PLOTTED SPEED = 1.04 (M/SEC)
NORDA 323 02/28/86

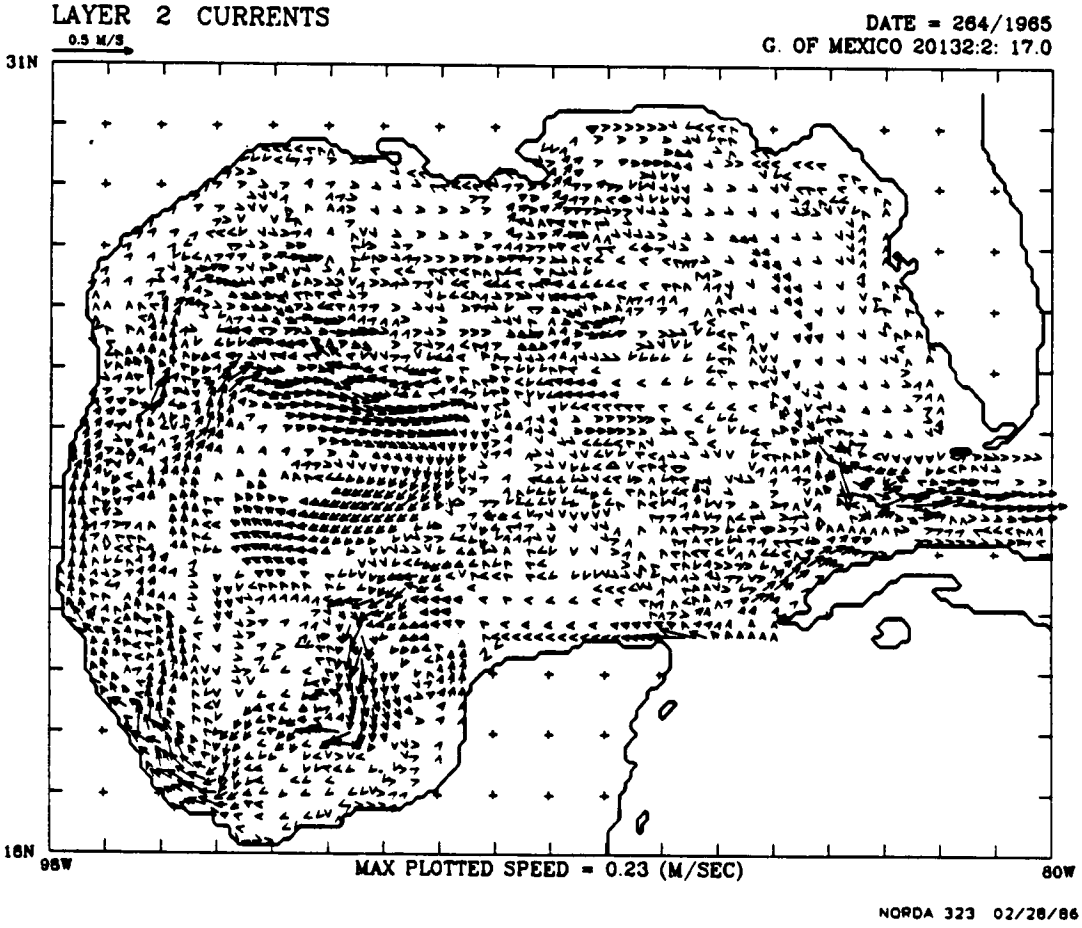
LAYER 2 CURRENTS
0.5 M/S
DATE = 264/1965
G. OF MEXICO 20132:2: 17.0
31N
16N
98W
80W
MAX PLOTTED SPEED = 0.23 (M/SEC)
NORDA 323 02/28/86

FIGURE 30

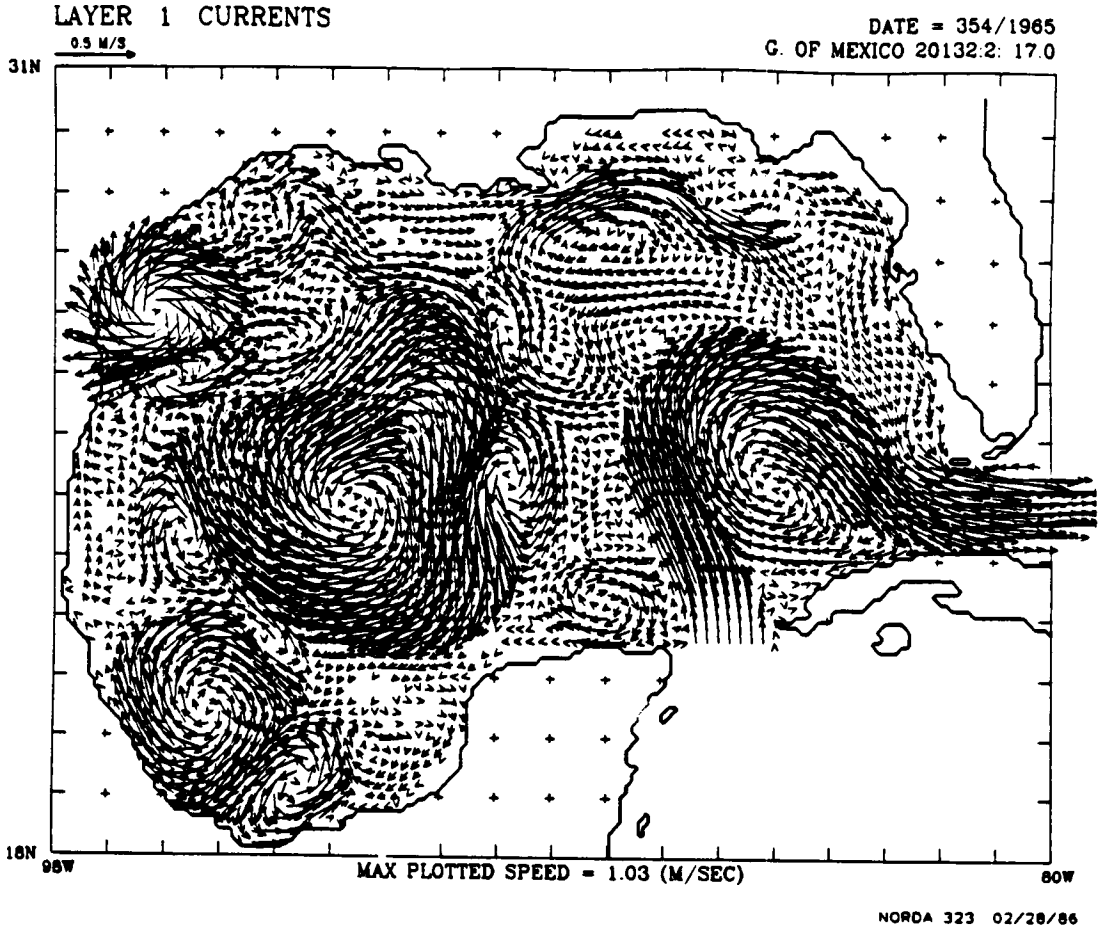
LAYER 1 CURRENTS
0.5 M/S
DATE = 354/1965
G. OF MEXICO 20132:2: 17.0
31N
18N
98W
80W
MAX PLOTTED SPEED = 1.03 (M/SEC)
NORDA 323 02/28/86

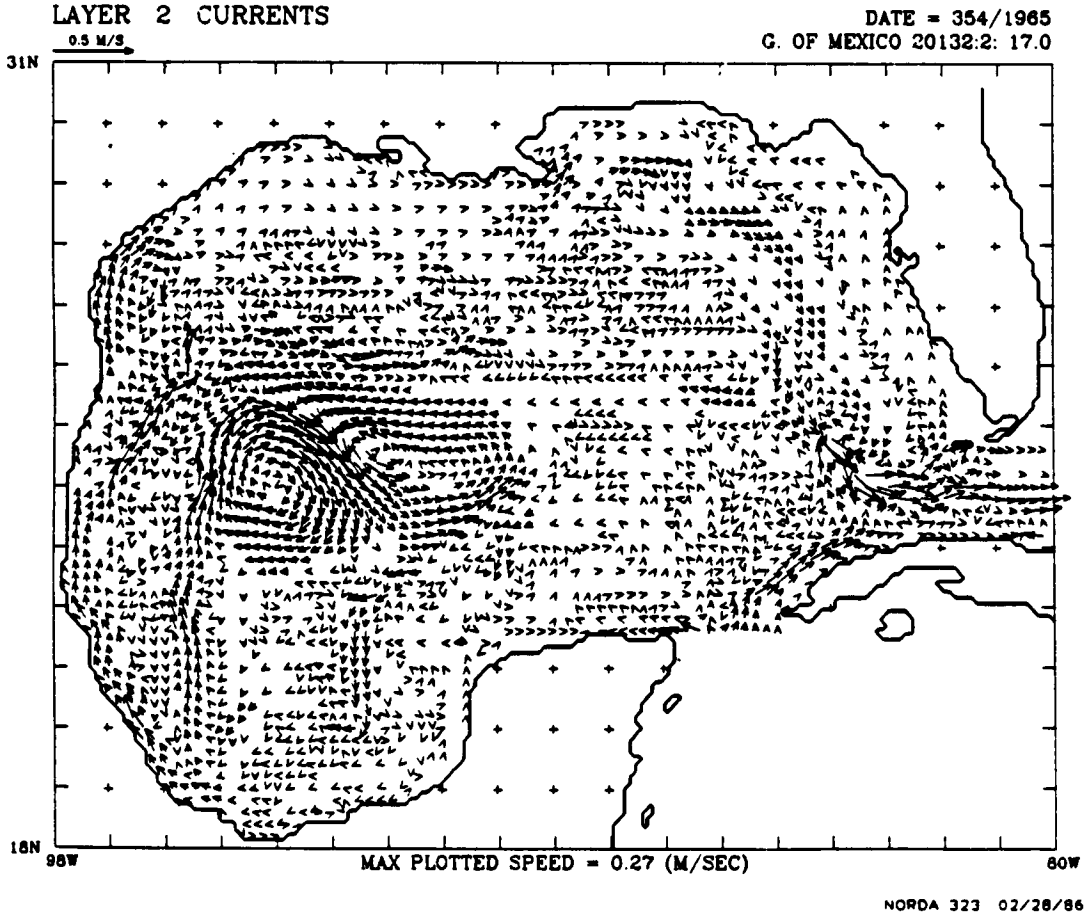
LAYER 2 CURRENTS
0.5 M/S
DATE = 354/1965
G. OF MEXICO 20132:2: 17.0
31N
18N
98W
80W
MAX PLOTTED SPEED = 0.27 (M/SEC)
NORDA 323 02/28/86

FIGURE 31

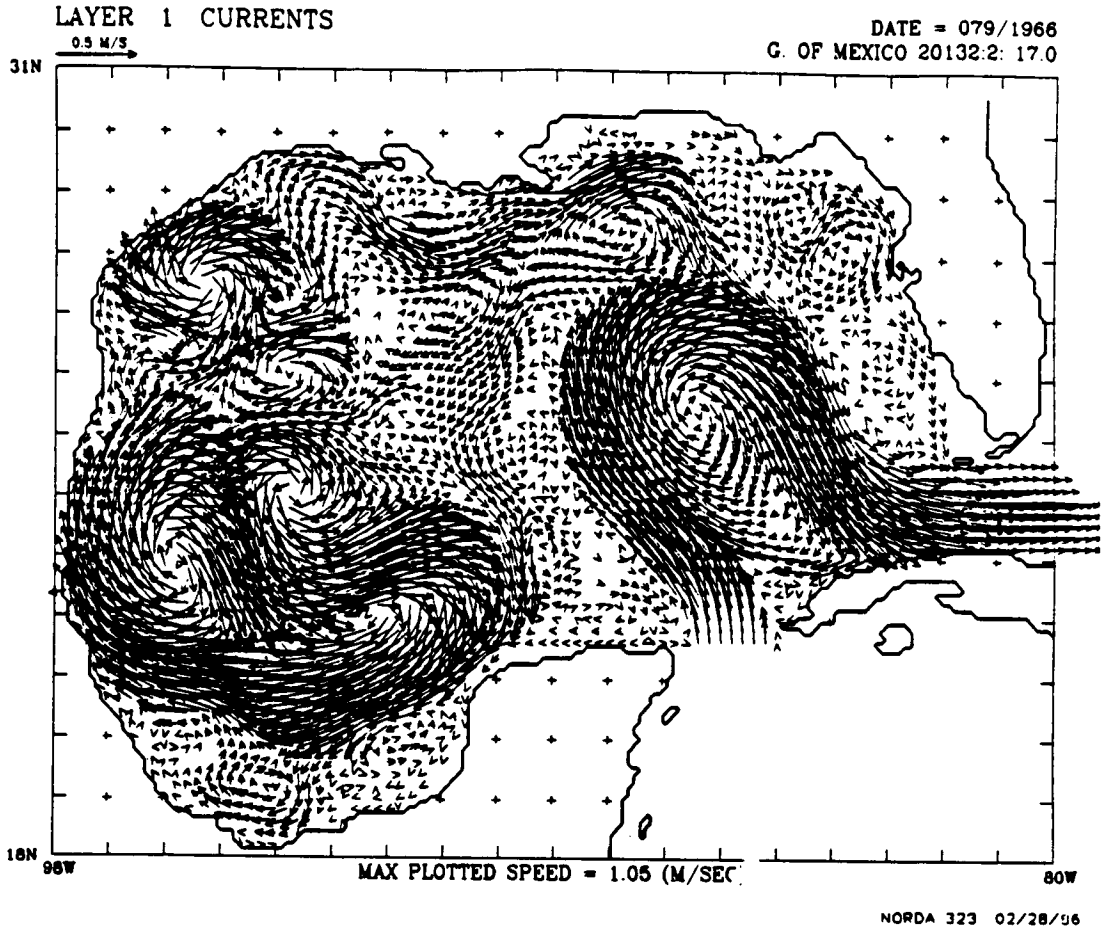
LAYER 1 CURRENTS
0.5 M/S
DATE = 079/1966
G. OF MEXICO 20132:2: 17.0
31N
18N
98W
80W
MAX PLOTTED SPEED = 1.05 (M/SEC)
NORDA 323 02/28/86

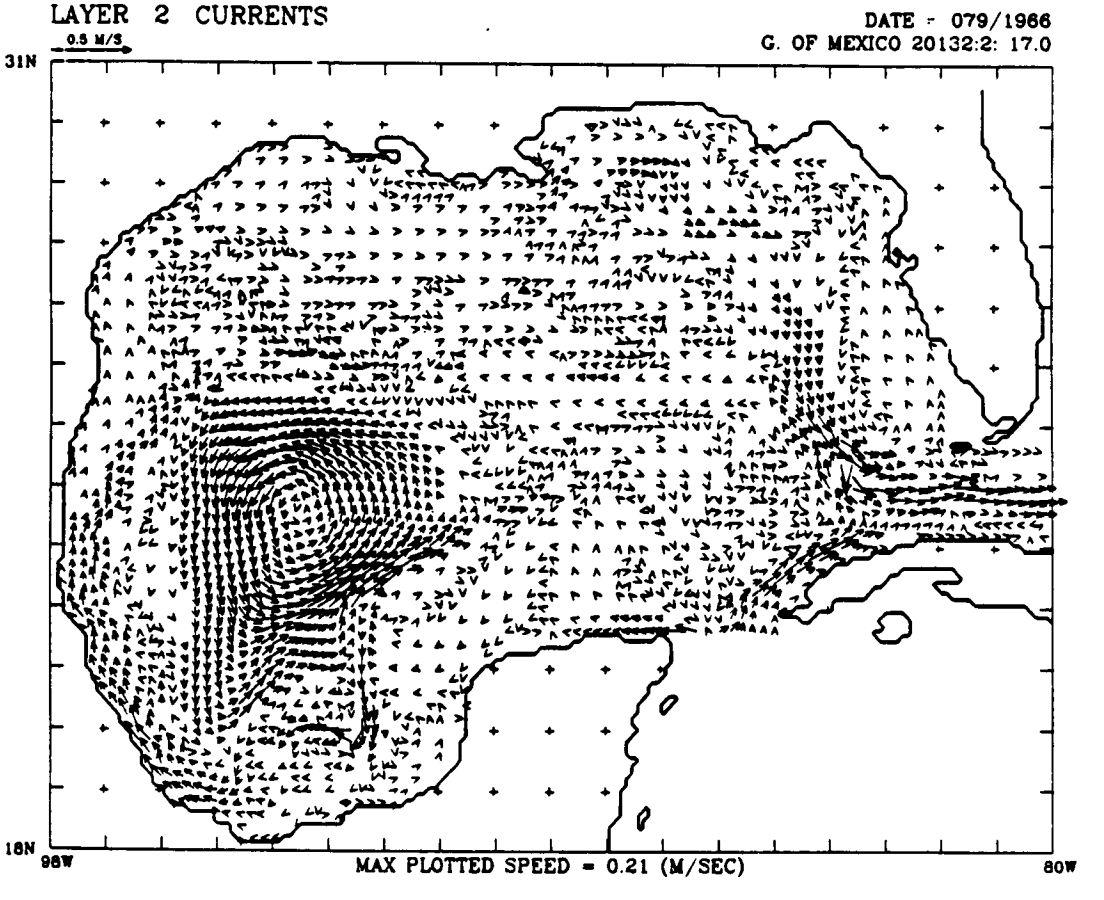
LAYER 2 CURRENTS
0.5 M/S
DATE = 079/1966
G. OF MEXICO 20132:2: 17.0
31N
18N
98W
80W
MAX PLOTTED SPEED = 0.21 (M/SEC)
NORDA 323 02/28/86

FIGURE 32

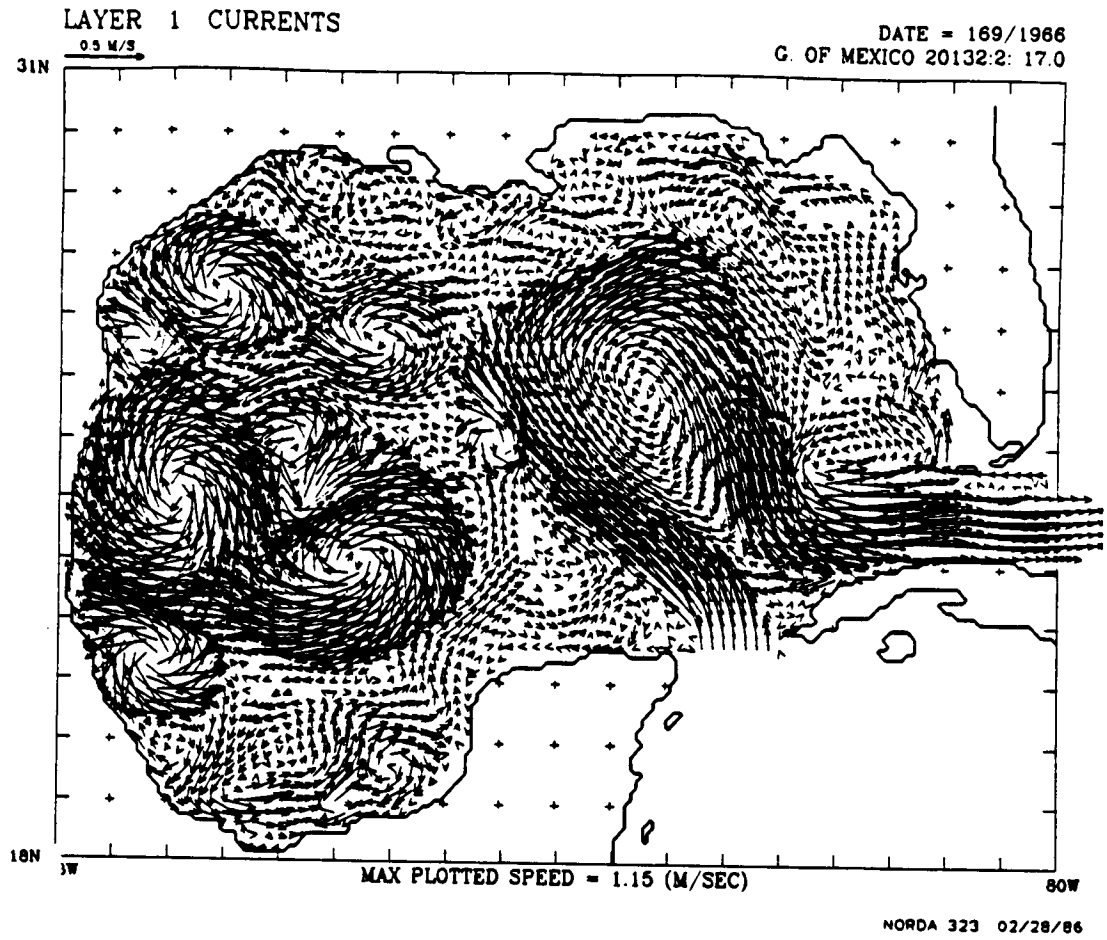
LAYER 1 CURRENTS
0.5 M/S
DATE = 169/1966
G. OF MEXICO 20132:2: 17.0
31N
18N
98W
80W
MAX PLOTTED SPEED = 1.15 (M/SEC)
NORDA 323 02/28/86

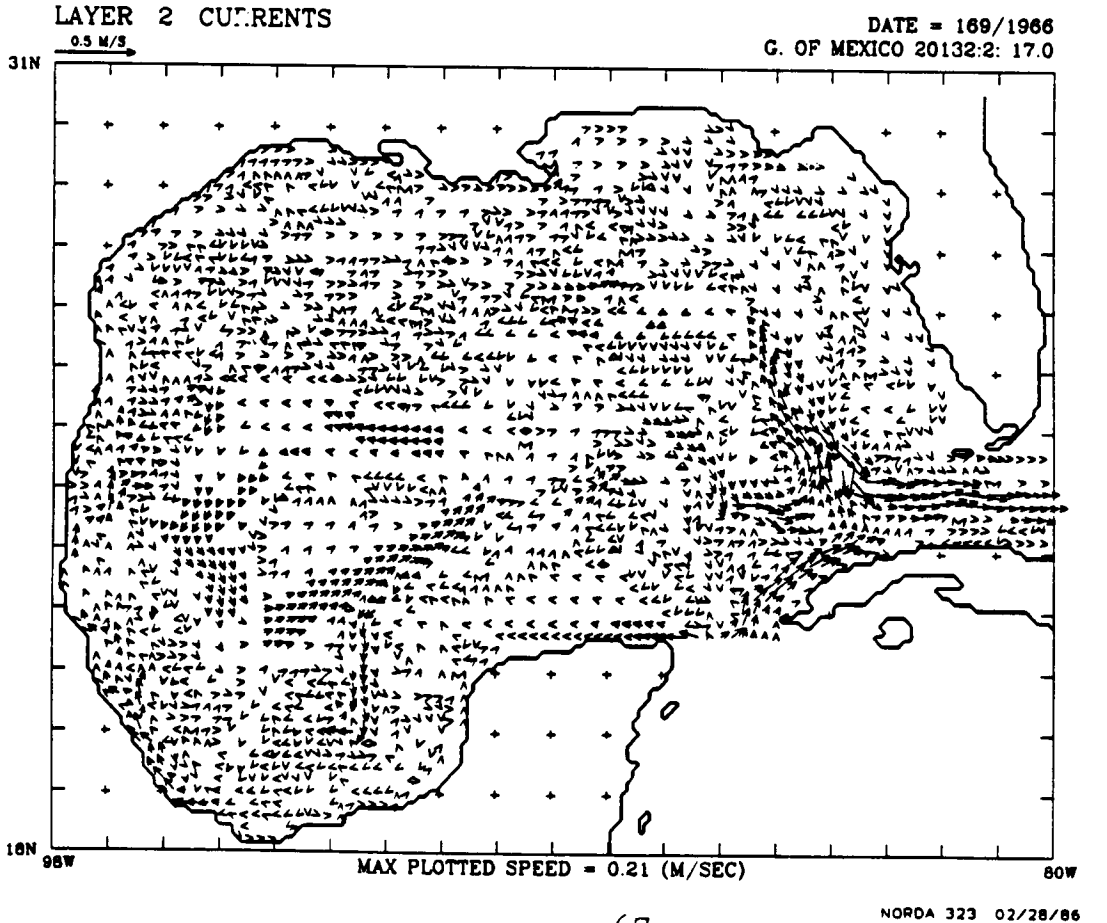
LAYER 2 CURRENTS
0.5 M/S
DATE = 169/1966
G. OF MEXICO 20132:2: 17.0
31N
18N
98W
80W
MAX PLOTTED SPEED = 0.21 (M/SEC)
NORDA 323 02/28/86

FIGURE 33

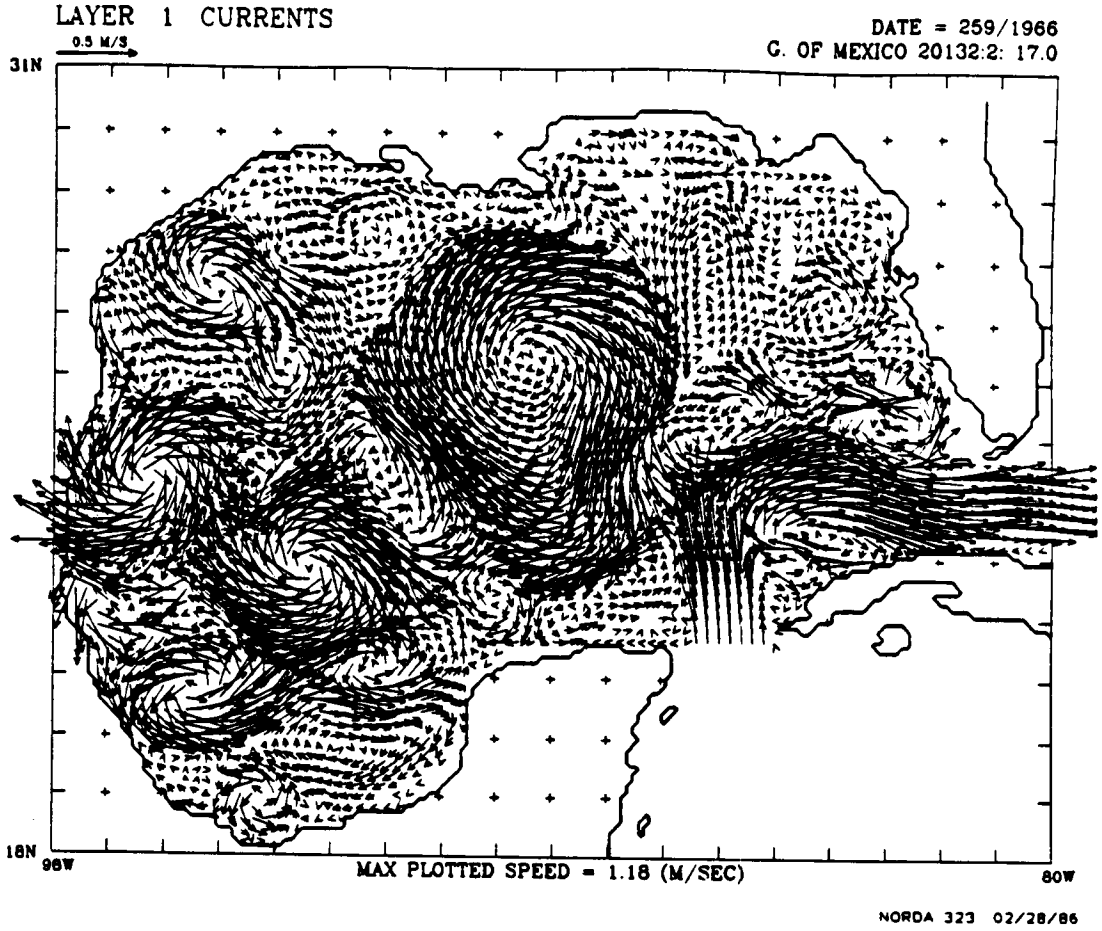
LAYER 1 CURRENTS
0.5 M/S
DATE = 259/1966
G. OF MEXICO 20132:2: 17.0
31N
18N
98W
80W
MAX PLOTTED SPEED = 1.18 (M/SEC)
NORDA 323 02/28/86

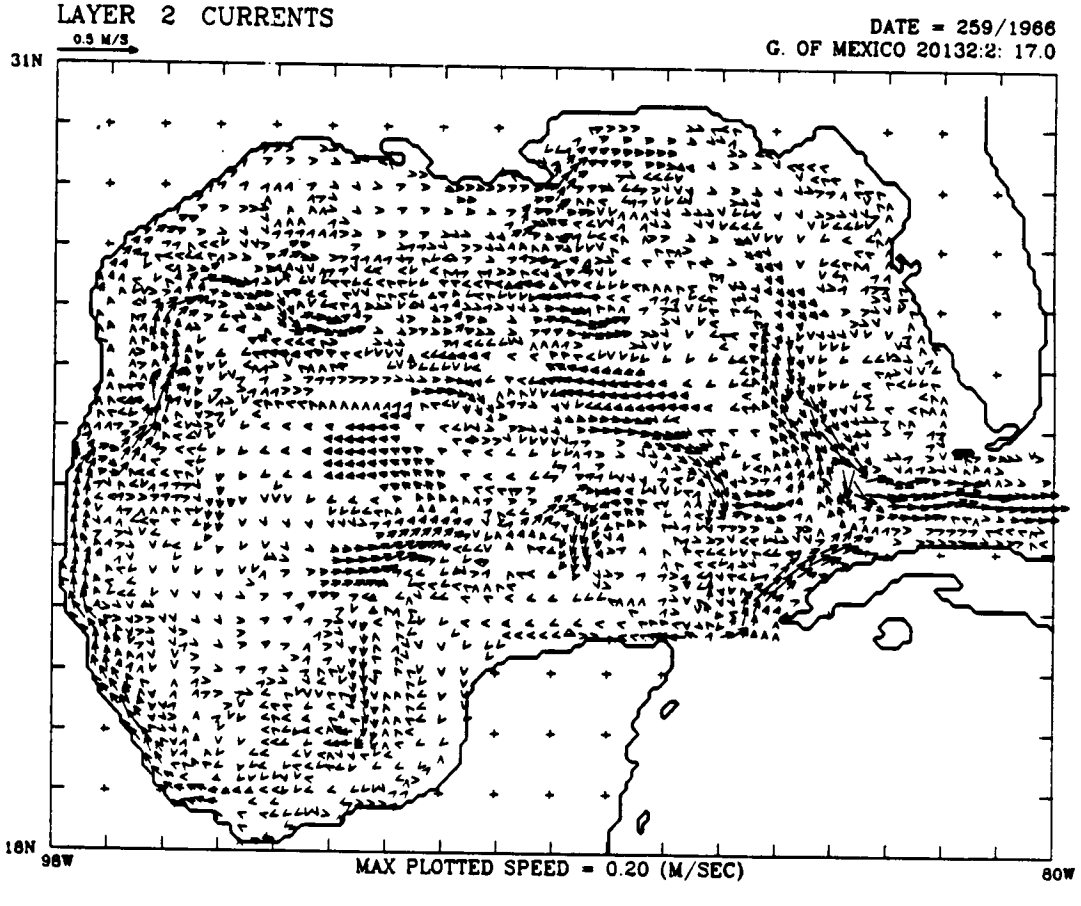
LAYER 2 CURRENTS
0.5 M/S
DATE = 259/1966
G. OF MEXICO 20132:2: 17.0
31N
18N
98W
80W
MAX PLOTTED SPEED = 0.20 (M/SEC)
NORDA 323 02/28/86

FIGURE 34

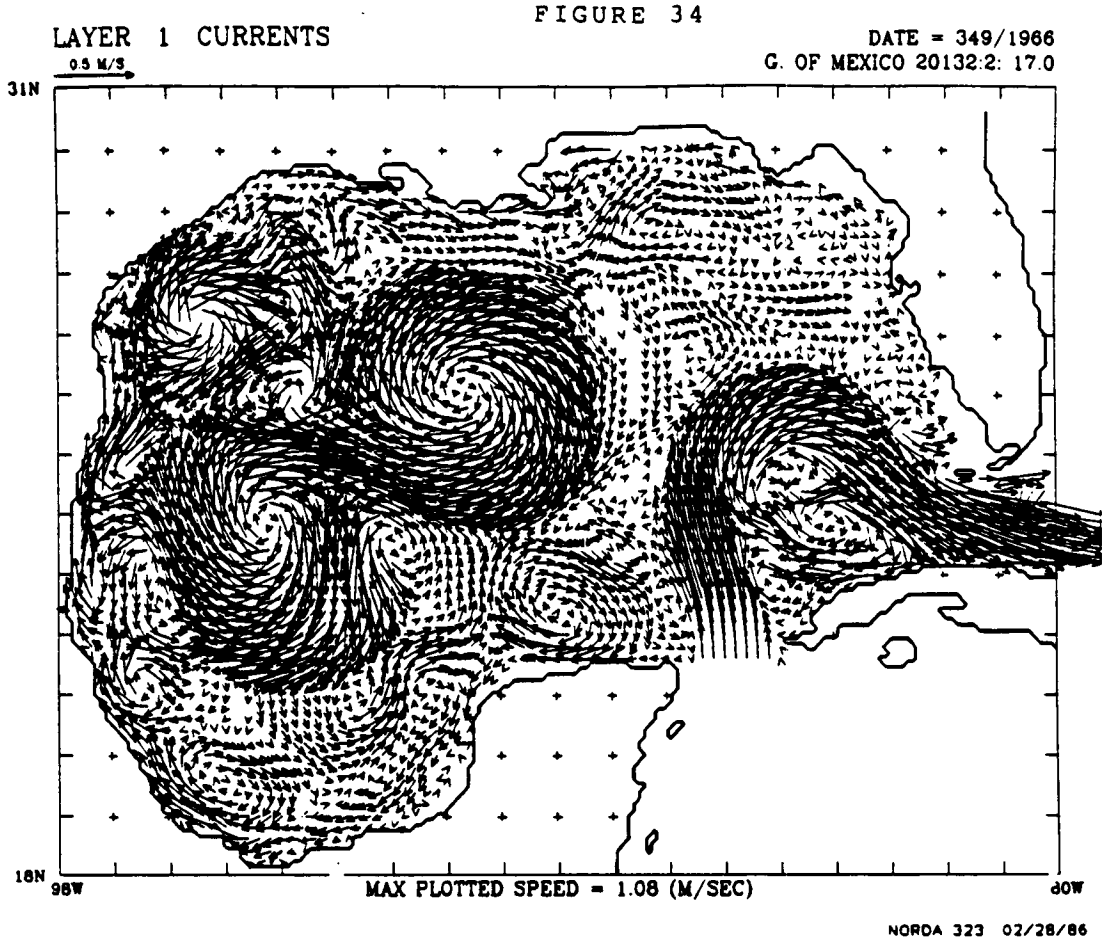
LAYER 1 CURRENTS
0.5 M/S
DATE = 349/1966
G. OF MEXICO 20132:2: 17.0
31N
18N
98W
MAX PLOTTED SPEED = 1.08 (M/SEC)
80W
NORDA 323 02/28/86

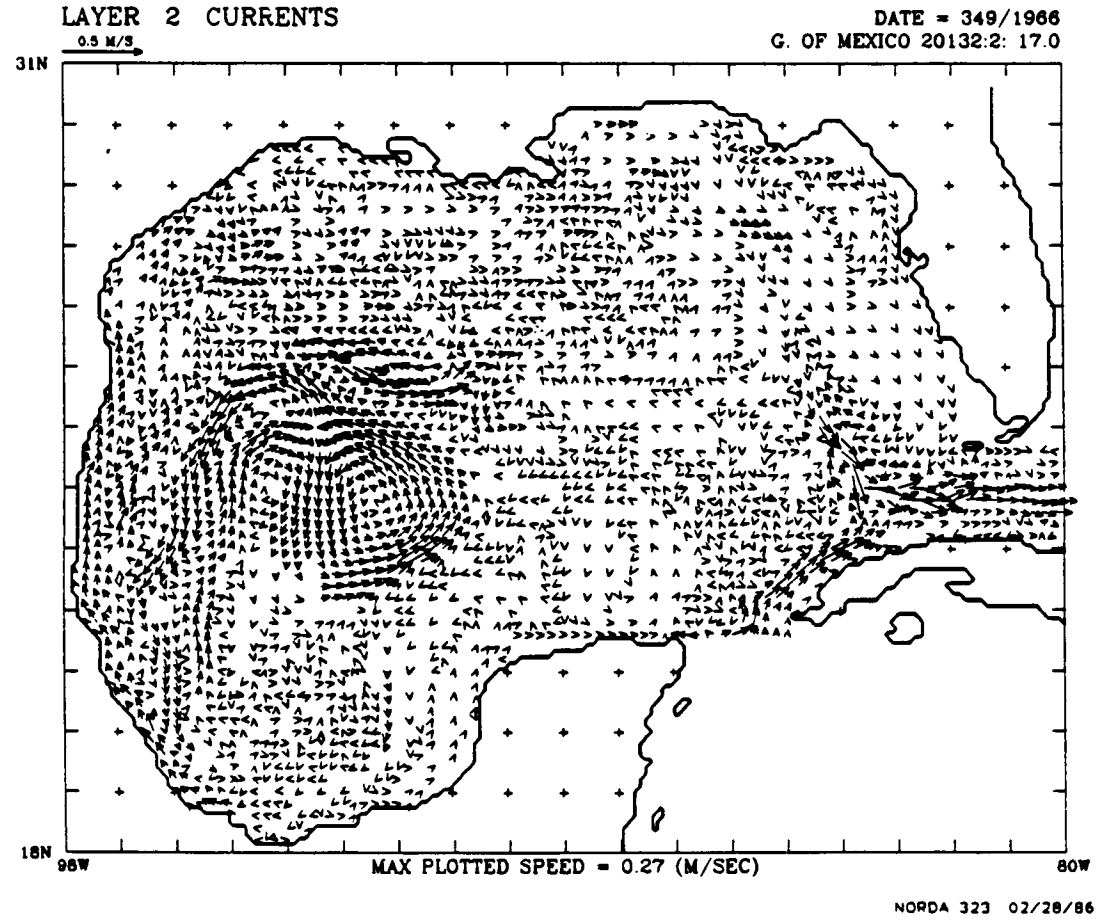
LAYER 2 CURRENTS
0.5 M/S
DATE = 349/1966
G. OF MEXICO 20132:2: 17.0
31N
18N
98W
MAX PLOTTED SPEED = 0.27 (M/SEC)
80W
NORDA 323 02/28/86

FIGURE 35: Instantaneous view of the upper layer averaged velocities from Experiment 201/16.0 on model days (a) 2880, and (b) 2970. The assigned dates (344/1967 and 069/1968) indicate the applied wind forcing, but the experiment was not a hindcast and the ocean currents in the Gulf on that date might have been quite different from those shown. Vectors are only plotted at every second model grid point, i.e., every 0.2 degrees, and all velocities greater than 50 cm/sec are plotted as 50 cm/sec.

FIGURE 36: Instantaneous view of the upper layer averaged velocities from Experiment 201/16.0 on model days (a) 3060, and (b) 3150. The assigned dates (159/1968 and 249/1968) indicate the applied wind forcing, but the experiment was not a hindcast and the ocean currents in the Gulf on that date might have been quite different from those shown. Vectors are only plotted at every second model grid point, i.e., every 0.2 degrees, and all velocities greater than 50 cm/sec are plotted as 50 cm/sec.

FIGURE 37: Instantaneous view of the upper layer averaged velocities from Experiment 201/16.0 on model days (a) 3240, and (b) 3330. The assigned dates (339/1968 and 063/1969) indicate the applied wind forcing, but the experiment was not a hindcast and the ocean currents in the Gulf on that date might have been quite different from those shown. Vectors are only plotted at every second model grid point, i.e., every 0.2 degrees, and all velocities greater than 50 cm/sec are plotted as 50 cm/sec.

FIGURE 38: Instantaneous view of the upper layer averaged velocities from Experiment 201/16.0 on model days (a) 3420, and (b) 2510. The assigned dates (153/1969 and 243/1969) indicate the applied wind forcing, but the experiment was not a hindcast and the ocean currents in the Gulf on that date might have been quite different from those shown. Vectors are only plotted at every second model grid point, i.e., every 0.2 degrees, and all velocities greater than 50 cm/sec are plotted as 50 cm/sec.

FIGURE 39: Instantaneous view of the upper layer averaged velocities from Experiment 201/16.0 on model days (a) 3600, and (b) 3690. The assigned dates (333/1969 and 058/1970) indicate the applied wind forcing, but the experiment was not a hindcast and the ocean currents in the Gulf on that date might have been quite different from those shown. Vectors are only plotted at every second model grid point, i.e., every 0.2 degrees, and all velocities greater than 50 cm/sec are plotted as 50 cm/sec.

FIGURE 35

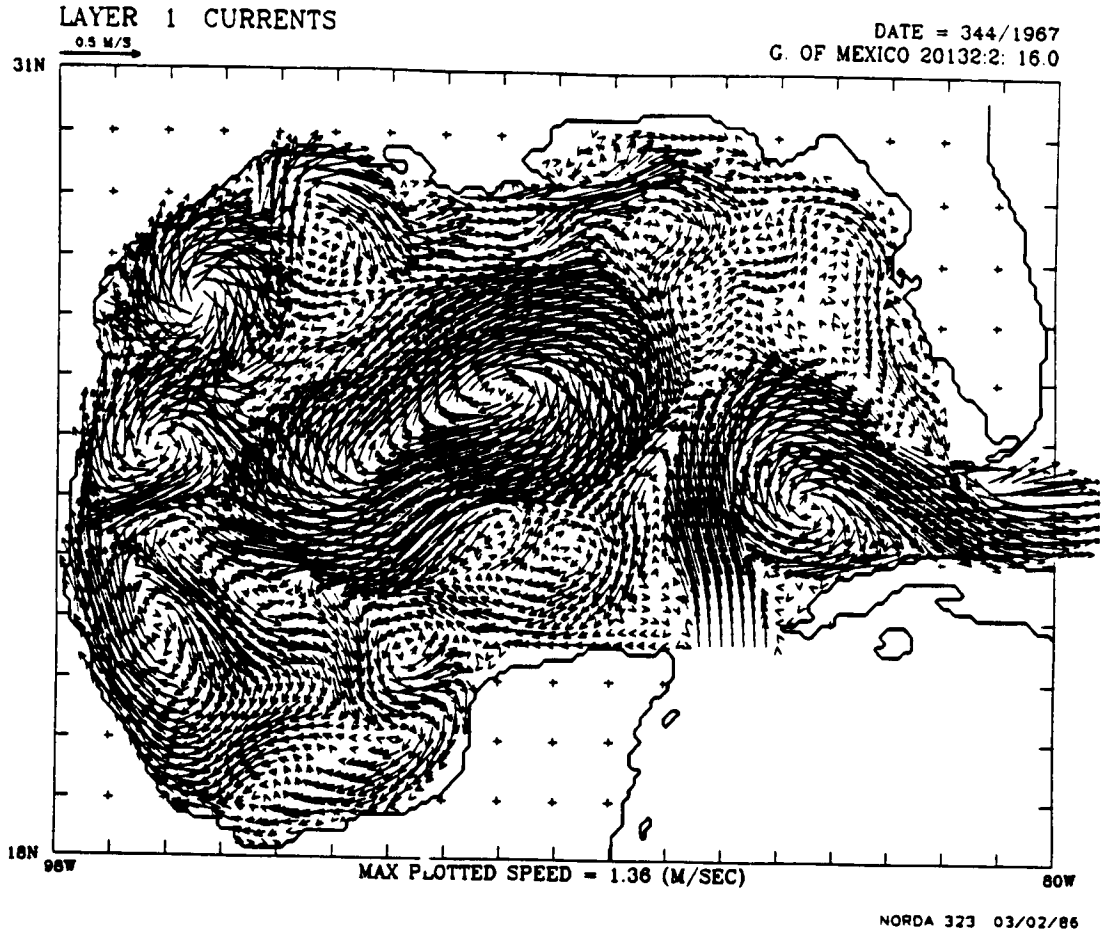
LAYER 1 CURRENTS
0.5 M/S
DATE = 344/1967
G. OF MEXICO 20132:2: 16.0
31N
18N
98W
80W
MAX PLOTTED SPEED = 1.36 (M/SEC)
NORDA 323 03/02/86

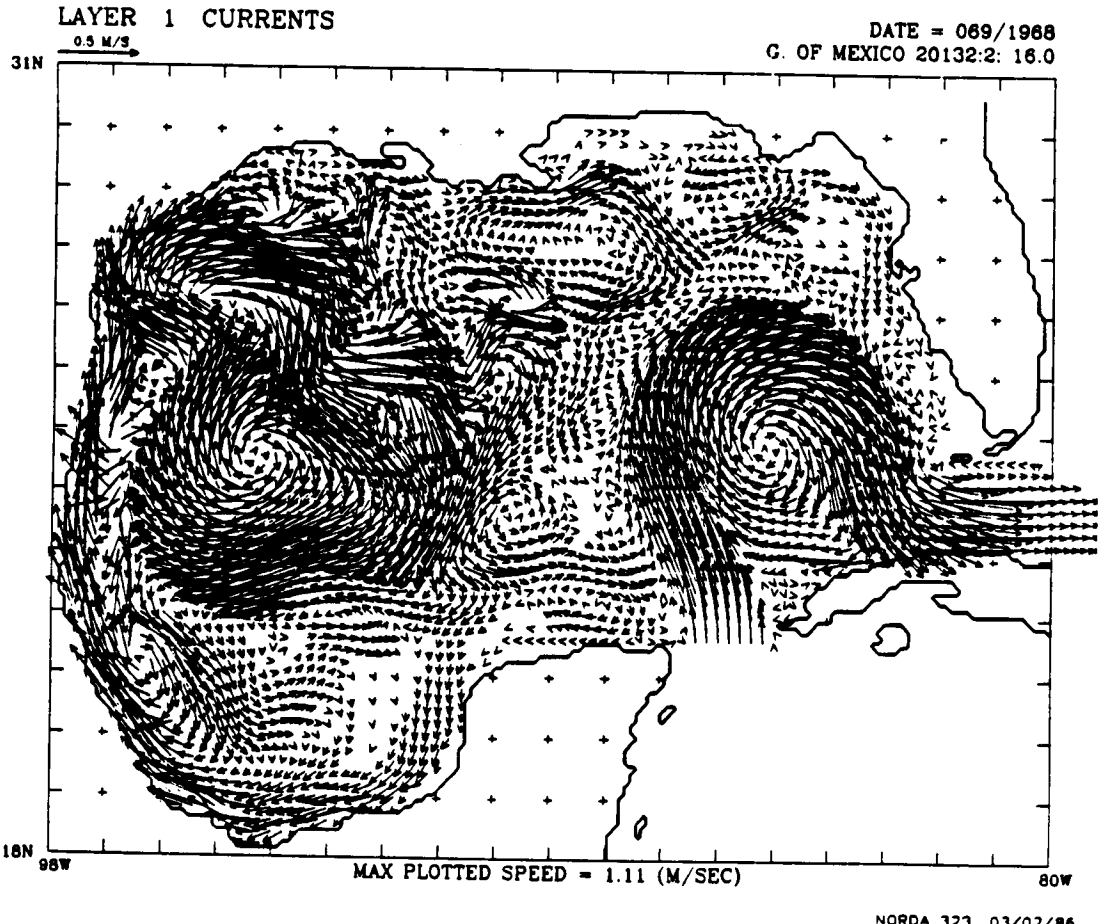
LAYER 1 CURRENTS
0.5 M/S
DATE = 069/1968
G. OF MEXICO 20132:2: 16.0
31N
18N
98W
80W
MAX PLOTTED SPEED = 1.11 (M/SEC)
NORDA 323 03/02/86

FIGURE 36

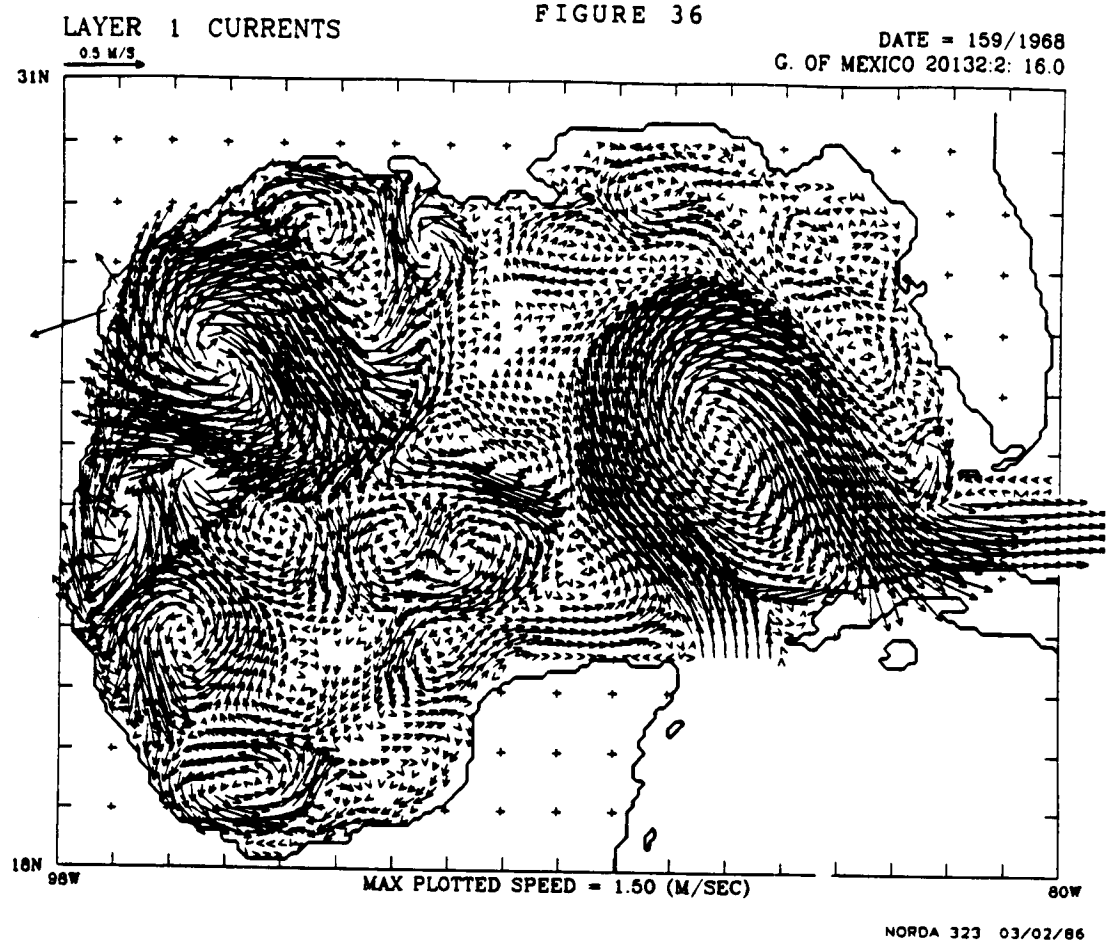
LAYER 1 CURRENTS
0.5 M/S
DATE = 159/1968
G. OF MEXICO 20132:2: 16.0
31N
18N
98W
80W
MAX PLOTTED SPEED = 1.50 (M/SEC)
NORDA 323 03/02/86

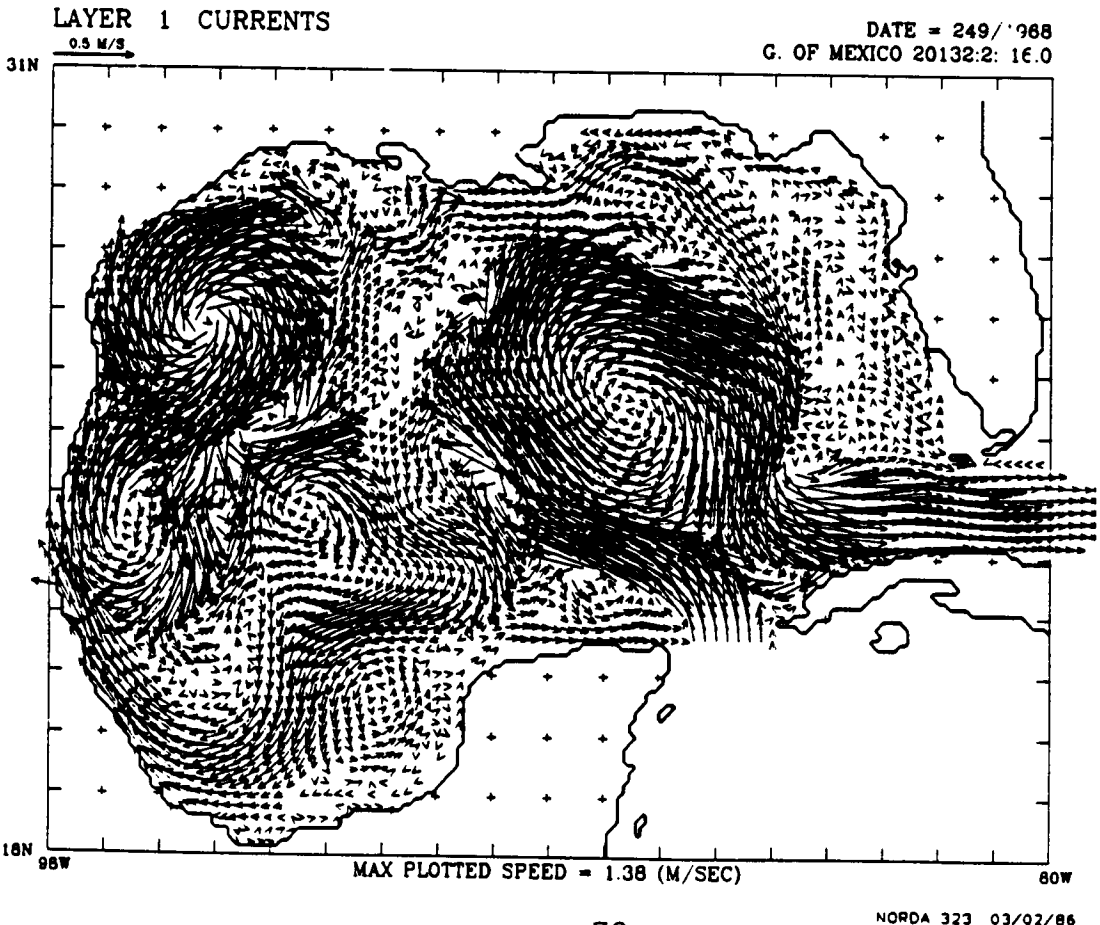
LAYER 1 CURRENTS
0.5 M/S
DATE = 249/1968
G. OF MEXICO 20132:2: 16.0
31N
18N
98W
80W
MAX PLOTTED SPEED = 1.38 (M/SEC)
NORDA 323 03/02/86

FIGURE 37

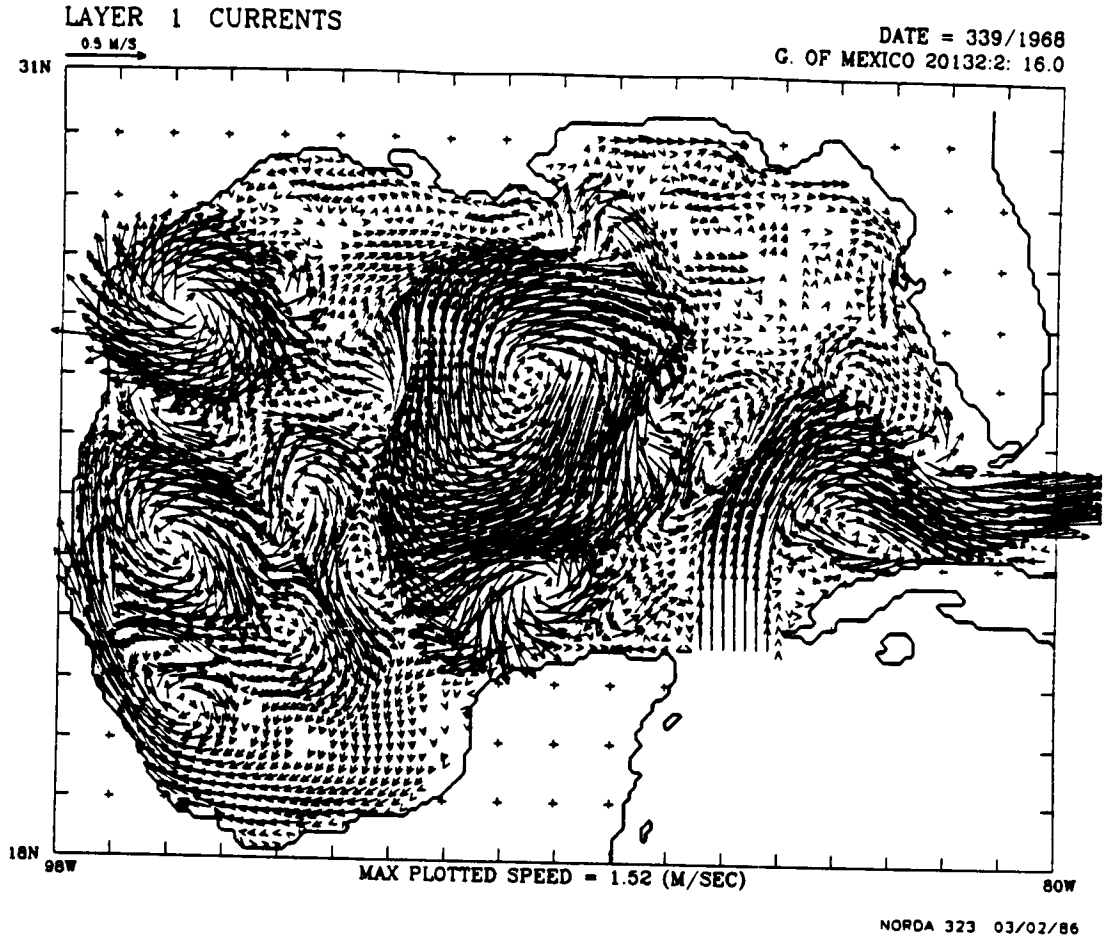
LAYER 1 CURRENTS
0.5 M/S
DATE = 339/1968
G. OF MEXICO 20132:2: 16.0
31N
18N
98W
80W
MAX PLOTTED SPEED = 1.52 (M/SEC)
NORDA 323 03/02/86

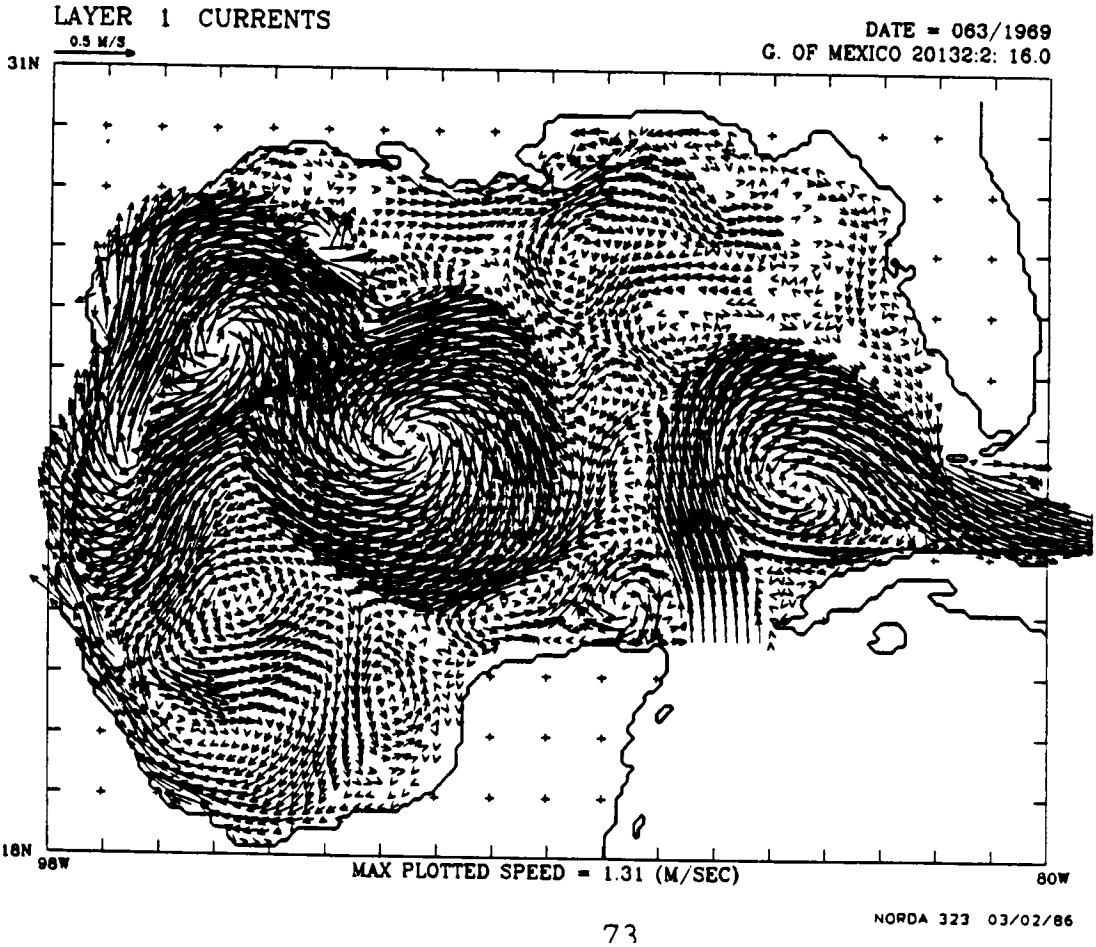
LAYER 1 CURRENTS
0.5 M/S
DATE = 063/1969
G. OF MEXICO 20132:2: 16.0
31N
18N
98W
80W
MAX PLOTTED SPEED = 1.31 (M/SEC)
NORDA 323 03/02/86

FIGURE 38

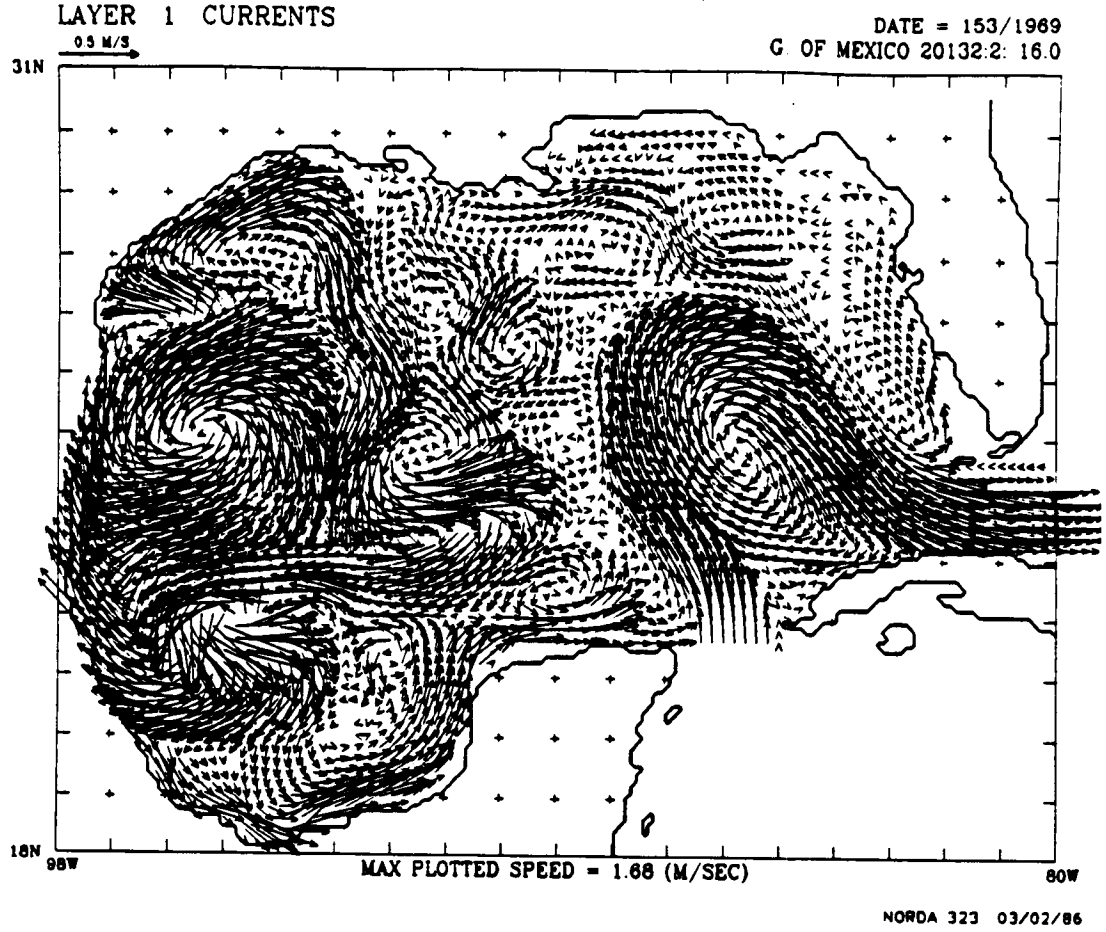
LAYER 1 CURRENTS
0.5 M/S
DATE = 153/1969
G. OF MEXICO 20132:2: 16.0
31N
18N
98W
80W
MAX PLOTTED SPEED = 1.68 (M/SEC)
NORDA 323 03/02/86

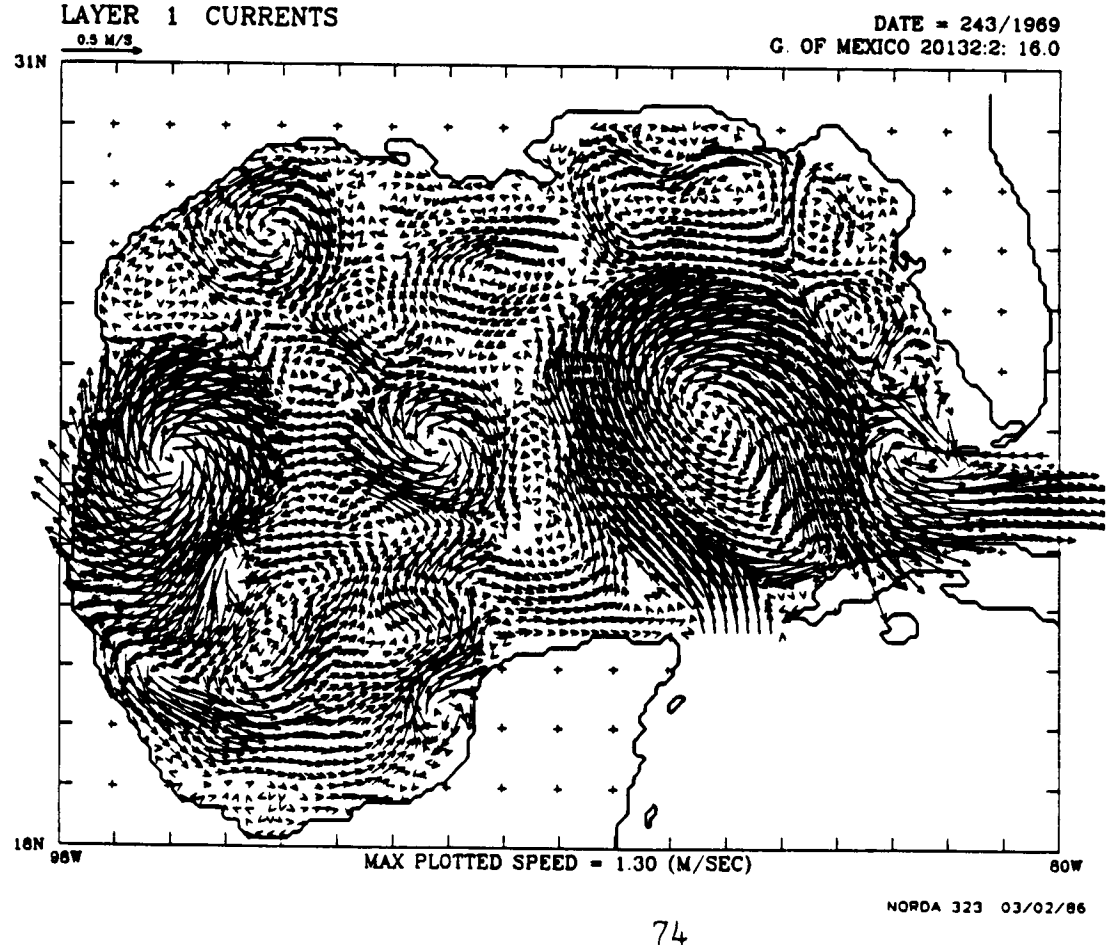
LAYER 1 CURRENTS
0.5 M/S
DATE = 243/1969
G. OF MEXICO 20132:2: 16.0
31N
18N
98W
80W
MAX PLOTTED SPEED = 1.30 (M/SEC)
NORDA 323 03/02/86

FIGURE 39

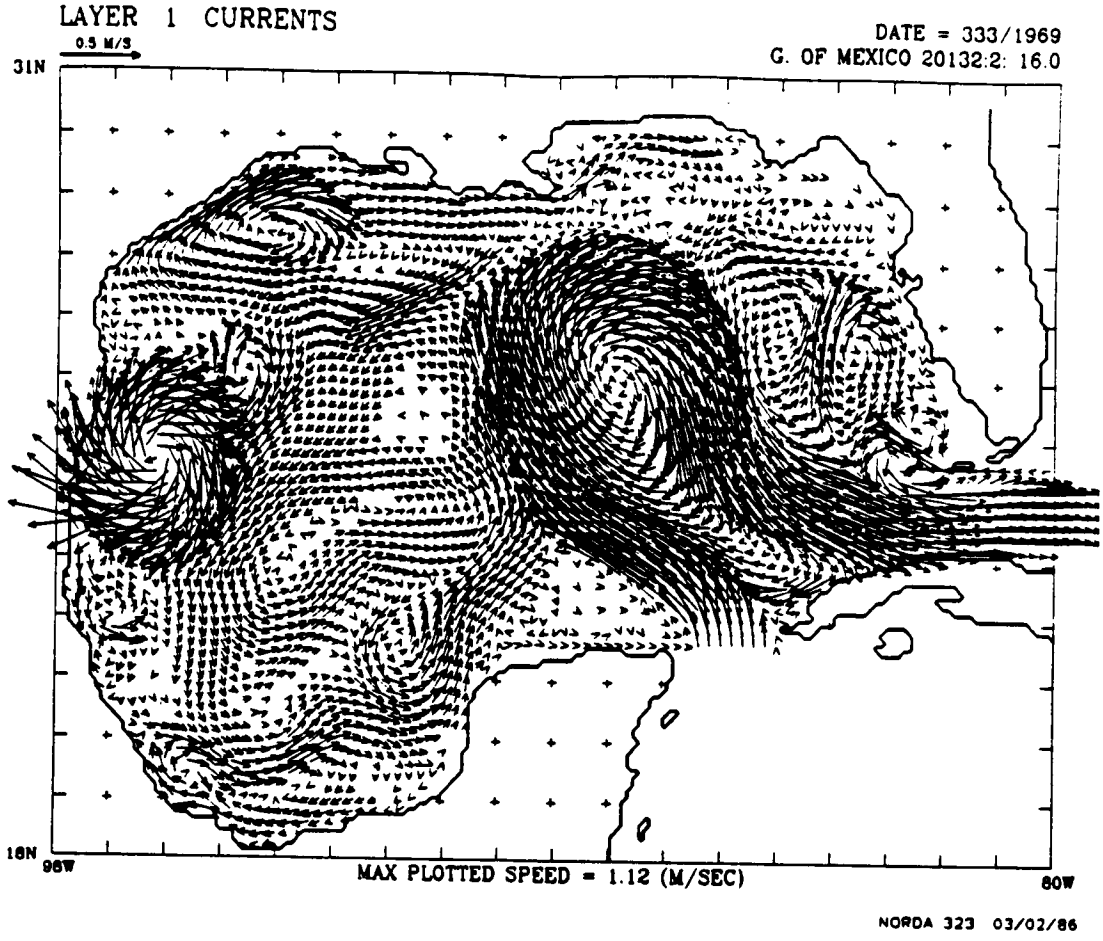
LAYER 1 CURRENTS
0.5 M/S
DATE = 333/1969
G. OF MEXICO 20132:2: 16.0
31N
18N
98W
80W
MAX PLOTTED SPEED = 1.12 (M/SEC)
NORDA 323 03/02/86

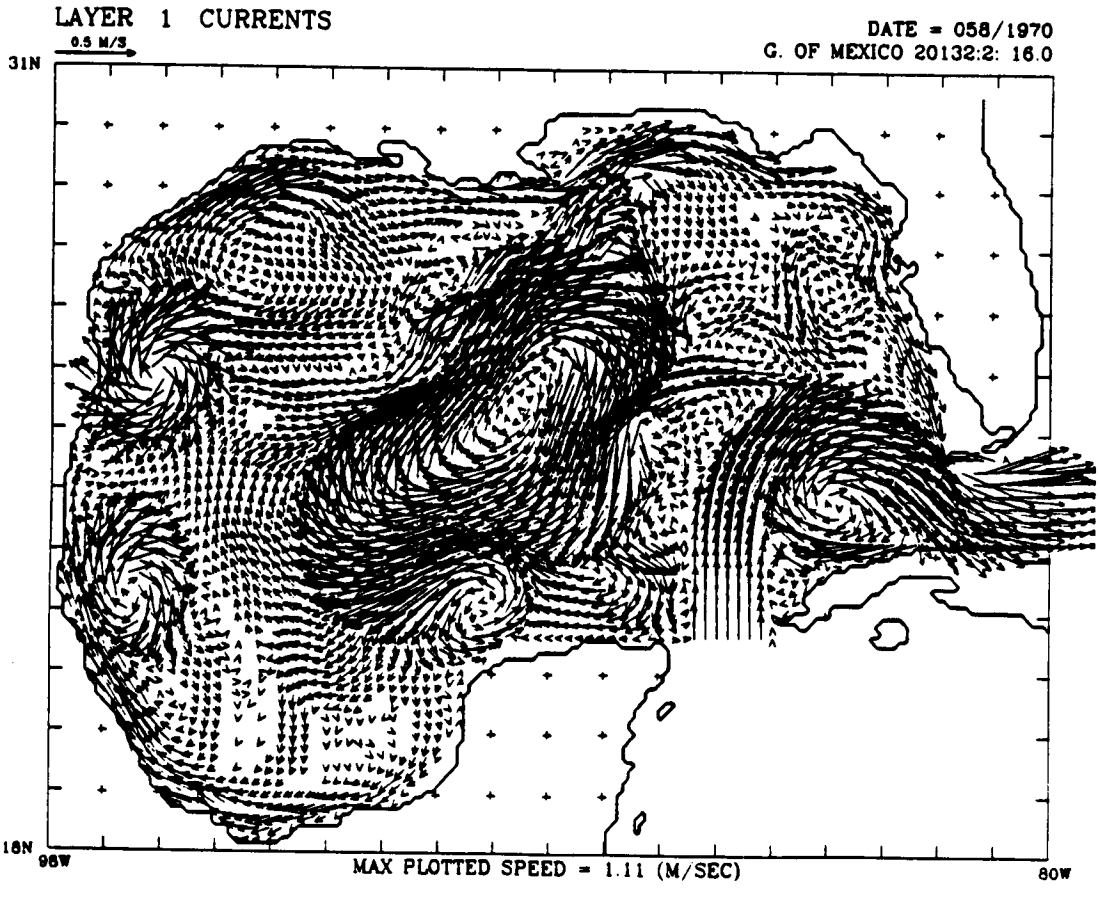
LAYER 1 CURRENTS
0.5 M/S
DATE = 058/1970
G. OF MEXICO 20132:2: 16.0
31N
18N
98W
80W
MAX PLOTTED SPEED = 1.11 (M/SEC)
NORDA 323 03/02/86

FIGURE 40: Location of moorings deployed in the eastern Gulf of Mexico for years 1 and 2 of the MMS sponsored Gulf of Mexico Physical Oceanography Study, from Waddell (1986). Locations V, W, X, Y, Z in the ocean model approximately coorespond to moorings G, A, C, D, F respectively.

FIGURE 41: Kinetic energy spectra at 100 m depth for (solid) experiment 201/13.0 at location X, and (dashed) mooring C. Variance is shown on a linear scale, but a logarithmic scale would be appropriate.

FIGURE 42: Kinetic energy spectra at 100 m depth for (solid) experiment 201/13.0 at location Z, and (dashed) mooring F. Variance is shown on a linear scale, but a logarithmic scale would be more appropriate.

FIGURE 40

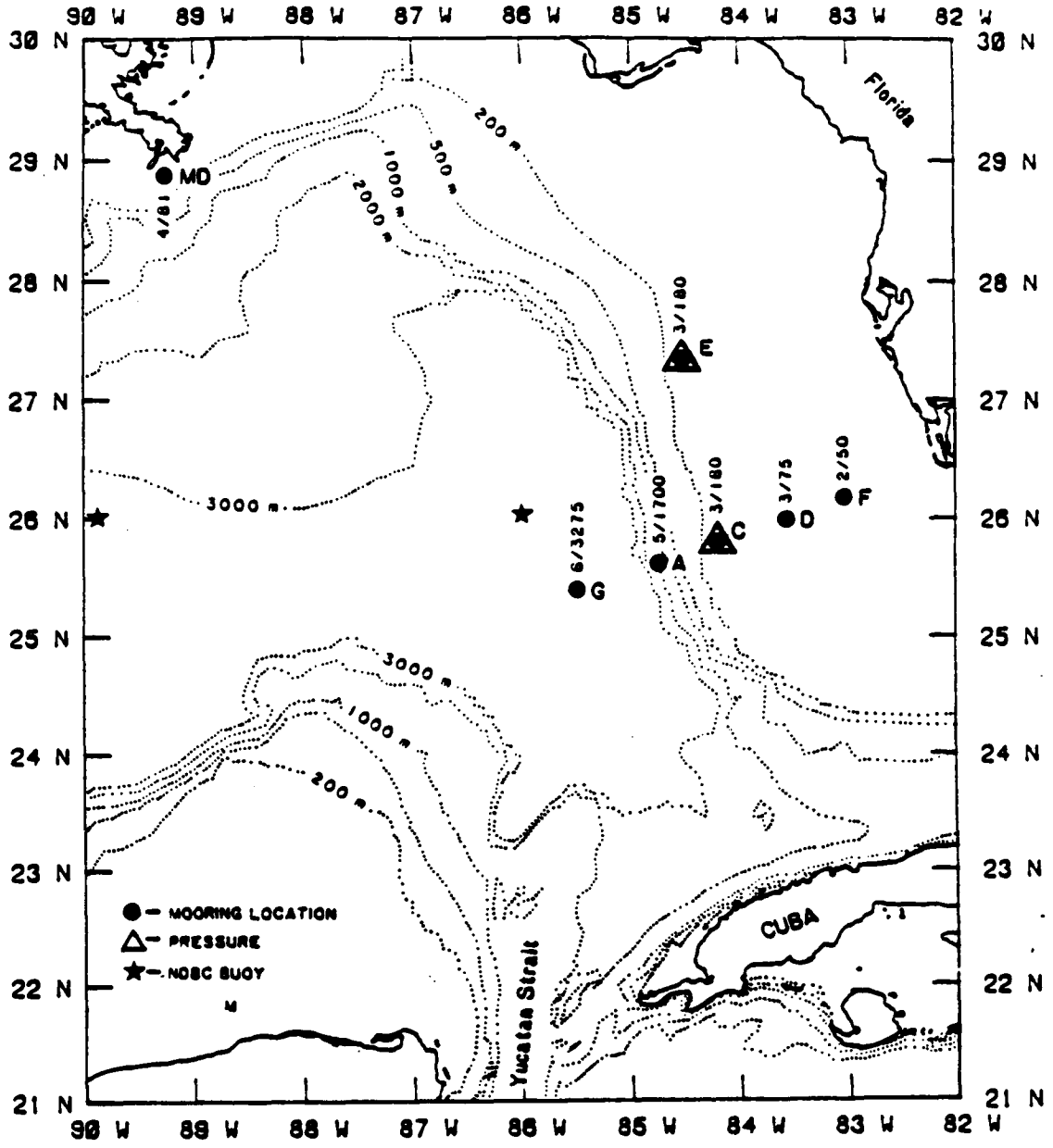
90 W
89 W
88 W
87 W
86 W
85 W
84 W
83 W
82 W
30 N
29 N
28 N
27 N
26 N
25 N
24 N
23 N
22 N
21 N
Florida
CUBA
Yucatan Strait
MD
4/81
200 m
500 m
1000 m
2000 m
3000 m
3/180
E
3/180
C
5/1700
A
6/3275
G
3/75
D
2/50
F
MOORING LOCATION
PRESSURE
NOSC BUOY

FIGURE 41

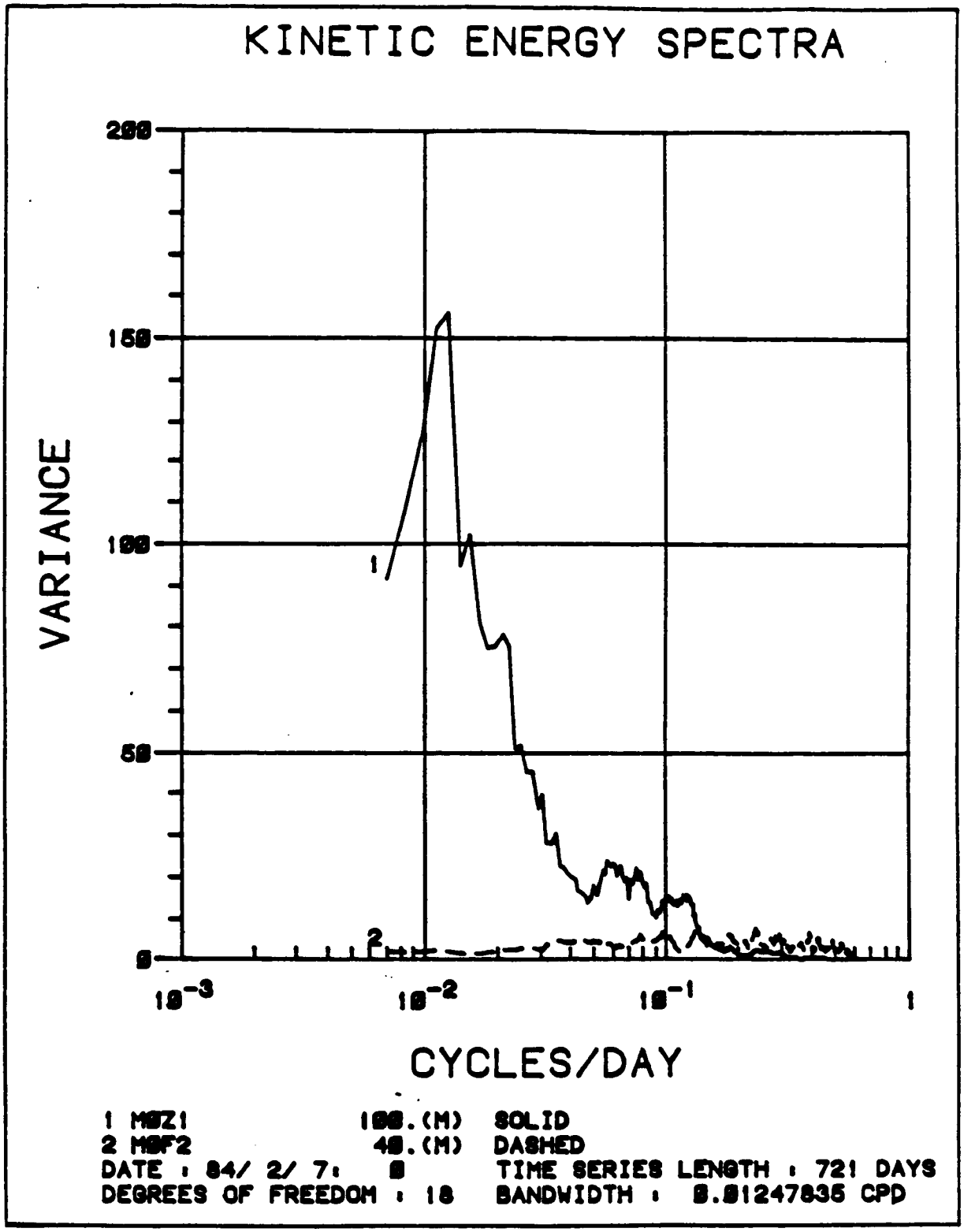
KINETIC ENERGY SPECTRA
200
150
100
50
0
VARIANCE
1
2
10^{-3}
10^{-2}
10^{-1}
1
CYCLES/DAY
1 MSZ1 100.(M) SOLID
2 MSF2 40.(M) DASHED
DATE : 84/ 2/ 7: 0 TIME SERIES LENGTH : 721 DAYS
DEGREES OF FREEDOM : 18 BANDWIDTH : 0.01247836 CPD

FIGURE 42

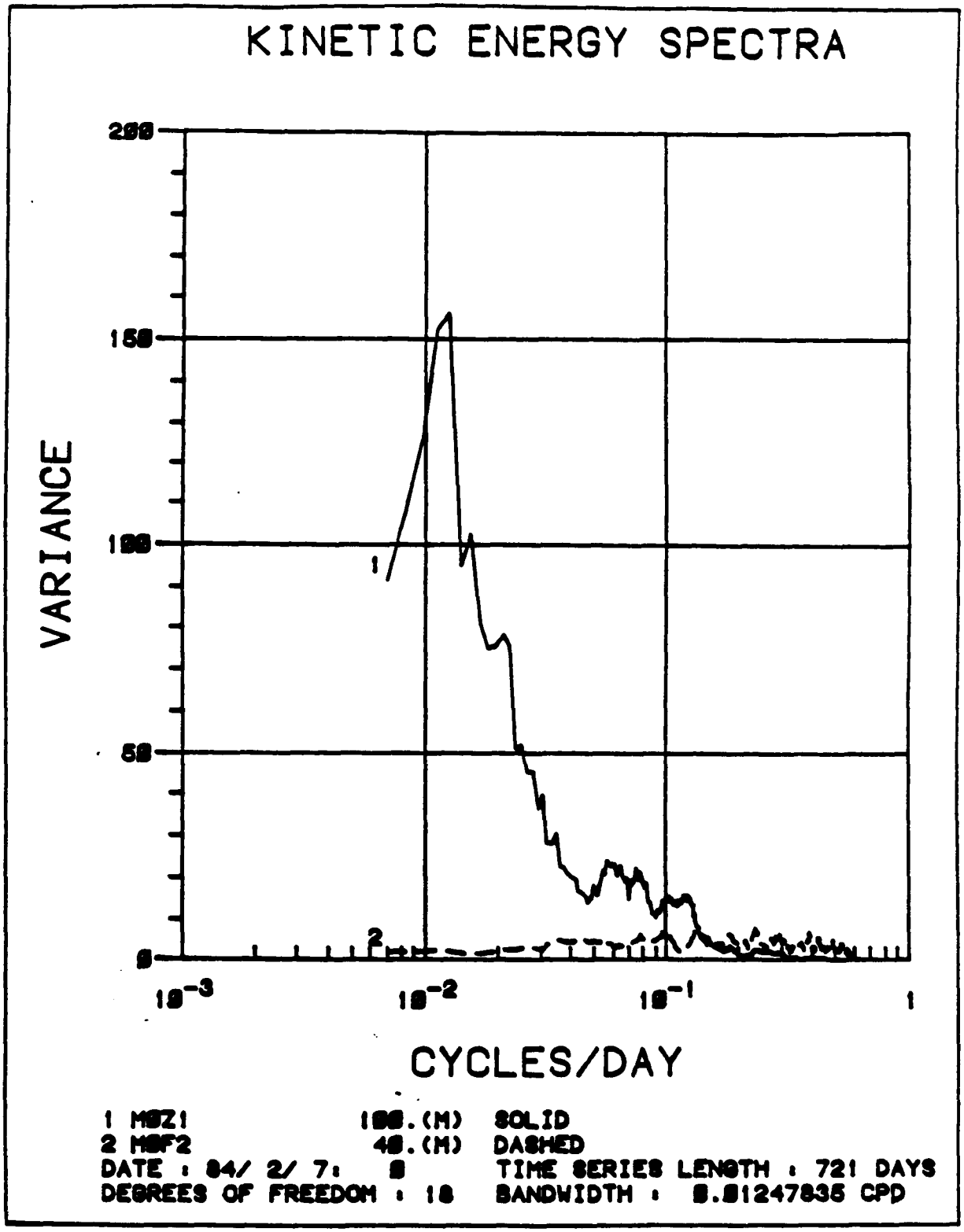
KINETIC ENERGY SPECTRA
200
150
100
50
0
VARIANCE
1
2
10^{-3}
10^{-2}
10^{-1}
1
CYCLES/DAY
1 MSZ1 100.(M) SOLID
2 MSF2 40.(M) DASHED
DATE : 84/ 2/ 7: 0 TIME SERIES LENGTH : 721 DAYS
DEGREES OF FREEDOM : 18 BANDWIDTH : 0.01247835 CPD

FIGURE 43: Instantaneous view of the layer depth at hour 0 from a simulation using a 2-D explicit version of the NORDA/JAYCOR ocean model that allows layer interfaces to intersect topography. The layer depth is positive, but very close to zero in the second basin.

FIGURE 44: Instantaneous view of the layer depth at hour 6 from a simulation using a 2-D explicit version of the NORDA/JAYCOR ocean model that allows layer interfaces to intersect topography. Water is being added to the center of the first basin.

FIGURE 45: Instantaneous view of the layer depth at hour 12 from a simulation using a 2-D explicit version of the NORDA/JAYCOR ocean model that allows layer interfaces to intersect topography. Water is being added to the center of the first basin.

FIGURE 46: Instantaneous view of the layer depth at hour 18 from a simulation using a 2-D explicit version of the NORDA/JAYCOR ocean model that allows layer interfaces to intersect topography. Water is being added to the center of the first basin.

FIGURE 47: Instantaneous view of the layer depth at hour 24 from a simulation using a 2-D explicit version of the NORDA/JAYCOR ocean model that allows layer interfaces to intersect topography. Water is being added to the center of the first basin.

FIGURE 48: Instantaneous view of the layer depth at hour 30 from a simulation using a 2-D explicit version of the NORDA/JAYCOR ocean model that allows layer interfaces to intersect topography. Water is being added to the center of the first basin.

FIGURE 49: Instantaneous view of the layer depth at hour 36 from a simulation using a 2-D explicit version of the NORDA/JAYCOR ocean model that allows layer interfaces to intersect topography. Water is being added to the center of the first basin.

FIGURE 50: Instantaneous view of the layer depth at hour 42 from a simulation using a 2-D explicit version of the NORDA/JAYCOR ocean model that allows layer interfaces to intersect topography. Water is being added to the center of the first basin.

FIGURE 51: Instantaneous view of the layer depth at hour 48 from a simulation using a 2-D explicit version of the NORDA/JAYCOR ocean model that allows layer interfaces to intersect topography. Water is being added to the center of the first basin.

FIGURE 43

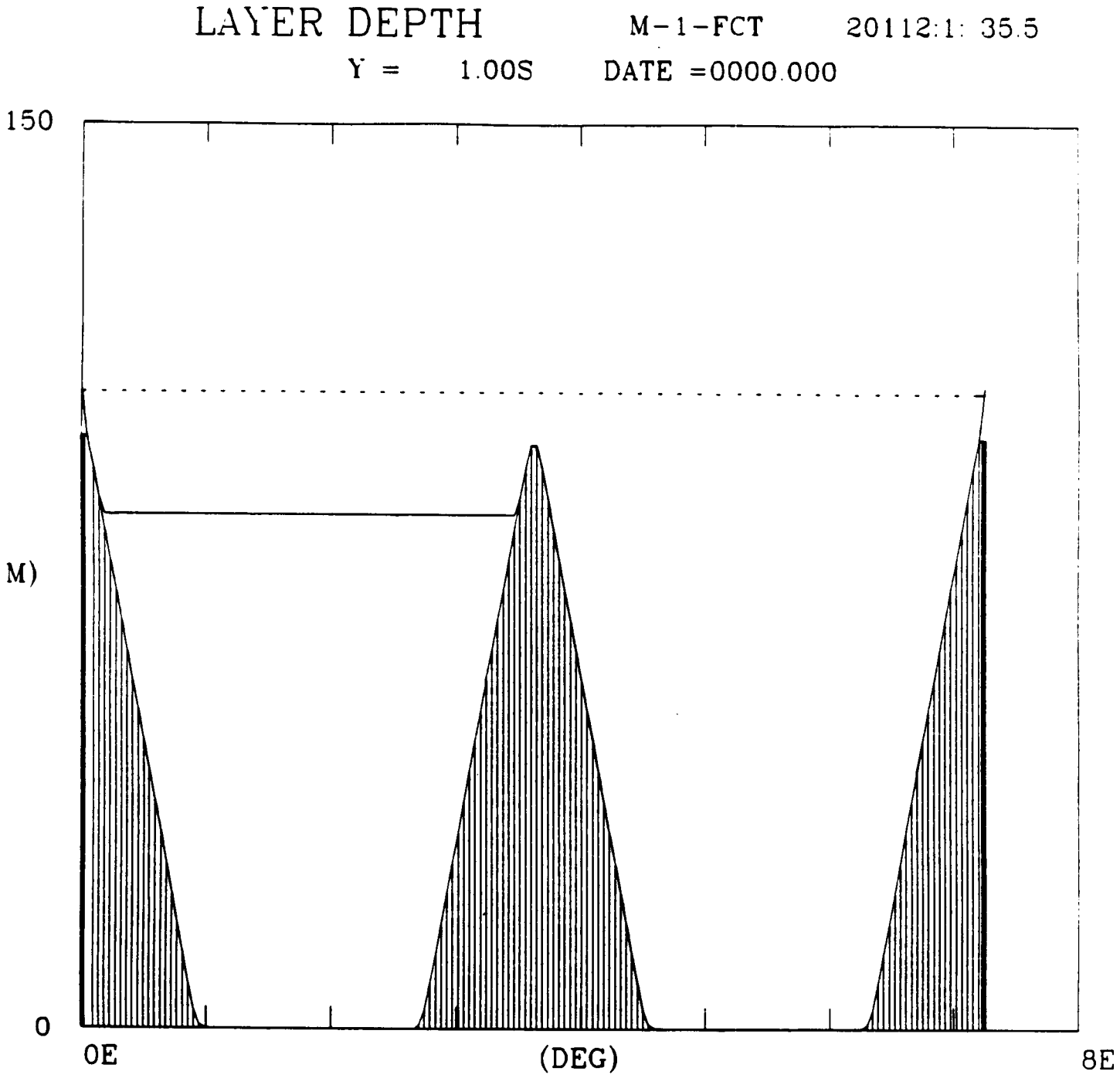
LAYER DEPTH
M-1-FCT
20112:1: 35.5
Y = 1.00S
DATE =0000.000
150
M)
0
0E
(DEG)
8E

FIGURE 44

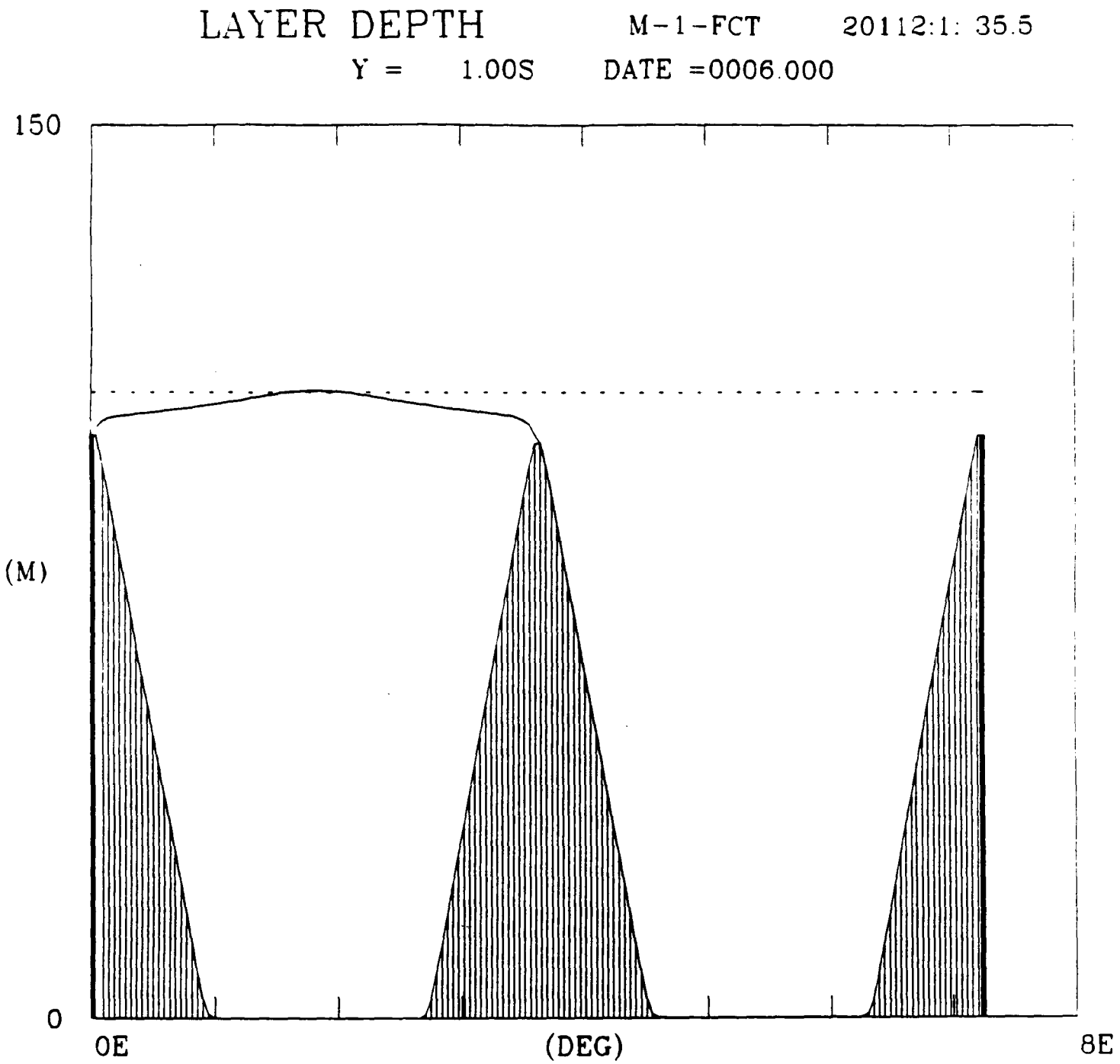
LAYER DEPTH
M-1-FCT
20112:1: 35.5
Y = 1.00S
DATE =0006.000
150
(M)
0
0E
(DEG)
8E

FIGURE 45

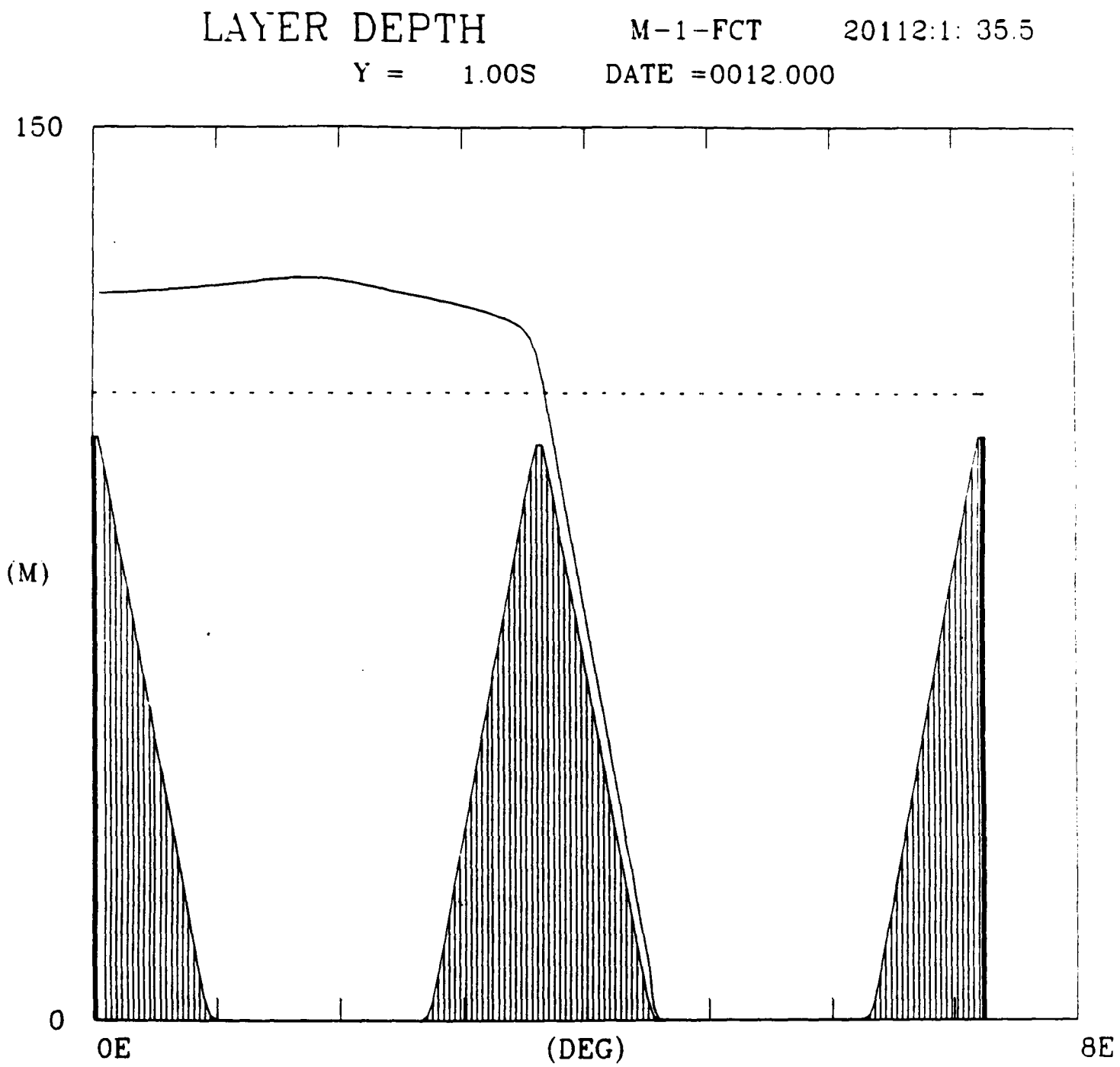
LAYER DEPTH
M-1-FCT
20112:1: 35.5
Y = 1.00S
DATE =0012.000
150
(M)
0
0E
(DEG)
8E

FIGURE 46

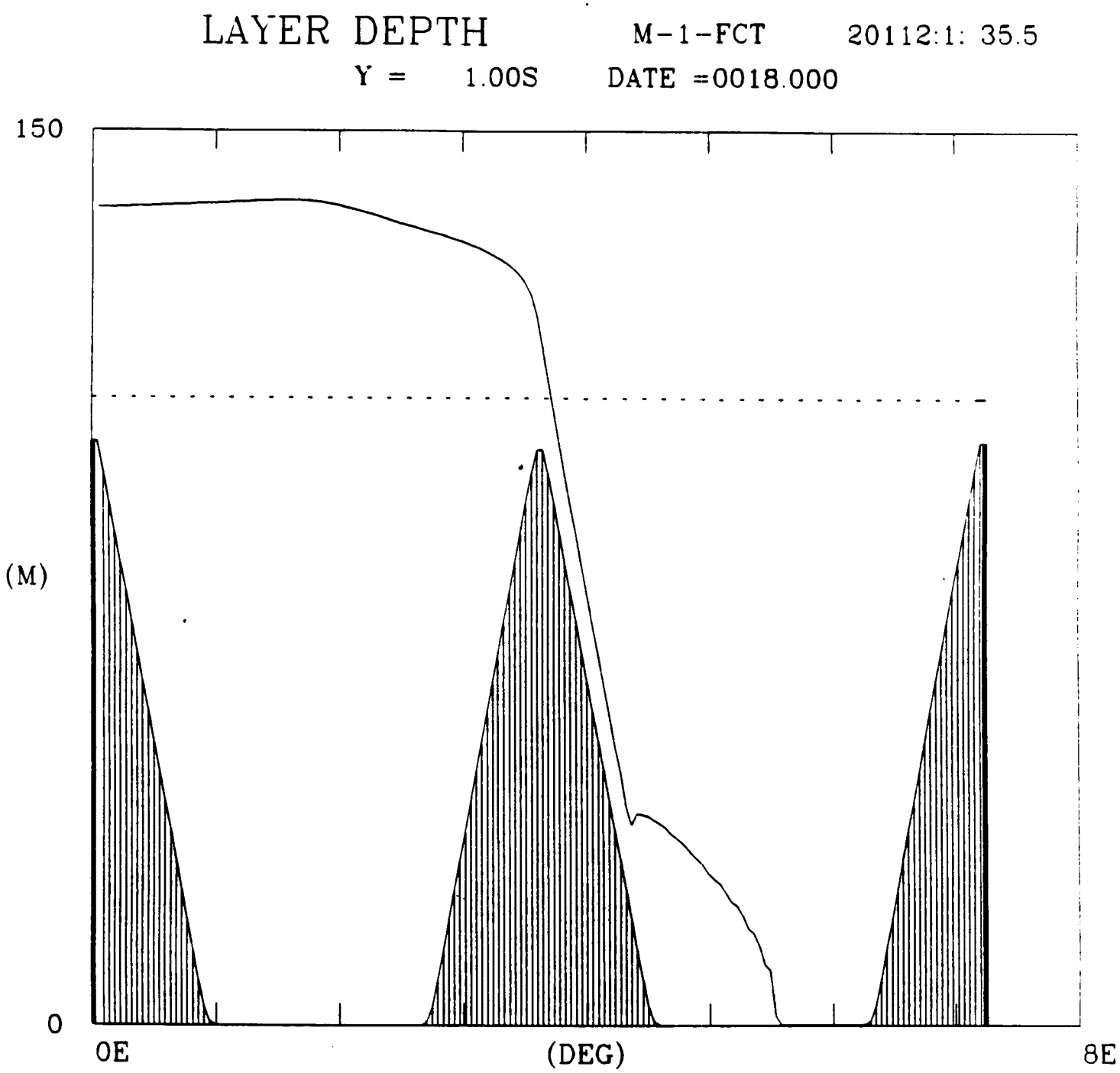
LAYER DEPTH
M-1-FCT
20112:1: 35.5
Y = 1.00S
DATE =0018.000
150
(M)
0
0E
(DEG)
8E

FIGURE 47

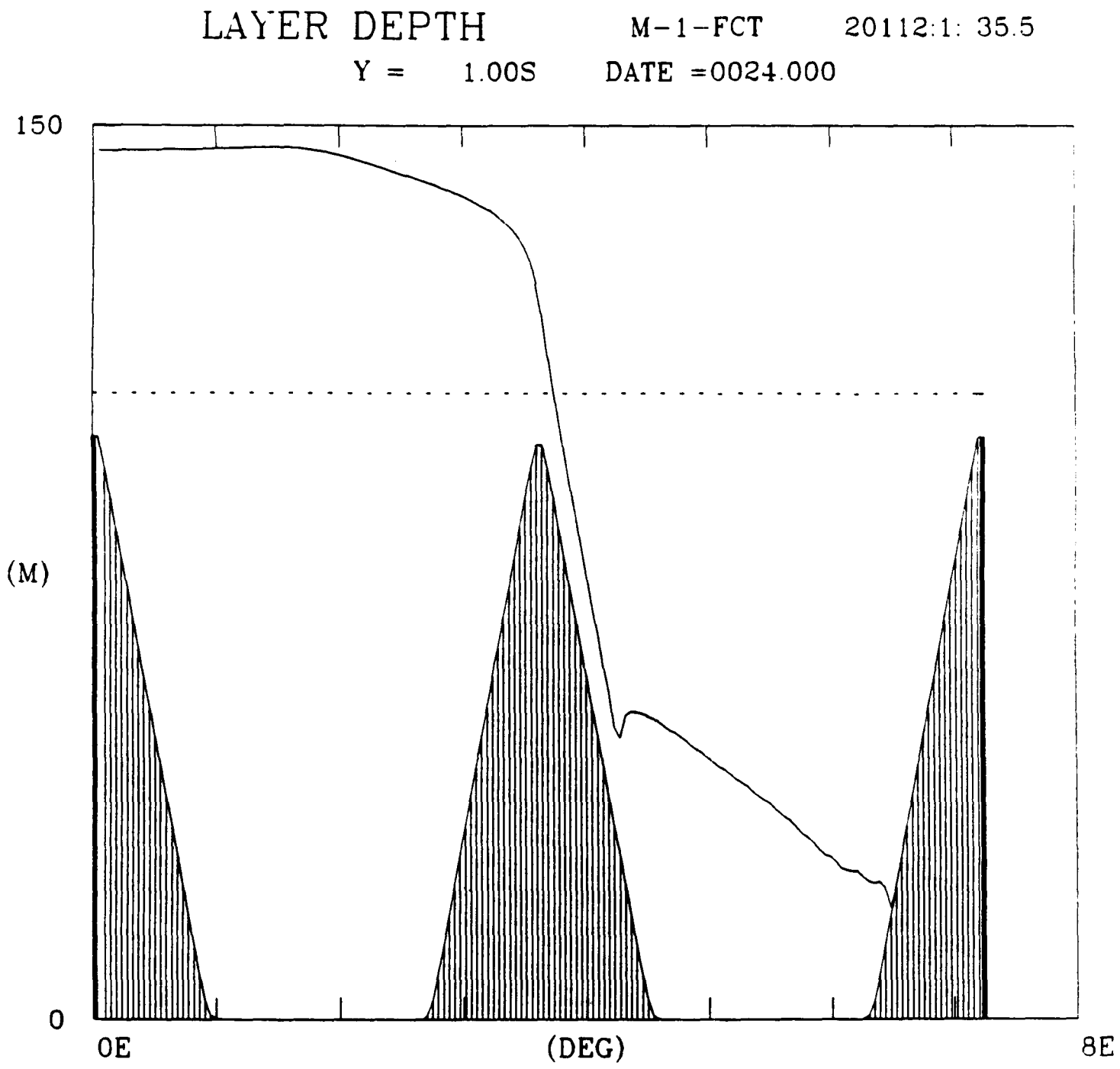
LAYER DEPTH
M-1-FCT
20112:1: 35.5
Y = 1.00S
DATE =0024.000
150
(M)
0
0E
(DEG)
8E

FIGURE 48

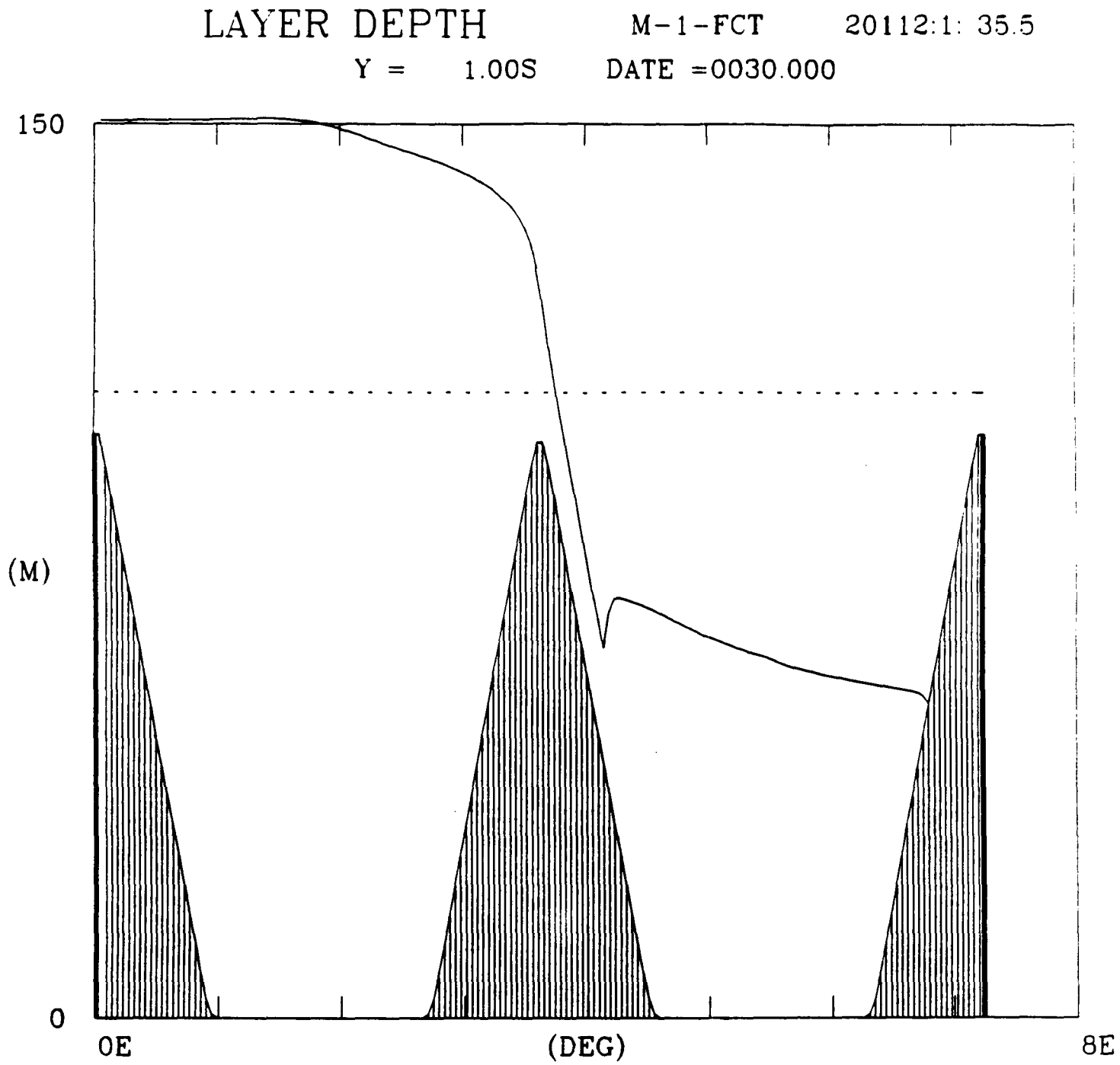
LAYER DEPTH
M-1-FCT
20112:1: 35.5
Y = 1.00S
DATE =0030.000
150
(M)
0
0E
(DEG)
8E

FIGURE 49

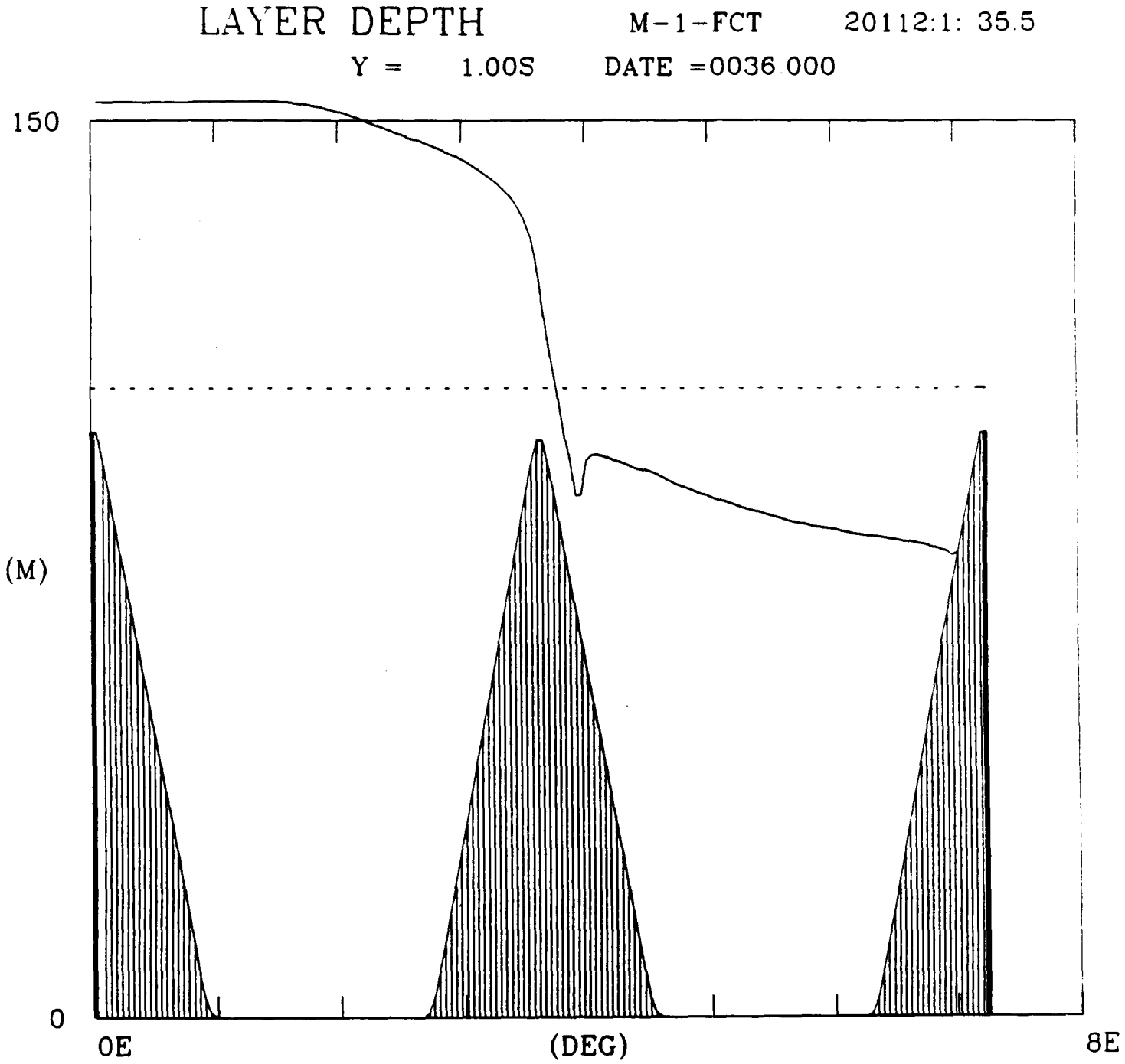
LAYER DEPTH
M-1-FCT
20112:1: 35.5
Y = 1.00S
DATE =0036.000
150
(M)
0
0E
(DEG)
8E

FIGURE 50

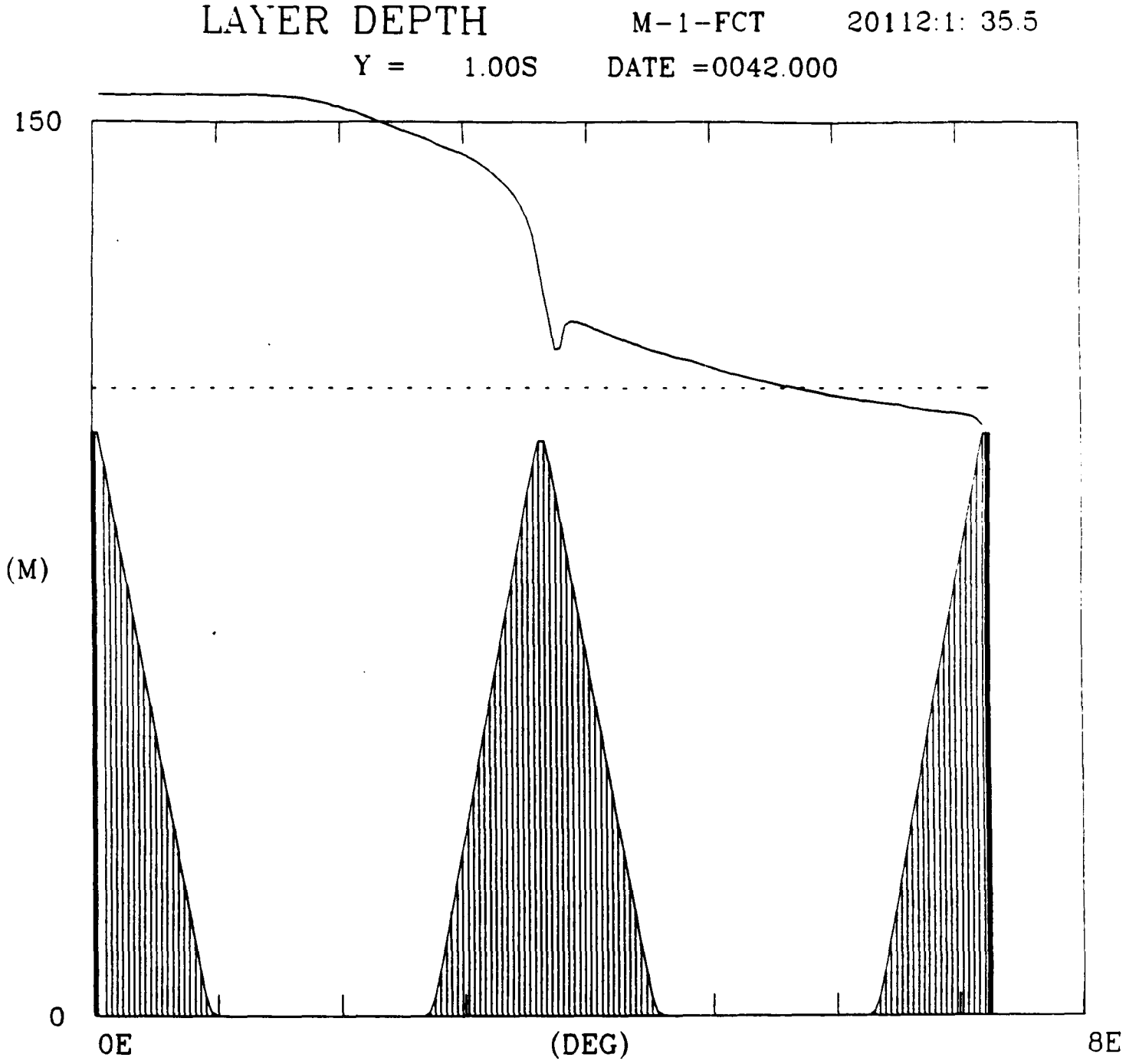
LAYER DEPTH
M-1-FCT
20112:1: 35.5
Y = 1.00S
DATE =0042.000
150
(M)
0
0E
(DEG)
8E

FIGURE 51

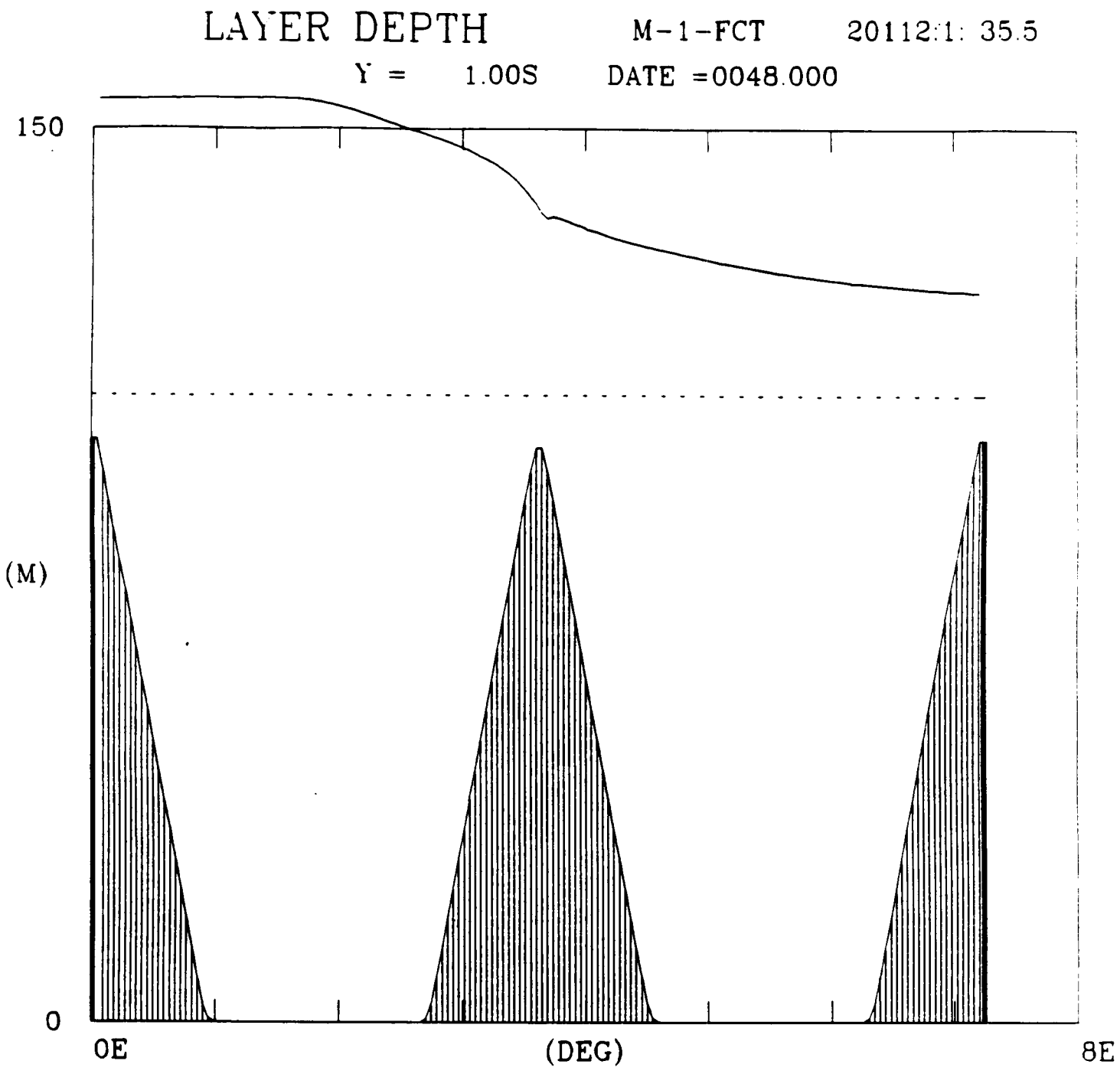
LAYER DEPTH
M-1-FCT
20112:1: 35.5
Y = 1.00S
DATE =0048.000
150
(M)
0
0E
(DEG)
8E

APPENDIX A

APPENDIX A: MODEL PARAMETERS

YEAR 1 REFERENCE PARAMETERS (EXPERIMENT 40):

- upper layer inflow transport = 20 x 10^6 m^3 sec^{-1} (= 20 Sv),
- lower layer inflow transport = 10 x 10^6 m^3 sec^{-1} (= 10 Sv),
- wind stress = 0,
- horizontal eddy viscosity, A = 300 m^2 sec^{-1},
- grid spacing = 20 by 22 km (0.2 by 0.2 degrees),
- upper layer reference thickness, H1 = 200m,
- lower layer reference thickness, H2 = 3300m,
- minimum depth of bottom topography = 500m,
- beta, df/dy = 2 x 10^{-11} m^{-1} sec^{-1},
- Coriolis parameter at the southern boundary, f = 4.5 x 10^{-5} sec^{-1},
- gravitational acceleration, g = 9.8 m sec^{-2},
- reduced gravity, g' = .03(H1 + H2)/H2 m sec^{-2},
- interfacial stress = 0,
- coefficient of quadratic bottom stress = .003,
- time step = 1.5 hours.

EXPERIMENT 9:

- upper layer inflow transport = 26 x 10^6 m^3 sec^{-1} (= 26 Sv),
- lower layer inflow transport = 4 x 10^6 m^3 sec^{-1} (= 4 Sv),
- grid spacing = 25 by 25 km,
- lower layer reference thickness, H2 = 3400m,
- Coriolis parameter at the southern boundary, f = 5 x 10^{-5} sec^{-1},
- coefficient of quadratic bottom stress = .002,
- time step = 1 hour,
- all other parameters as in the Year 1 reference experiment.

EXPERIMENT 31:

- upper layer inflow transport = 0,
- lower layer inflow transport = 0,
- wind stress from seasonal climatology based on ship observations,
- coefficient of quadratic bottom stress = .002,
- all other parameters as in the Year 1 reference experiment.

EXPERIMENT 40:

- the Year 1 reference experiment.

EXPERIMENT 68:

- wind stress from 12 hourly Navy Corrected Geostrophic Wind set,
- all other parameters as in the Year 1 reference experiment.

YEAR 2 REFERENCE PARAMETERS (EXPERIMENT 201/13.0):

- upper layer inflow transport = 20 x 10^6 m^3 sec^{-1} (= 20 Sv),
- lower layer inflow transport = 10 x 10^6 m^3 sec^{-1} (= 10 Sv),
- wind stress = 0,
- horizontal eddy viscosity, A = 100 m^2 sec^{-1},
- grid spacing = 10 by 11 km (0.1 by 0.1 degrees),
- upper layer reference thickness, H1 = 200m
- lower layer reference thickness, H2 = 3450m,
- minimum depth of bottom topography = 500m,
- beta, df/dy = 2 x 10^{-11} m^{-1} sec^{-1},
- Coriolis parameter at the southern boundary, f = 4.5 x 10^{-5} sec^{-1},
- gravitational acceleration, g = 9.8 m sec^{-2},
- reduced gravity, g' = .03 m sec^{-2}
- interfacial stress = 0,
- coefficient of quadratic bottom stress = .002,
- time step = 1.0 hours.

EXPERIMENT 202/11.0

- upper layer inflow transport = 0,
- lower layer inflow transport = 0,
- wind stress is monthly climatology for 6 years and then monthly winds for 1967, 1968, 1969, etc. from the Navy Corrected Geostrophic Wind data set.
- horizontal eddy viscosity, A = 300 m^2 sec^{-1},
- grid spacing = 20 by 22 km (0.2 by 0.2 degrees),
- time step = 1.5 hours,
- all other parameters as in the Year 2 reference experiment.

EXPERIMENT 201/13.0

- the Year 2 reference experiment.

EXPERIMENT 201/16.0

- wind stress is zero for 6 years and then monthly winds for 1967, 1968, 1969, etc. from the Navy Corrected Geostrophic Wind data set.
- interfacial stress is space- and layer-thickness-dependent: for an upper layer thickness of 200 m the frictional e-folding time varies from 3 years in the east to 115 days in the west of the Gulf, for a layer thickness of 100 m the range is 75 days to 7 days, and for a layer thickness of 50 m it is 4.5 to 0.5 days.
- time step = 0.5 hours,
- all other parameters as in the Year 2 reference experiment.

EXPERIMENT 201/17.0

- horizontal eddy viscosity, $A = 50\ m^2\ sec^{-1}$,
- coefficient of quadratic bottom stress = .003,
- all other parameters as in the Year 2 reference experiment.

The Department of the Interior Mission

As the Nation's principal conservation agency, the Department of the Interior has responsibility for most of our nationally owned public lands and natural resources. This includes fostering sound use of our land and water resources; protecting our fish, wildlife, and biological diversity; preserving the environmental and cultural values of our national parks and historical places; and providing for the enjoyment of life through outdoor recreation. The Department assesses our energy and mineral resources and works to ensure that their development is in the best interests of all our people by encouraging stewardship and citizen participation in their care. The Department also has a major responsibility for American Indian reservation communities and for people who live in island territories under U.S. administration.

The Minerals Management Service Mission

As a bureau of the Department of the Interior, the Minerals Management Service's (MMS) primary responsibilities are to manage the mineral resources located on the Nation's Outer Continental Shelf (OCS), collect revenue from the Federal OCS and onshore Federal and Indian lands, and distribute those revenues.

Moreover, in working to meet its responsibilities, the **Offshore Minerals Management Program** administers the OCS competitive leasing program and oversees the safe and environmentally sound exploration and production of our Nation's offshore natural gas, oil and other mineral resources. The MMS **Minerals Revenue Management** meets its responsibilities by ensuring the efficient, timely and accurate collection and disbursement of revenue from mineral leasing and production due to Indian tribes and allottees, States and the U.S. Treasury.

The MMS strives to fulfill its responsibilities through the general guiding principles of: (1) being responsive to the public's concerns and interests by maintaining a dialogue with all potentially affected parties and (2) carrying out its programs with an emphasis on working to enhance the quality of life for all Americans by lending MMS assistance and expertise to economic development and environmental protection.